1-1-2012

Modifying Crystal Morphology And Framework Composition Of Composition Of Zeolite L (LTL) – A Co-Solvent Approach

Adriana Gaona-Gomez
Ryerson University

MODIFYING CRYSTAL MORPHOLOGY AND FRAMEWORK COMPOSITION OF ZEOLITE L (LTL) – A CO-SOLVENT APPROACH

by

ADRIANA GAONA-GÓMEZ
B.Sc. in Chemical Engineering
Universidad del Valle, Colombia, 2008

A Thesis

presented to Ryerson University

in partial fulfilment of the requirements

for the degree of

Master of Applied Science
in the Program of
Chemical Engineering

Toronto, Ontario, Canada, 2012

AUTHOR'S DECLARATION

I hereby declare that I am the sole author of this thesis. This is a true copy of the thesis, including any required final revisions, as accepted by my examiners.

I authorize Ryerson University to lend this thesis to other institutions or individuals for the purpose of scholarly research.

_____

Adriana Gaona-Gómez

I further authorize Ryerson University to reproduce this thesis by photocopying or by other means, in total or in part, at the request of other institutions or individuals for the purpose of scholarly research.

I understand that my thesis may be made electronically available to the public.

_____

Adriana Gaona-Gómez

ABSTRACT

Modifying Crystal Morphology and Framework Composition of Zeolite L (LTL)
A Co-Solvent Approach

Adriana Gaona-Gómez
Master of Applied Science
Chemical Engineering
Ryerson University
2012

The first part of this study investigates synthesis protocols to tune the size and the morphology of zeolite L (LTL) crystals using three different glycols. The outcomes clearly demonstrate that the formation of pure LTL phase is greatly facilitated at 150 ºC for 6 days only when using triethylene glycol (TEG) as the co-solvent, verified by powder X-ray diffraction (PXRD). SEM images show that LTL crystals present a cylinder-like structure with an aspect ratio of one. The formation of pure LTL phase is dramatically deteriorated when the synthesis conditions are changed to higher temperature (180 ºC), various synthesis durations (1-3 days) and aging time, and using other co-solvents (ethylene glycol and diethylene glycol). Inspired by published results indicating the interactions between Ge and glycols, I developed three synthesis approaches exploring the feasibility of incorporating germanium (Ge) into LTL framework using TEG in the second part of this study. Moreover, studies report that the incorporation of Ge in zeolite frameworks can enhance zeolites' catalytic performances. The results from my investigation show that highly crystalline and well-defined LTL crystals are attained at 150 ºC for 3 days. X-ray fluorescence (XRF) shows the presence of Ge in LTL samples, indicating that the incorporation of Ge is very promising using the developed synthesis approaches. The outcomes are expected to be very useful to other researchers in the zeolites research field.

ACKNOWLEDGMENTS

First and foremost, my sincere gratitude to my advisor, Dr. Chil-Hung Cheng, not only for his diligent work on this thesis, but also for his continuing efforts to help preparing me in this research path. From him, I have learned the value of precision, perseverance, understanding of the fundamentals, and to take the extra time to push work from *good enough* to *excellent*. I deeply appreciate his support and vast patience during my time in Ryerson and to encourage the presentation of this work in scientific conferences.

I also thank both Dr. Jiangning Wu and Dr. Huu Doan for being part of my thesis committee and for providing invaluable feedback to this work. I thank the academic and financial support received from the Department of Chemical Engineering at Ryerson University. I am also thankful for the financial support provided by Natural Science and Engineering Research Council of Canada (NSERC)-Discovery Grant program and Seed Grant of the Dean's Office of Faculty of Engineering, Architecture, and Science at Ryerson University.

My deepest thanks to Dr. Srebri Petrov, from the Department of Chemistry at University of Toronto, for conducting almost all the powder X-ray analyses. I also thank Dr. Mike Gorton from the Department of Geology of University of Toronto, for conducting the X-ray Fluorescence analyses. I would like to thank Dr. Russell Viirre from the Department of Chemistry at Ryerson University, for allowing me to conduct NMR analyses. Many thanks to the help received from Mr. Quiang Li, from the Department of Mechanical Engineering at Ryerson University, who conducted SEM analyses. I acknowledge the assistance received from Dr. Glynis de Silveira from the Brockhouse Institute for Materials Research (BIMR) at MacMaster University for conducting powder X-ray analyses.

I thank the support of Dr. Cheng's group members. Specially thanks to Jia Hua Ou and Samuel Porter. I really appreciate Samuel's enthusiasm towards my research work. I also thank him for helping me to conduct some of the experiments. I would also like to thank my graduate fellows who have helped me over my time in Ryerson: Ilya Kosukhi, Shideh Fathi, Sossina Gezahegn, Wahib Al-Abdallah, Kashif Syed, Hiva Movafagh, Amira Abdelrasoul, Shahzad Baig and Julio Hernandez. My thanks to Hamza Nakhoda and Ciro Lecompte who are valuable friends and from them, I have received constructive feedbacks regarding my research. I thank the support and the great time spent with the ELS team at Ryerson University: Christopher Brierley, Kathryn Oda and Elizabeth Ollerhead.

I would like to especially thank Dr. Ruben Camargo, Dr. Gustavo Bolaños, Dr. Nilson Marriaga and Professor Jaime Jaramillo for their unconditional help and guidance. I thank Lina Montes de Oca for contributing in my academic progress. Fabio Misnaza, you have been my ally in this quest of knowledge. Without you, I would have not be able to have come this far. I feel really blessed to have you in my life. My most sincere gratitude and appreciation to the wonderful women in my life: my grandmas (Emma and Celina), my aunts (Rosa, Amanda, Rubiela, Carmen, Sonia, Marina, Nancy and Nohra) and cousins (Gloria Amanda and Cristina).

I finalize by thanking my most important collaborators, my mom Gloria and my dad Santiago, who have supported me in every single stage of my life, for their unconditional love and for filling my life with joy. I thank Yahweh for allowing me to have both of you in my life.

I also offer regards and greetings to all those who supported me in any way during the completion of this work and whose names were not mentioned.

TABLE OF CONTENTS

LIST OF TABLES

Page

LIST OF FIGURES

Page

LIST OF APPENDICES

Page

NOMENCLATURE

Acronyms

a.u	Arbitrary units
AFM	Atomic force microscopy
Al_2O_3	Aluminium oxide
$AlPO_4$s	Aluminophosphates
BCHP	N-butyl-N-cyclohexyl-pyrrolidinium cation
D6R	Double six-membered ring
D4R	Double four-membered ring
DEG	Diethylene glycol
EG	Ethylene glycol
Et_3N	Triethylamine
EtOH	Ethanol
FAU	Faujasite structure
FER	Ferrierite
FTIR	Fourier transform infrared spectroscopy
Ge	Germanium
GeO_2	Germanium oxide
IR	Infrared raman spectroscopy
ITQ	Instituto de tecnología química
K_2O	Potassium oxide
LTL	Linde type L
MAS-NMR	Magic angle spinning nuclear magnetic resonance
MFI	ZSM-5
NMR	Nuclear magnetic resonance
OECD	Organization for economic co-operation and development
OMS	octahedral molecular sieves
PXRD	Powder X-ray diffraction
PG	Propane-1,3-diol
Py	Pyridine
SEM	Scanning electron microscopy

SiO_2	Silicon oxide
SOD	Sodalite
SSA	Stainless steel autoclave
SDAOH	1,3,3-trimethyl-6-azonium-tricyclo[3.2.1.$4^{6,6}$]dodecane hydroxide
SAXS	Small-angle X-ray scattering
TEG	Triethylene Glycol
TMABr	Tetramethylammonium bromide
TPABr	Tetrapropylammonium bromide
TPAOH	Tetrapropylammonium hydroxide
TEOS	Tetraethyl orthosilicate
XRF	X-ray fluorescence spectroscopy
ZSM-5	Zeolite Socony Mobil - five

Greek Symbols

λ	Wavelength of the X-rays
θ	Angle of the incident X-rays

CHAPTER 1
INTRODUCTION

Industrial synthetic zeolites were first reported by Union Carbide in 1954[1]; however, the use of these materials did not become important until the 1960s when zeolite Y was developed and applied to Fluid Catalytic Cracking (FCC) continuous process,[1,2] where heavy hydrocarbon molecules are breaking down to lighter molecules for gasoline production. Zeolite catalysts in FCC yielded an increase in the production of gasoline from 14 gallons per barrel in the 1960s to 20 gallons per barrel in the late 1980s, thus revolutionizing the petrochemical industry.[3]

Nowadays, the implementation of zeolites has also been considered to reduce harmful environmental emissions and to minimize energy consumption in established chemical processes. For instance, Goodyear chemical company[4] (Akron, OH) investigated the use of carbon-modified zeolites to reduce the energy consumption in the separation of hydrocarbon mixtures, where they estimated that the annual benefit to the industry was 64 trillion Btu/year in energy savings and a 2400-ton increase in synthetic zeolite manufacturing. Moreover, the scarcity of fossil fuel resources has initiated a search for alternative energies. It has been observed the potential use of zeolites as materials to uptake, store and release hydrogen (H_2), where Canada is the largest per-capita hydrogen producer in the Organization for Economic Co-operation and Development (OECD).[5,6]

Successful applications of zeolites in the various aforementioned areas are strongly correlated with the morphology and size of zeolite crystals. Hence, it has promoted the development of novel synthesis protocols to systematically "tailor" the morphology and the size of zeolite crystals. Fundamentally, the development of synthesis protocols could be established through the understanding of zeolite crystallization mechanisms, where the crystallization mechanisms are still unclear to date[7,8]. Experimentally, the development of synthesis protocols has been achieved to tune zeolite size and morphology through adjusting synthesis variables (compositions of synthesis gels, synthesis temperature, and synthesis duration), through adopting various synthesis methods (hydrothermal vs. Microwave), and through adding organic compounds and/or co-solvents.

In the case of zeolite L (LTL), intense research efforts have also been focused to understand, improve and tune the size of crystals. The main problem that researchers have encountered is the

difficulty to develop a method to tune the size LTL crystals with high crystallinity and homogeneous surface (i.e., without intergrowth). The LTL which can meet all the aforementioned characteristics could be effectively applied in areas, such as the catalyst in the aromatization reaction of *n*-alkanes[9], where the performance of the catalyst will be greatly improved due to the reduction of the diffusion time, as membranes, and as host-guest materials.[10] The majority of the synthesis techniques reported in the literature to obtain zeolite crystals have been focused on adjusting the gel composition and the synthesis conditions, such as time and temperature.[11,12] However, the studies conducted thus far have only allowed partially obtaining some of the specific characteristics already mentioned.

Zeolite L is one of few zeolites featuring one-dimensional pore structure. A recent investigation illustrated that zeolite crystals with a shorter diffusion path exhibit better catalytic performance, due to better dispersion of clusters of precious metals (e.g., Pt).[13] Many studies have reported to tune the size and the morphology of LTL crystals by varying the composition of synthesis gels, such as the silica content, the water content, or the mineralizing agent content. To the best of our knowledge, the tuning of the shape and size of LTL crystals by applying organic compounds or co-solvents is the subject of only a few works.[14,15] A successful development of the synthesis protocols using organic compounds or co-solvents will provide the zeolite science community an alternative route of tuning LTL crystals. With this motivation in mind, the first part of the research project systematically investigates the identity and the concentration effects of co-solvents.

Furthermore, isomorphous substituted LTL crystals has demonstrated a better catalytic performance in Fischer-Tropsch reactions.[16] To date, all published studies on isomorphous substituted LTL focus on replacing Al atoms in the zeolite framework. No study has been reported to substitute Si atoms with Ge atoms in LTL framework. However, studies carried out for Ge-incorporated ZSM-5 has demonstrated better catalytic performances in dehydration and Friedel-Crafts acylation reactions.[17] Thus, it is believed that a successful development of Ge-incorporated zeoltie L crystals will expand the horizon of zeoltie L applications. Hence, the second part of the research project investigates the synthesis conditions to incorporate Ge atoms into LTL framework using the aforementioned co-solvent synthesis protocols.

1.1. OBJECTIVES

Zeolites possess well-defined structures. Moreover, depending on the type of zeolite structure, their pore sizes can range from 3 to 15 Å. Thus, zeolites are known as molecular sieves. This characteristic allows the use of these microporous materials in areas such as catalysis, ion exchange and separations. In the case of the catalysis area, zeolites are used, for instance, in the conversion of light naphtha for the attainment of highly valuable products such as benzene. However, the successful application of any zeolite is strongly correlated with their size and morphology. Therefore, the zeolite customizability, depending on the process used, is of paramount importance.[1]

In the case of zeolite L (LTL), the successful application of this zeolite in the catalysis area requires the following characteristics: a crystal with a short channel length, possessing a coin-like shape and smooth surfaces (i.e., without intergrowth). These specifications may allow the enhancement of the diffusion rates as well to avoid the generation of undesired path reactions.[13] Until now, great efforts have been done to change the morphology of zeolite L (LTL) by modifying the molar composition of each of the elements or adding supplemental elements that behave as templates. The outcome from these efforts, although predominantly positive, has occasionally resulted in the undesired intergrowth. For example the presence of amorphous and other phases with the non-uniform crystals could be noticed occasionally.[56] Hence, my research project focuses on developing an alternative synthesis protocol to tune the size and the morphology of LTL crystals, and to incorporate heteroatoms into LTL framework using co-solvents. This investigation is intended to provide insights on tuning LTL crystals. The synthesis protocols can contribute, in the future, to the successful application of LTL in catalysis and separations processes. The specific objectives of this research are:

1. To evaluate and identify the effect of the co-solvent identity towards the formation of LTL crystals.
2. To determine how synthesis conditions can affect the synthesis of LTL such as temperature, time and gel aging.
3. To develop a procedure that can incorporate heteroatoms into LTL framework.
4. To systematically study and learn about the formation of LTL phase when heteroatoms are incorporated.

CHAPTER 2
LITERATURE REVIEW

2.1. GENERAL OVERVIEW

The purpose of this part of the thesis is to provide a comprehensive review of zeolites. This includes the general properties of zeolites, classification depending of pore size and connections, synthesis of zeolites and crystallization mechanism; this chapter also describes and reviews the characteristics, crystallization mechanism and applicability of zeolite L. Finally, this literature review also encompasses the isomorphous substitution of Si by Ge atoms in zeolites.

2.1.1. Molecular Sieves

A molecular sieve is a porous material which exhibits the screening property at the molecular scale.[8,18] To classify a material as a molecular sieve, it should demonstrate the capability to separate the components of a gas or liquid mixture based on its pore size and shape. By 1932, two classes of molecular sieves were identified: the natural zeolites and a particular class of microporous charcoals.[18] At present, a large number of materials have been included in this category, such as silicates, metal aluminates, phosphates, aluminophosphates ($AlPO_4$s), and pillared clays. It is worth mentioning that the terms of molecular sieves and zeolites are used interchangeably. However, only materials whose elemental composition is aluminisilicates can be categorized as zeolites.[1]

Figure 2.1 presents a classification of molecular sieves based on three main groups: silicates, phosphates and others such as pillared clays, octahedral molecular sieves (OMS), among others.[19] Although molecular sieves have been described to provide a general concept, the scope of this study will only be focused on the zeolite materials, specifically LTL.

2.1.2. Zeolites

Zeolites are crystalline materials with well-defined microporous geometry.[18,20] The framework of zeolites is assembled by the connections of 4-coordinated atoms forming tetrahedra of SiO_4 or AlO^-_4. The connections among tetrahedra are accomplished by the sharing of oxygen atoms, yielding regular intra-crystalline cavities and channels at a molecular scale, which can be observed in Figure 2.2. The sizes of the cavities and channels can range from 3 Å to 15 Å.[18,20]

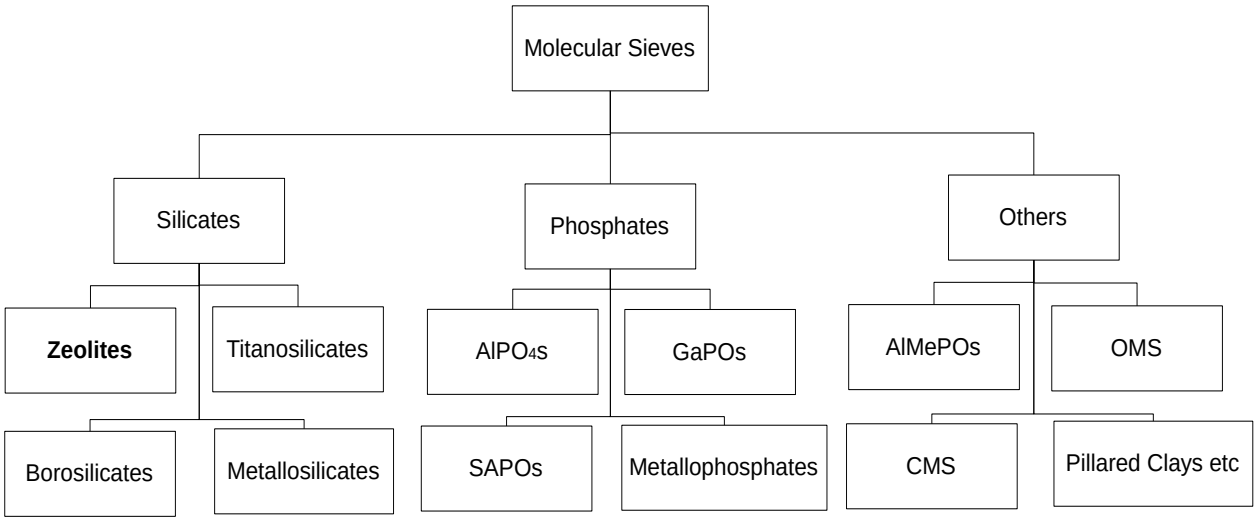

Figure 2.1. Classification of molecular sieves based on three main families.[3]

Zeolites can be classified depending on the size of their pores. The pore size is defined by the number of tetrahedral atoms that are associated together to form the largest pore window within the zeolite structure. For instance, zeolite A and chabazite possess 8-membered rings as the largest pore window. The 8-membered ring is classified as the small-pore and its dimension is approximately 4 Å × 4 Å. The medium-pore zeolites are comprised of 10-membered rings with a dimension of 5.5 Å × 5.5 Å. ZSM-5 stands as a representative in this class.[21] Finally, large-pores zeolites constitute of 12-membered rings with the dimension of 7.5 Å × 7.5 Å in their framework. Zeolite Beta and zeolite Y fall into this category. Figure 2.3 illustrates the different types of pore sizes according to the grouping of the tetrahedra.

When tetrahedra contain aluminum (Al) atoms, the units are charged negatively. The units require balancing charges using alkali metal ions (Na^+, K^+) to maintain the neutrality in the structure.[20] The ratio between Al atoms and silicon (Si) atoms determines the hydrophobicity of zeolite frameworks. As the Si/Al ratio of the framework increases, the hydrophobicity increases. This feature also dictates the zeolites applicability. Therefore, zeolites can also be classified depending on the Si/Al ratio, which are low-silica zeolites with Si/Al < 5, are intermediate zeolites with 5< Si/Al < 10, and are high-silica zeolites with Si/Al >10.[21] Low-silica zeolites are hydrophilic, whereas high-silica zeolites are hydrophobic.[22]

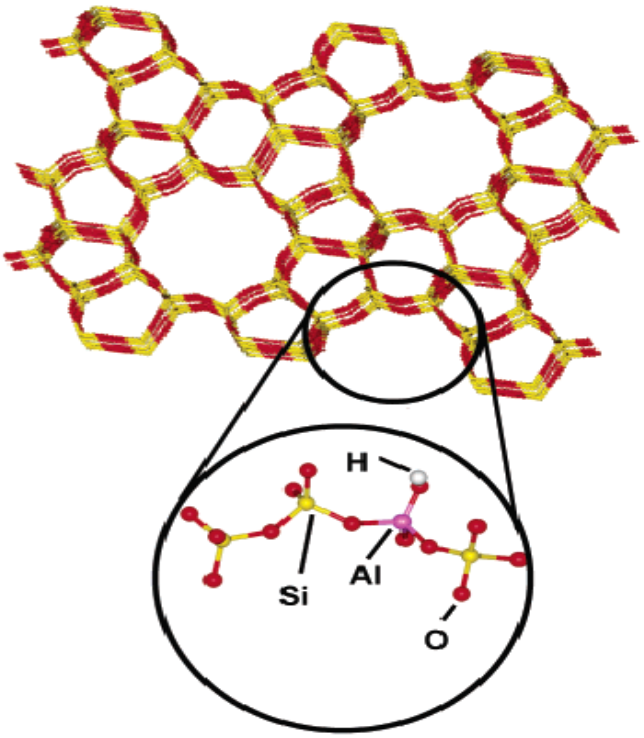

Figure 2.2. Schematic representation of ZSM-5 framework.[23]

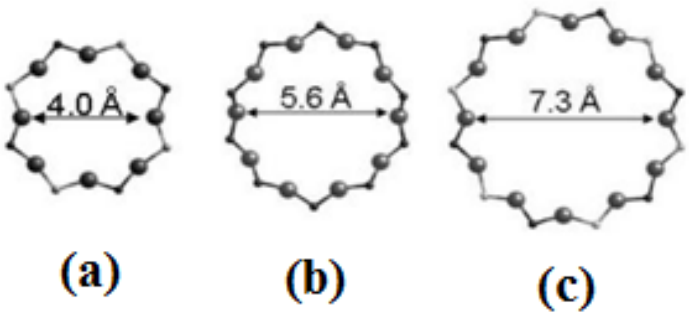

Figure 2.3. Classification of zeolites based on their pore size. (a) 8-membered rings; (b) 10-membered rings; (c) 12-memebered rings.[24]

The formation of a specific type of zeolite is determined by the nature of the starting materials, the starting gel composition, alkalinity and the synthesis conditions, such as temperature, time, and pH. Observing the syntheses of zeolites from a thermodynamic perspective, zeolites are metastable phases. During the course of the syntheses, initial phases are created which are replaced by more stable phases until the most stable phases are formed. This sequence of formation of stable phases is known as Ostwald's law,[8,25] e.g. quartz with SiO_2.

Synthetic zeolites are commonly attained via the hydrothermal synthesis route to their precursor solutions. The zeolite precursor solutions are prepared by combining an alumina source, a silica source

and a mineralizing agent in an aqueous solution. Water plays an important role in the hydrothermal synthesis because of its versatility to interact with both cations and anions. Moreover, the relevance of water is observed to solubilise the different components, as well as the final stabilization of the zeolite framework.[26] The hydrothermal synthesis is usually conducted at a temperature range of 80-200 °C with a duration between hours and days.[23] Figure 2.4 shows a schematic representation of the hydrothermal synthesis.

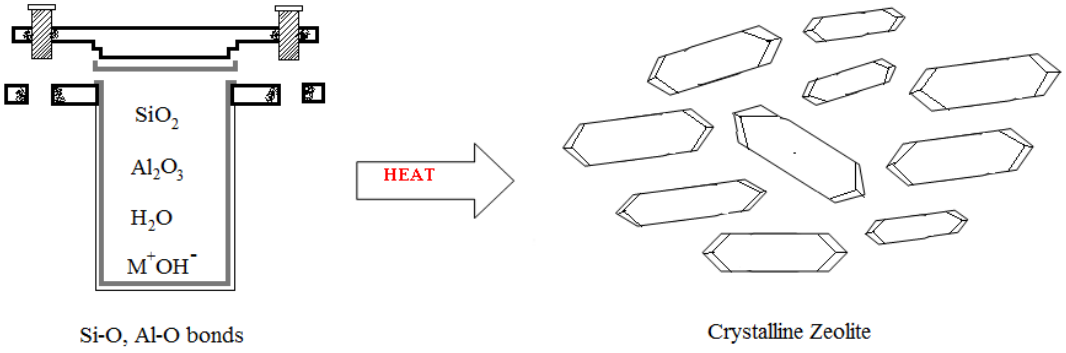

Figure 2.4. Schematic representation of the hydrothermal zeolite synthesis.[7]

In Figure 2.4, the silica sources applied in the hydrothermal synthesis includes fumed silica, sodium silicates, and organosilicates. Aluminum oxide, aluminum powder, and organoaluminates are usually used as the alumina sources in the zeolite precursor solution. The widely adopted mineralizing agents are alkali metal hydroxides and alkali earth metal hydroxides. The mineralizing agent serves as a complexing agent, which can act as acid or base to bring oxides and hydroxides into the precursor solution.[27] The composition of the zeolite precursor solution is usually expressed as:

$$\mathbf{SiO_2: TO_2: M_2O: H_2O}$$

where, M_2O is the oxide form for the mineralizing agent and TO_2 is the oxide form for Al.

It is worth mentioning that before the 1960s the reaction mixtures for hydrothermal syntheses of zeolites were previously prepared using solely the aforementioned components.[20] However after the 1960s, researchers started adding organic components to “tailor” the crystallization of targeted zeolites as well as to alter the Si/Al ratio of zeolite frameworks. These organic components are defined as templates, which are amines and quaternary ammonium compounds.[28] Adding these templates in zeolite precursor solutions contributed to the successful synthesis of ZSM-5 and offretite.[29]

Furthermore, zeolite syntheses have been conducted using seeds to induce the formation of preferred zeolite phase[30,31] and to grow oriented zeolite membranes for gas separation applications.[32] The formation of the preferred zeolite phase can also be achieved using salts as the function of seeds. Therefore, the template compounds, seeds, and salts have been included to the molar composition of the starting gel or the reaction mixture.[13] Thus, the composition of zeolite precursor solution is also expressed as:

$$\mathbf{SiO_2: TO_2: R_2O: M_2O: H_2O + Seed + Salt}$$

Table 2.1 summarizes each component of the zeolite precursor solution, its roles and introduces brief comments on the special features of each of the components.

Table 2.1. Zeolite gel composition for the hydrothermal synthesis.[33]

Component	Role	Comments
SiO_2, TO_2	Framework Components	* Si may be replaced by Ge * T may be Si, Al, B, Fe, Ga, Ti, etc * Ratio of T/Si affects framework charge and properties
M_2O	Mineraliser or base	* Base (OH) * M is usually an alkali metal or a quaternary ammonium compound * Na→ K→ Rb→ Cs can alter product but also crystal morphology and size * Concentration can affect product purity, crystallization rate and framework composition
R_2O	Template	* Structure direction * Structure blocking * Framework stabilisation * Crystal morphology and size
Seed	Seed	* Structure directing (rare) * Increase rate (overall) of crystallization.
Salt	Direct/Indirect	* Direct addition * Crystal size and morphology * Indirect addition through use, for example, of $Al_2(SO_4)_3$ as Al source * Salts may act as framework stabilisers

2.1.3. Crystallization Mechanism

According to Cundy and Cox,[7,23] zeolite crystallization mechanisms take place in a mixture of liquid, amorphous and crystalline solid phases. The depiction of crystallization mechanisms depends on the specific type of zeolite and its properties. Although zeolite synthesis procedures are straightforward, detail understandings of zeolite formation from precursor solutions to crystalline materials are still lacking due to the complexity of several occurring phenomena inside the reactor, such as the variation of solubility, equilibrium, as well as intricate chemical reactions.[8,18] Figure 2.5 represents a potential description of zeolite Y (FAU) crystallization mechanism proposed by Breck.[23] The gel structure is decomposed into simpler compounds by hydroxide ions (OH^-). The hydrated cations (Na^+ or K^+) induce the rearrangement of aluminosilicate and silicate ions present in the hydrous

gel. The tetrahedra (SiO_4, AlO_4^-) are assembled around hydrated cations to form polyhedral units. Subsequently the formation of more polyhedra and their linkages produce the crystal structure of the zeolite.

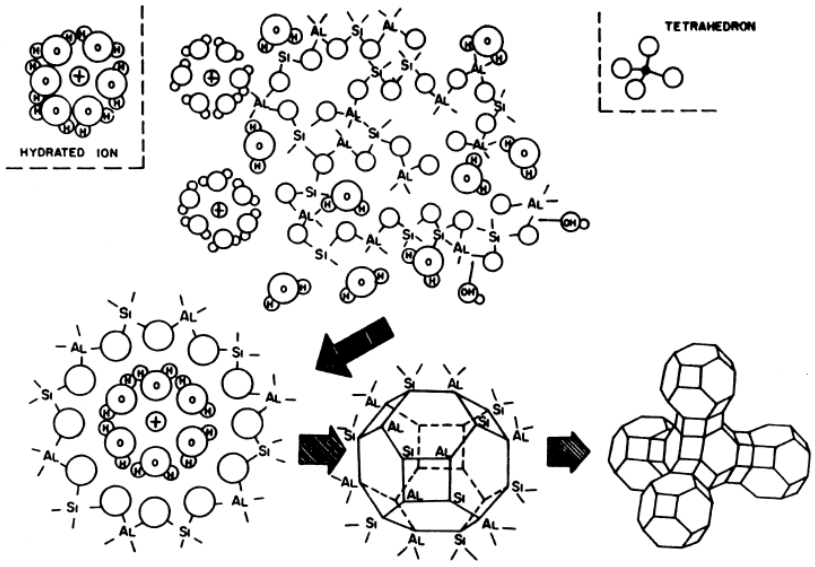

Figure 2.5. Schematic description of zeolite crystallization mechanism.[23]

2.2. ZEOLITE L (LTL)

Among almost 180 zeolites, LTL presents an unique one dimensional pore (1-D) pore structure and several significant applications in catalyst,[9,34,13,35] and in sustainable energy.[10,36-43] It is reported that the morphology of LTL crystals affects the performance of this materials. Thus, the synthesis variables of tuning LTL morphology merit thorough investigations. The framework structure of LTL is constituted by $(Si,Al)O_4$ tetrahedra, which are the primary building units. The primary building units are assembled into secondary building units called cancrinite cages (Figure 2.6 (a)-(b)).[44] The cancrinite cages are connected together by double 6-rings (D6R) to form columns in ***c***-direction (Figure **2.6** (c)-(d)). The 1-D channels of LTL crystals are created by associating 6 cancrinite columns with oxygen bridges, resulting in the 12-membered-ring pore structure with the diameter of 7.1 Å (Figure 2.6 (e)-(f)).[45-47]

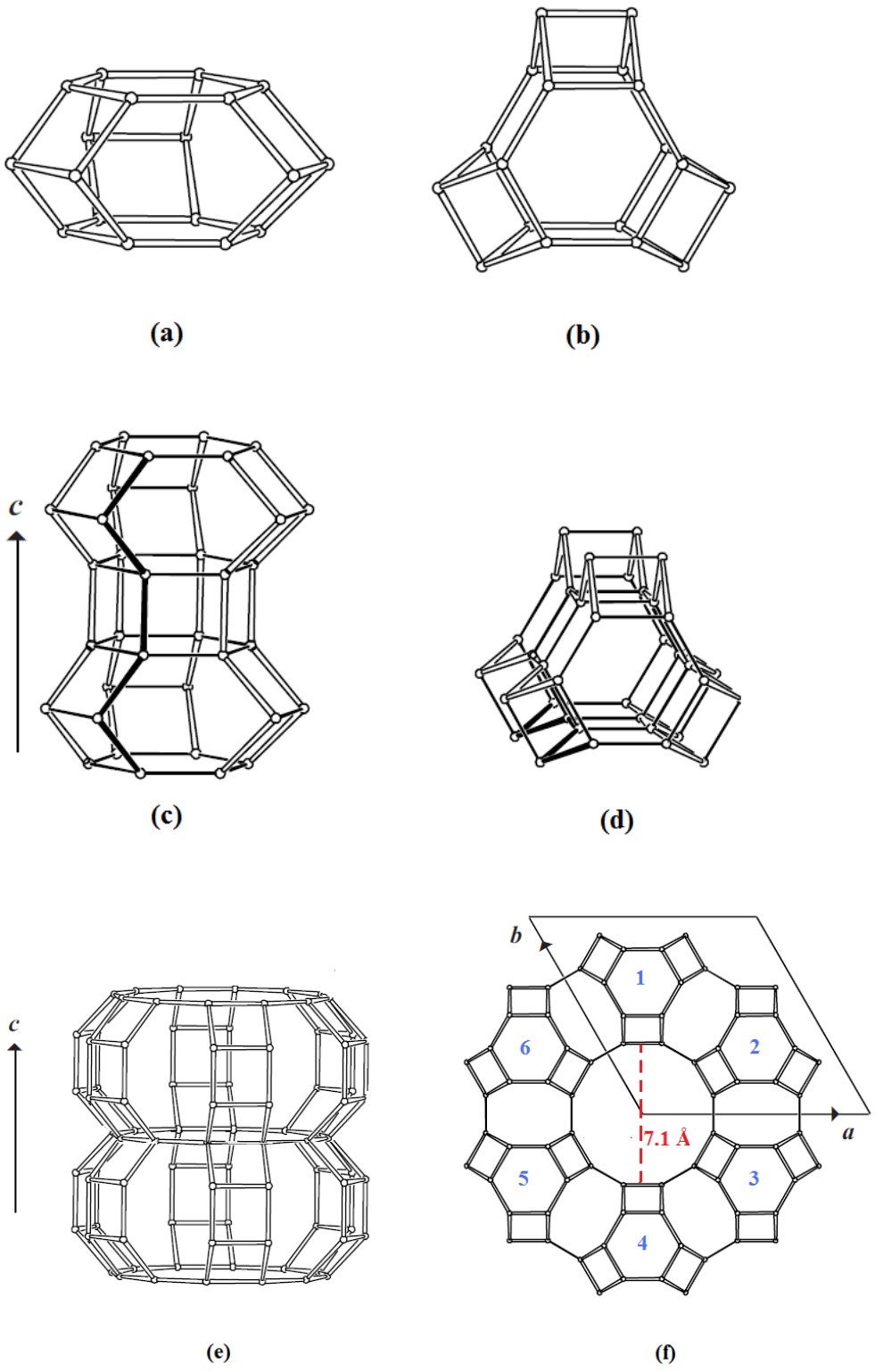

Figure 2.6. (a) Cancrinite cage as the secondary unit building of LTL; (b) View of cancrinite cage along the*c*-direction; (c) Two cancrinite cages connected together by one double 6-ring (D6R) to form a column in *c*-direction (d) View of the column formed in (c) along the c-direction; (e) View of one dimensional channel of LTL; (f) LTL framework projected along c-direction. The numbers in blue (1-6) represent the six cancrinites cages required to form the 12-membered ring structure of LTL with a diameter of 7.1 Å.[48]

2.2.1. Hydrothermal Synthesis of LTL

The first synthesis of the LTL was reported by Breck and Acara[49] in the late 1950s using potassium as the cationic species, where the crystals exhibited a hexagonal cylinder morphology**.** Hereafter, researchers direct all their efforts to understand the structure of LTL. Examples of these studies are the investigations from Barrer[46] in 1969, and Terasaki[45] in 1984. Due to its unique one-dimensional pores, the synthesis and the tuning of LTL crystals started to gain attention. For instance, in 1985, Wortel[50] reported in a patent the attainment of cylindrical crystals with an aspect ratio (i.e. length/diameter) of about 0.5 to 1.5. The starting gel composition consisted of alumina, silica, potassium and water. Wortel also reported the attainment of disc-shape crystals while varying the concentration of the constituents in the starting gel composition. The syntheses of LTL crystals were carried out from 120 °C to 225 °C. It was also observed that an increase in the temperature resulted in a reduction of reaction time.

In 1995, Tsapatsis *et al*[51] synthesized LTL nanoclusters employed as seeds for the formation of micro-sized LTL crystals and films. The crystal length along *c*-axis was around 60 nm. The preparation of the starting gel consisted of dissolving the silica source into the potassium solution, which was subsequently heated at 80 °C for 12h while stirring. After the silicate solution was cooled to room temperature, the aluminate solution was slowly added to the silicate solution, obtaining a clear homogeneous solution. The final solution was subjected to the hydrothermal synthesis under rotating conditions.

Ko and Ahn[12] presented a method to shorten the synthesis time of LTL by increasing synthesis temperature and by incorporating NaOH as an additional mineralizing agent. The effect of Na^+ ions was also investigated when it replaced K^+ ions. The synthesis was carried out at 170 °C and LTL crystals were attained at designated synthesis durations of 12, 20, and 24 hours. The average crystal sizes based on the synthesis time were 300, 1200 and 1400 nm correspondingly. From elemental analyses, the authors observed that the Na content in LTL crystals was minimal compared to that of K. Therefore, it was deduced that LTL favours the incorporation of K^+ ions.

Calzaferri's group has claimed that, to successfully implement dye-zeolite composites as artificial photonic systems, the morphology of LTL crystals are preferable to be a disc-like shape with aspect ratios inferior to one and high crystallinity.[41] Thus, Megelski and Calzaferri[38] reported syntheses of LTL crystals with sizes ranging from 30 nm up to 3000 nm at 160 °C for 6 days. Three main

synthesis parameters were studied: water content, K_2O/SiO_2 molar ratio, and the substitution of K^+ ions by Na^+ ions. The size of the crystals increased with water content of the synthesis gel; however, a limit amount of water content of the synthesis gels was observed to obtain LTL crystals. The crystals showed a cylindrical morphology with a smooth surface. The influence of KOH content was manifested in the decrease of the length along *c*-direction and the diameter of the crystals were not significantly altered. An intergrowth was also developed as the potassium content was increased. The morphology of the crystals resembled a disc shape with a length of about 300 nm and a diameter of about 650 nm. The effect of Na^+ ions was investigated by substituting 50% of K^+ by Na^+ in the starting gel composition. As a consequence of this variation, some of the crystals showed a formation of intergrowth specifically on the prismatic face. The rest of the crystals showed a cylindrical morphology.

Bhat *et al*[52] investigated the effect of the contents of KOH, H_2O, and SiO_2 in the gel composition. It was also analyzed the effect of silica and alumina sources on the morphology of LTL. The gel preparation was similar to that reported by Tsapatsis *et al*.[51] However, all the experiments were carried out at 170 °C and static condition. Their results were categorized based on the variation of molar ratios (SiO_2/Al_2O_3, K_2O/SiO_2, H_2O/SiO_2) from the gel mixture. Different types of morphology were reported with varying from clam shape agglomerates, a mixture of spherical particles and clam shape particles, and round shape particles when the SiO_2/Al_2O_3 was decreased. On the other hand, when the content of K_2O/SiO_2 was increased the size of the particles decreased. An increase in the water content permitted the attainability of well-define cylinders. In addition, the authors concluded that the morphology of LTL was not influenced by the nature of alumina and silica sources. However, when using fumed silica instead of silica sol, the former favours the formation of clam shape agglomerates. The crystal sizes attained were in the range of 400 to 1000 nm and from 1500 nm to 2000 nm.

Larlus *et al*[11] also investigated the effect of synthesis variables on the size and the morphology of LTL crystals, such as the composition of starting gel (i.e., contents of H_2O, KOH, Na^+ ions, introduction of Ba^{2+}, Si/Al ratio), the aging time of the gel, and the synthesis temperature. All syntheses were carried out at 170 °C for 3 days under static conditions. They reported that the water content showed the most prominent effect on the morphology of LTL crystals in which the aspect ratio increased from 0.5 to 3. The morphology of the crystals changed from a coin-like shape to cylindrical crystals as the water content was increased. They also reported a maximum water content to

successfully synthesize LTL crystals, consistent with the observation published by Megelski and Calzaferri.[38]

The alkalinity of the synthesis gel affected the particle size distribution. When the KOH content was increased from 0.25 to 0.5 moles, the crystal size was reduced from 250 to 150 nm, respectively. The effect of KOH content is accompanied with the occurrence of the overgrowth on the pinacoidal face, making the crystals resemble a bi-pyramidal shape. Moreover, the substitution of K^+ by Na^+ and the incorporation of Ba^{2+} did not evidence a salient effect on the morphology of LTL. The effect of Si/Al ratio (SAR) in the gel composition was observed in the purity and the growth kinetics of the final product. The SAR of 5 produced a CHA-type zeolite, while crystalline LTL was attained for a $10<Si/Al<15$. An increase of SAR equal to 17 yielded a mixture of amorphous material and LTL. Further increase of SAR to 20 resulted in the formation of amorphous materials only.

An increase of the aging time (1-4 weeks) did not cause changes in the morphology of crystals. Instead, the gel aging reduced the formation of LTL agglomerates. The synthesis temperature was varied between 150 and 200 ºC. No crystalline material was formed at 150 ºC for 3 days. Successively temperature increments yielded the formation of zeolite merlinoite (160 ºC), an increase along the c-direction (3000-4000 nm at 180 ºC) and even higher temperatures resulted in formation of long LTL, with an aspect ratio equal to 2, and formation of clusters.

In 2004, Zabala Ruiz *et al*[53] conducted a systematic study on the morphology and the size of LTL crystals in terms of gel composition, types of silica source, crystallization with or without rotation, reaction time, as well as temperature. The preparation of the starting gel consisted of preparations of silica and alumina solutions separately; however, both solutions were brought to 120 °C to further dissolution before they were mixed together at room temperature. Similar to what were summarized in previous paragraphs, the authors reported that the small size crystals were obtained using the highest content of alkaline source, silica source, water content and the shortest synthesis duration.

Moreover, the gel compositions for the medium sizes were conducted to study the alkalinity effect on the crystal size and to compare their findings to the results reported by Megelski and Calzaferri.[38] It was noted that an increase in KOH lead to the decrease of particle size; yet increasing of intergrowth at the crystal ends was also observed. Their results were also in agreement with Megelski and Calzaferri.[38] Larger crystals were prepared by increasing the water content. It was observed that the

crystals grew preferably along *c*-direction when the amount of water was increased. A similar result has been achieved by other researchers.[38,52-54] Small- and medium-size crystals were prepared in dynamic conditions, whereas large-size crystals were carried out in static conditions. It was determined that the dynamic rotation only influenced the crystals larger than 1000 nm and no significant effect was noticed for smaller size crystals.

A year later, Lee *et al*,[55] motivated by the lack of studies, focused on the synthesis of flat faceted forms, decided to conduct a thorough and systematic study. The morphology and the size of LTL crystals were tuned by varying each component content of the staring gel mixture. The main attributes the authors' study were: the attainment of high crystalline materials with hexagonal cylinder morphology, the use of easy to handle chemicals, the preparation of the starting gel without the extra step observed in the method used by Zabala Ruiz *et al*,[53] and all the experiments conducted were conducted at 180 ℃ for 3 days. It was observed from their results, when the water content was increased (400-1400 moles) this modification favoured the growth in *c*-direction, obtaining large crystal sizes in the range of 700-7000 nm. Additionally, the authors studied other parameters, such as the variation of Al sources from aluminum sulphate to aluminum. It was found that Al sources can also influence or tune the crystal size. Moreover, the effect of salts and NaOH was studied and a change on the morphology was reported.

Ban *et al*[56] reported the use of alkanolamine to tune the size and the morphology of LTL. The preparation of the starting gel consisted of dissolving metallic aluminum powder in an aqueous solution of KOH immersed in an ice bath under a nitrogen atmosphere. The potassium-alumina solution was stirred for 2 hours at room temperature under nitrogen atmosphere, followed by filtration to remove impurities (e.g., Fe traces). The silica source was then added to the alumina-alkaline solution. After hydrothermal synthesis, the crystal sizes attained for the following gel composition *x*KOH: 1.0Al: 4.5SiO_2: 80H_2O were 5200 × 900 nm, 3700 × 2500 nm, and 1300 × 1700 nm in length x diameter, for the following synthesis conditions KOH/Al= 2.2, 2.5, 2.5 at 130 °C, 175 °C, 175 °C, respectively. The increase of KOH content yielded a smaller particle size and an increment in the intergrowth, which have also been reported by other researchers.[52,53,55]

In order to study the effect of the K^+ concentration, a series of experiments were carried out adding KCl to the gel composition (2.26KOH: 1.00Al: 4.55SiO_2: 82.0H_2O: ***y*** KCl) to adjust the amount of cations. The syntheses were carried out at 175 °C for 3 days, where the amount of ***y*** was varied from

0 to 5.2 moles. The addition of KCl yielded a formation of an unknown by-product, which was increased when the KCl content was also increased. Moreover, the crystal morphology shared similar characteristics to the samples when KOH/Al was varied; however, the length and the diameter changed significantly, possibly due to the slight change in the molar composition. At a higher content of KCl, a clam-like shape was observed. Hexagonal cylinder crystals were formed using a lower content of KCl.

The effect of alkalonamine was first studied in the following gel composition: (2.2 or 2.5 moles) KOH: 1.0Al: 4.5SiO_2: 80H_2O by varying the temperature (130 °C, 175 °C); however, it was found an increase in the formation of zeolite W. The authors suspected that alkalonamine formed a complex anion with Al^{3+} ions, leading to the formation of zeolite W. To decrease the formation of zeolite W phase, Ban *et al* increased the concentration of SiO_2 in the starting gel. The change in the SiO_2 concentration also allowed attaining better LTL phase. Moreover, experiments varying the temperature were effectuated as well to obtain the optimal temperature for alkalonamine. The optimal temperature was found to be 120 ºC and the alkalonamine amount was varied in a range of 0.0 to 8.0 moles. When no alkalonamine was added, the morphology of LTL was indistinct shape. A well-defined clam-like shape was attained with a diameter of 1500 nm and a thickness of 300 nm at the alkalonamine content of 2.0 moles. Further increase in the concentration led to form smaller crystals with clam-like shapes.

In 2008, Ko and Ahn,[57] based on their study published in 1999,[12] reported a recent systematic study on the same starting gel composition. The synthesis variables investigated were: starting raw materials, synthesis temperature, gel aging, and concentration of the components. In the case of the raw materials, they investigated the effect of three different silica sources (i.e., Ludox® HS-40 colloidal silica, fine silica powder of Zeosil® 77, and sodium silicate solution). Meanwhile, three different alumina sources were also studied, which were sodium aluminate, aluminum hydroxide and aluminum sulphate. It was observed that the type of raw materials greatly influence the morphology of LTL, varying from clam-like shape to smaller crystal clusters. The average crystal sizes when using Ludox® HS-40, Zeosil® 77, and sodium silicate were 1460, 390 and 410 nm, respectively.

On the other hand, the variation of the alumina source did not alter the morphology of LTL, except for its crystallinity. While using sodium aluminate yielded the highest crystallinity LTL, the aluminum sulphate presented the lowest one. Temperature also had a great effect on the morphology of LTL. It appears that the increment of temperature lead to the formation of crystals with larger average sizes. This is likely due to the fact that nucleation and crystallization were much faster at high

temperatures.[53] Several experiments were carried out to observe the effect of the concentration of the components in the starting gel. The authors concluded that to attain pure LTL crystals, the ratio of SiO_2/Al_2O_3 must be kept among 25-33. Moreover, they found an optimal ratio for each of the elements used in the starting gel in order to avoid formation of unknown by-products and other types of zeolites.

Brent *et* al[15] conducted a study to investigate the effects of the addition of crown ether, which is a ring shaped organic molecule, in the formation of LTL. The authors' hypothesis was based on previous studies[28,58] which have shown that organic molecules can behave as structure directing agents or templates. In order to confirm their hypothesis, a simulation was carried out to observe which type of crown ether and some types of tetraalkyl-ammonium cations were more suitable to generate the template effect. It was found 18-crown-6, and 21-crown-7 were the most effective ones, due to their stronger interactions with LTL framework. A set of experiments was conducted to validate the simulation analyses.

The experiments consisted in varying the molar concentration of the two crown ethers, following the same synthesis procedure published by Lee *et al*.[55] A control experiment was conducted as the benchmark to elucidate the crown ether effect on the zeolite morphology using SEM technique. The results indicated that the addition of crown ether to the starting gel composition yielded a change in the size of LTL crystals. From the SEM images, it was observed that the crystals had a hexagonal cylindrical shape. In the case of 21-crown-7 ether, the sizes attained were 3800, 2000, 1800 and 1800 nm when the molar content varied from 0, 1, 2 and 4. On the other hand, when using 18-crown-6 ether, it did not yield LTL phase; instead, an unknown crystalline phase was formed. They suspected that the effect of crown ether could be understood as an identity that inhibits the growth along *c*-direction of LTL. Brent *et al*. were able to corroborate the presence of the crown ether in LTL using TGA and NMR techniques; however, they were not able to confirm the exact location of the crown ether in LTL structure.

It was reported by White *et al*[59] the synthesis of LTL to prepare zeolite membranes with controlled thickness. The types of structure obtained from the synthesis were a disc-shape LTL, with a size distribution ranging from 500-2000 nm in diameter. Nanocrystalline materials were also prepared. Both gel compositions differed in their KOH molar content. The KOH molar content for the nanocrystalline material was higher when compared to the content for synthesizing disc-shape crystals. The result in the decrease of the size of the LTL crystals was in accordance with the trend observed in

previous studies.[38,40,53,55] Table 2.2 to Table 2.5 show a summary of the synthesis conditions required to attain LTL crystals by using the hydrothermal synthesis approach.

Table 2.2. Summary of representative hydrothermal synthesis conditions used to attain zeolite L (LTL)

		Crystallization parameters				
Crystal length (nm)	**Starting gel composition Al_2O_3: SiO_2: K_2O: H_2O**	**t (h)**	**T (°C)**	**Cond.[a]**	**Silica source[b]**	**Ref.**
60	1.00: 20.00: 10.00: 400.00	1-8	175	d	FS	[51]
300-1400	1.00: 30.00: 5.40: 500.00: 5.70[c]	24	170	s	L	[12]
300	1.00: 10.70: 2.99: 169.3	144	160	s	AK	[38]
	1.00: 9.72: 2.55: 161.3	144	160	s	AK	
	1.00: 20.00: 10.00: 400.00	144	160	s	AK	
400-1000; 1500-2000	1.00: 20.00: 8.00: 400.00	10-50	170	s	FS	[52]
	1.00: 10.00: 4.00: 100.00	10-50	170	s	FS	
	1.00: 10.00: 4.00: 100.00	10-50	171	s	FS	
	1.00: 10.00: 4.00: 101.00	10-50	172	s	FS	
	1.00: 8.00: 3.20: 80.00	10-50	170	s	FS	
	1.00: 8.00: 2.40: 80.00	10-50	170	s	FS	
	1.00: 8.00: 2.00: 80.00	10-50	170	s	FS	
	1.00: 8.00: 2.00: 100.00	10-50	170	s	FS	
	1.00: 8.00: 2.00: 133.00	10-50	170	s	FS	
250-150; 3000-4000	0.08: 1.00: 0.25: 15.00	72	170	s	L	[11]
	0.08: 1.00: 0.25: 10.00-30.00	72	170	s	L	
	0.08: 1.00: 0.25: 15.00	72	170	s	L	
	0.08: 1.00: 0.30: 15.00	72	170	s	L	
	0.08: 1.00: 0.30: 15.00	72	170	s	L	
	0.08: 1.00: 0.30: 15.00	72	180	s	L	

[a] Crystallization Conditions: d = dynamic, s = static; [b] AO = Aerosil OX-50, AK = Aerosil K-330, L = Ludox HS-40, FS = Fumed silica; [c] $1.00Al_2O_3$: $30.00SiO_2$: $5.40K_2O$: $500.00H_2O$: $5.70Na_2O$; [I] Aluminum source varied for every reference: Ref [51]: Aluminum foil; Ref [12] : Aluminum Hydroxide $Al(OH)_3$; Ref [38]: Sodium Aluminate ($NaAlO_2$) ; Ref [52]: Aluminum Isopropoxide and $Al(OH)_3$; Ref [11]: Aluminum Isopropoxide.

Table 2.3. Summary of representative hydrothermal synthesis conditions used to attain zeolite L (LTL)

		Crystallization parameters				
Crystal length (nm)	**Starting gel composition Al_2O_3: SiO_2: K_2O: H_2O**	**t (h)**	**T (°C)**	**Cond.[a]**	**Silica source[b]**	**Ref.**
30-70	1.00: 20.20: 9.34: 412.84	6	170	d	AO	[53]
200-550	1.00: 9.83: 3.17: 168.52	42	160	d	AO	
400-1300	1.00: 9.83: 2.55: 165.60	42	160	d	AO	
	1.00: 9.83: 2.70: 165.60	42	160	d	AO	
	1.00: 9.83: 2.83: 165.60	42	160	d	AO	
	1.00: 9.83: 3.13: 165.60	42	160	d	AO	
250-450	1.00: 30.00: 5.40: 416.08: 5.50[d]	48	160	d	L	
1000-3000	1.00: 10.70: 2.99: 182.00	144	160	s	AK	
	1.00: 10.70: 2.99: 194.60	144	160	s	AK	
	1.00: 10.70: 2.99: 199.20	144	160	s	AK	
	1.00: 10.70: 2.99: 250.70	144	160	s	AK	
	1.00: 10.70: 2.99: 299.70	144	160	s	AK	
	1.00: 10.70: 2.99: 332.40	144	160	s	AK	
	1.00: 9.72: 2.55: 161.30	144	160	s	AK	
4000-6000	1.00: 9.00: 2.21: 164.60	72	175	s	L	
700	1.00: 20.00: 10.90: 400.00	72	180	s	L	[55]
1100	1.00: 20.00: 10.90: 600.00	72	180	s	L	
1700	1.00: 20.00: 10.90: 800.00	72	180	s	L	
3600	1.00: 20.00: 10.90: 1000.00	72	180	s	L	
6100	1.00: 20.00: 10.90: 1200.00	72	180	s	L	

[a] Crystallization Conditions: d = dynamic, s = static; [b] AO = Aerosil OX-50, AK= Aerosil K-330, L= Ludox HS-40, FS = Fumed silica; [d] $1.00Al_2O_3$:$30.00SiO_2$:$5.400K_2O$:$416.08H_2O$:$5.50Na_2O$; [l] Aluminum source varied for every reference: Ref [53]: $Al(OH)_3$ and Aluminum powder; Ref [55]: $Al(SO_4)_3$ and $Al(OH)_3$.

Table 2.4. Summary of representative hydrothermal synthesis conditions used to attain zeolite L (LTL)

		Crystallization parameters				
Crystal length (nm)	**Starting gel composition Al_2O_3: SiO_2: K_2O: H_2O**	**t (h)**	**T (°C)**	**Cond.[a]**	**Silica source[b]**	**Ref.**
7000	1.00: 20.00: 10.90: 1400.00	72	180	s	L	[55]
7800	1.00: 20.00: 10.20: 1030.00	72	180	s	L	
5900	1.00: 20.00: 10.50: 1030.00	72	180	s	L	
3900	1.00: 20.00: 11.40: 1030.00	72	180	s	L	
3300	1.00: 20.00: 11.90: 1030.00	72	180	s	L	
2200	1.00: 16.00: 10.90: 1030.00	72	180	s	L	
3300	1.00: 18.00: 10.90: 1030.00	72	180	s	L	
4600	1.00: 20.00: 10.90: 1030.00	72	180	s	L	
5200	1.00: 22.00: 10.90: 1030.00	72	180	s	L	
4700	1.00: 24.00: 10.90: 1030.00	72	180	s	L	
1800	0.70: 20.00: 10.90: 1030.00	72	180	s	L	
6500	1.30: 20.00: 10.90: 1030.00	72	180	s	L	
10400	1.70: 20.00: 10.90: 1030.00	72	180	s	L	
4100	1.00: 20.00: 10.90: 1030.00	72	180	s	L	
2700	1.50: 20.00: 10.90: 1030.00	72	180	s	L	
2600	2.00: 20.00: 10.90: 1030.00	72	180	s	L	
1900	2.50: 20.00: 10.90: 1030.00	72	180	s	L	
5200	1.00: 4.50: 2.20: 80.00	72-168	175	s	L	[56]
3700	1.00: 4.50: 2.50: 80.00	72-168	175	s	L	

[a] Crystallization Conditions: d= dynamic, s=static; [b] AO= Aerosil OX-50, AK= Aerosil K-330, L= Ludox HS-40, FS = Fumed silica; [I] Aluminum source varied for every reference: Ref [55]: $Al(SO_4)_3$ and $Al(OH)_3$; Ref [56]: Metallic Aluminum.

Table 2.5. Summary of representative hydrothermal synthesis conditions used to attain zeolite L (LTL)

		Crystallization parameters				
Crystal length (nm)	**Starting gel composition Al_2O_3: SiO_2: K_2O: H_2O**	**t (h)**	**T (°C)**	**Cond.[a]**	**Silica source[b]**	**Ref.**
1300	1.00: 4.50: 2.50: 80.00	72-168	130	s	L	[56]
5200	1.00: 4.55: 2.60: 82.00	72-168	175	s	L	
3000	1.00: 4.55: 2.26: 82.00: 0.65[e]	72-168	175	s	L	
2600	1.00: 4.55: 2.60: 82.00: 0.60[f]	72-168	175	s	L	
-	1.00: 15.00: 10.00: 250.00	72-168	120	s	L	
-	1.00: 15.00: 10.00: 250.00:1.00[g]	72-168	120	s	L	
300	1.00: 15.00: 10.00: 250.00: 2.00[h]	72-168	120	s	L	
-	1.00: 15.00: 10.00: 250.00: 2.00 [i]	72-168	120	s	L	
1500	1.00: 15.00: 10.00: 250.00: 2.00 [j]	72-168	120	s	L	
-	1.00: 30.00: 5.40: 500.00: 5.70[k]	70	170	s	L	[59]
-	1.00: 20.00: 10.00: 400.00	6	170	d	L and LS	

[a] Crystallization Conditions: d= dynamic, s= static; [b] AO= Aerosil OX-50, AK= Aerosil K-330, L= Ludox HS-40, FS = Fumed silica, LS= Ludox LS-30 (nano); [e] $1.00Al_2O_3$: $4.55SiO_2$: $2.26K_2O$: $82.00H_2O$: 0.65KCl; [f] $1.00Al_2O_3$: $4.55SiO_2$: $2.26K_2O$: $82.00H_2O$: 0.60KCl;[g] $1.00Al_2O_3$: $15.00SiO_2$: $10.00K_2O$: $250.00H_2O$:$1.00H_3$tea; [h] $1.00Al_2O_3$: $15.00SiO_2$: $10.00K_2O$: $250.00H_2O$: $2.00H_3$tea; [i] $1.00Al_2O_3$: $15.00SiO_2$: $10.00K_2O$: $250.00H_2O$: $2.00H_2$dea; [j] $1.00Al_2O_3$: $15.00SiO_2$: $10.00K_2O$: $250.00H_2O$:2.00 bis-tris[*]; [k] $1.00Al_2O_3$: $30.00SiO_2$: $5.400K_2O$: $416.08H_2O$: $5.50Na_2O$; [I] Aluminum source varied for every reference: Ref [55]: Metallic Aluminum; Ref [56]: $Al(OH)_3$.; [*]bis-tris: $((HOC_2H_4)_2NC(CH_2OH)_3)$

2.2.2. Crystallization Mechanism of LTL

Atomic Force Microscopy (AFM) has been used to study the crystal growth mechanism of zeolites and to observe any defect in their formation.[2] The surface topography of crystal can be visualized due to the nanometer resolution of AFM technique. The study of the growth mechanism of LTL using AFM was reported by Rhea Brent and Michael W. Anderson[60] in 2008. The synthesis of LTL was based on the preparation method described by Lee *et al.*[55]

In the LTL AFM images, it can be observed from the side-wall face of crystals that the growth is favoured along *c*-direction due to the presence of elongated and narrow-shaped terraces, which can be visualized in Figure 2.7. The formation of the narrow-shape terraces is an indication of the crystal inability to grow in *a*-direction or [100] direction. It was found that the narrowest terraces had a step height of 1.2 nm, while wider terraces had a step height of 1.6 nm. For the terraces with a step height of 1.2 nm, it was suggested that a single cancrinite column is formed and supported on the surface of the crystal, shown in Figure 2.7 a) ii). The wider terraces represent the subsequent addition of cancrinite column, which ultimately forms the 12-memebered pore structure, shown in Figure 2.7 a) iii).

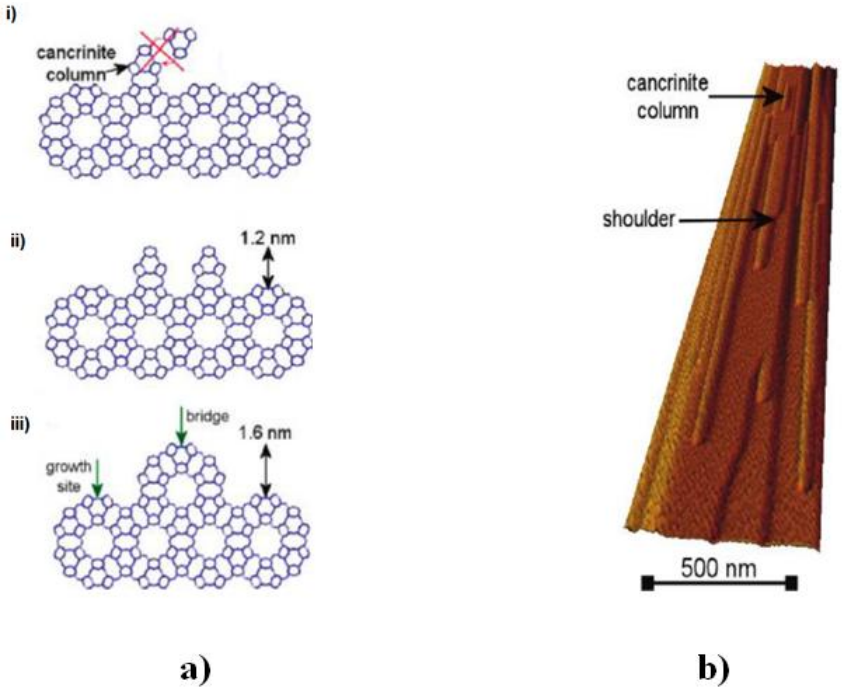

Figure 2.7. a) Proposed arrangement of the cancrinite columns to form LTL structure: i) Individual cancrinite placed on the surface; ii) Subsequent linkage of cancrinite units, showing the step height; iii) Visualization of the cancrinite bridge to form the 12-memebered ring having a step height of 1.6 nm. b) Atomic force micrograph of the side wall face of LTL, showing cancrinite columns and shoulder surface features.[15]

2.3. SOLVOTHERMAL SYNTHESIS

In pursuit of finding new methods to change the morphology, and therefore, the properties of molecular sieves, a new approach for their syntheses was developed. The alternative consists of adding organic solvents to the molecular sieve synthesis gels.[61,2] This type of syntheses using organic solvents is called as the solvothermal synthesis.[2] It is based on the total or partial replacement of water which is usually the principal solvent. The organic solvents that have been applied to synthesize molecular sieves are alcohols, ethylene glycol, diethylene glycol, pyridine, hydrocarbons, among others.[61,19]

The first researchers who successfully used this method were Bibby and Dale[62] in 1985. They obtained sodalite by using ethylene glycol as the solvent in the gel composition. In addition, they reported that the morphology of sodalite was strongly altered by increasing SiO_2/Al_2O_3 ratio. Ruren Xu's group[63] reported the syntheses of silicalite-1, ZSM-39, and ZSM-48 using solvents such as ethylene glycol, glycerol and butyl alcohol, as well as the use of organocations. It was noticed that the balance and selection between organocations and solvents are significant for the formation of crystalline materials.[63] On the other hand, the same group also synthesized different types of aluminophosphastes and gallophosphates from organic systems in the presence of different amine compounds.[64,65] The type of solvents included ethylene glycol, hexanol, and propane-1,3-diol. This solvothermal synthesis approach allowed obtaining larger crystals compared to the crystals obtained by hydrothermal syntheses.[64,65]

Solvothermal syntheses were adopted to form KZSM-48 and CT-5 by Professor Wenyang Xu's group.[66,67] Compared with ZSM-48 synthesized from the hydrothermal synthesis route, the authors reported that a much lower SAR (54) of KZSM-48 was noticed when using triethylene amine ($(C_2H_5)_3N$) as the solvent and hexaethylenediamine as the template. Later, the author reported the formation of CT-5 when applying methanol as the solvent and pentaerythritol as the template. In addition, the author showed the morphology of CT-5 is a rod-shape, instead of the needle-shape crystals prepared from the hydrothermal synthesis route.

In 1993, Kuperman *et al*[68] synthesized different types of molecular sieves in the presence of fluoride ions. This became a new synthesis approach that would allow the crystallization and the tuning of crystal sizes. They reported the synthesis of Dodecasil-3C, FER and silicalite-1 with sizes around 0.4-5.0 nm. Subsequently, several researchers have been applying the solvothermal synthesis in

combination with the use of fluoride ions.[69] Frequent materials synthesized from this approach are ferrierite (FER) and sodalite (SOD).[70] For instance, the crystal sizes for FER can vary from 100 μm[71] 600 μm.[72] Moreover, it was observed that heteroatoms (Al, B) were incorporated in the synthesis gel composition from Reddy Marthala *et al*[72] studies. The combination of solvothermal synthesis, fluoride media and incorporation of heteroatoms made possible to attain larger crystals in comparison with the crystals attained by only using solvothermal synthesis. Similar approaches were adopted to study the crystallization of SOD by Yang *et al*.[70] An enhancement of crystal size was also observed.

In 2009, Chen *et al*[73] investigated the effect of co-solvents on the crystallization of Si-MFI crystals using ethylene glycol (EG), diethylene glycol (DEG), and triethylene glycol (TEG). The solvothermal synthesis was implemented with the assistance of microwave heating. The results from their experiments indicated a relationship between the co-solvent identity and their molar concentration in the gel precursor. For instance, when using EG at molar concentrations of 6, 7, 8 and 9, the lengths of the crystals were 0.56, 1.05, 1.03, and 1.33 μm, respectively. When using TEG at the corresponding concentrations, the attained crystals sizes were about 1.04, 1.19, 1.29, 1.32 μm. However, the crystals attained the largest size when DEG was utilized as the co-solvent. The content of water and the interaction of DEG with water may be attributed to the unexpected large crystal size. For instance, when the molar concentration of DEG was kept at 7, and the water content was increased from 21.55 to 45.5 moles the crystal sizes of Si-MFI were decreased from 1.23 to 0.46 μm.

Chen *et al*[74] also investigated the relationship between the dielectric constant (ε) of co-solvents and the morphology of Si-MFI. The solvothermal synthesis was carried out using microwave heating, instead of the conventional oven heating. The main solvent used was isopropanol (^{i}PrOH) and the secondary solvent was EG or *n*-butanol (BuOH). The molar ratio of secondary solvent/^{i}PrOH was varied while keeping the content of (EG + secondary solvent) the same. When the molar ratio of EG/^{i}PrOH was increased from 0/8 (ε = 38.5) to 2/6 (ε = 41.0), the morphology of Si-MFI crystals comprised stacked crystals, with an average length of 1.95, 1.57, and 1.20 μm, respectively. Further increase the ratio from 3/5 (ε = 42.3) to 4/4 (ε = 43.6) lead to the co-existence of stacked and isolated crystals, with an average length of 0.93 and 0.64 μm. As the ratio was greater than 5, isolated crystals were formed. The average length was not measured for the former crystals because the calculation of the average length was based solely on the measurement of self-stacked Si-MFI crystals.

On the other hand, when BuOH was used, the dielectric constant changed from 38.5 (BuOH/^{i}PrOH = 0/8) to 36.4 (BuOH/^{i}PrOH = 8/0). The morphology attained for all the experiments were stacked crystals. No clear correlation could be observed between the average length and the dielectric constant when BuOH was used as the secondary solvent. However, the use of BuOH allowed attaining larger crystals compared to the crystals attained by using EG. The smallest average length attained for the Si-MFI crystals was 1.79 μm while the largest one was 2.73 μm.

It has been observed that the selection of one of these organic solvents over the others only depends on the success to obtain zeolite crystals. In other words, choosing an organic solvent is similar to a trial-and-error method. The difficulty in the solvent selection is originated from the complexity of the organic solvent interactions in the synthesis gel and the lack of adequate equipment that can register the experiment *in situ* at mild temperatures (120-250 °C) and the autogenous pressures.[61,75]

In terms of the dielectric constant of organic solvents, Morris and Weigel[19] attempted to classify the organic solvents in four categories depending on the affinity to form hydrogen bonds: high, high-medium, low-medium and non-hydrogen-bonding. Table 2.6 shows a summary of the classification. Based on their definitions, they hypothesized that the most suitable solvents are the ones that form high-medium and low medium hydrogen bonds due to their moderate interactions with active species in the synthesis gel. Thus, these moderate interactions between solvent molecules and active species in the synthesis gel facilitate the nucleation step and, therefore, lead to the crystallization of zeolites.

Table 2.6. Classification of the formation of hydrogen bond for an organic molecule[19]

Formation of Hydrogen bonds	**Interaction with other species**
High	Prevent interaction and nucleation
High-medium	Allows interaction among the species
Low-medium	Allows interaction among the species
Non-hydrogen bonding	Not enough linking (association) among species causing no crystallization

Table 2.7 shows a summary of the authors; types of solvents and molecular sieves obtained using the solvothermal synthesis approach. To the best of my knowledge from an extensive literature survey conducted. To the best of our knowledge, the tuning of the shape and size of LTL crystals by applying organic compounds or co-solvents is the subject of only a few works.[14,15]

Table 2.7. Summary of zeolites formed from solvothermal synthesis

Molecular Sieve	Solvent	Molar Gel composition	Temperature (ºC)	Duration (days)	Ref
Sodalite	Ethylene glycol (EG)	2 SiO_2: 3NaOH: 40EG	150	15-25	[51]
Silicalite-1	Ethylene glycol (EG)	1.50NaOH: 2.00SiO_2: 40.00EG: 0.30TPABr	180	25	
ZSM-39	Glycerol (GE)	(1.00-10.00)$PrNH_2$: (2.00-6.00)NaOH: (10.00-20.00)GE	150-180	30-70	[52]
ZSM-48	Ethylene glycol (EG) and Butyl alcohol (BuOH)	1.00NaOH: 2.00 SiO_2: 20.00EG: 12.00BuOH: 0.10TMABr	180	25	
$AlPO_4$-5	Propane-1,3-diol (PG)	1.00Al_2O_3: 1.80P_2O_5: 45.00PG: 5.90 Et_3N	180	20	
$AlPO_4$-5	Ethylene Glycol (EG)	1.00 Al_2O_3: 2.50P_2O_5: 60.00EG: 9.80Et_3N	180	30	[59]
$AlPO_4$-11	Ethylene Glycol (EG)	1.00 Al_2O_3: 1.80P_2O_5: 45.00EG: 2.40Bu_2NH	180	30	
$AlPO_4$-21	Ethylene Glycol (EG)	1.00 Al_2O_3: 1.80P_2O_5: 45.00EG: 2.40Bu_2NH	180	30	
KZSM-48	Triethylamine $(C_2H_5)_3N$)	1.0 Al_2O_3:(4.5-5.5)K_2O: (26-16)$H_2N(CH_2)_6NH_2$:(50-600)SiO_2: (100-800)$(C_2H_5)_3N$	180-200	1-4	[61]
CT-5	Methanol (CH_3OH)	1.0 Al_2O_3: (8-25)$C(CH_2OH)_4$: (2-20)Na_2SO_4: (8-16)Na_2O:(60-200)SiO_2: (60-500)CH_3OH	150-200	5-16	[63]
Dodecasil-3C	Pyridine (Py)	1.50SiO_2: 2.00HF/Py: 6.00H_2O: 16.00Py	200	7	
Ferrierite (FER)	Pyridine (Py)	1.50SiO_2: 2.00HF/Py: 8.00H_2O: 4.00$PrNH_2$: 16.00Py	180	7	[55]
Silicalite-1	Triethlyamine (Et_3H)	2.00SiO_2: 2.00HF/Et_3N: 6.00H_2O: 2.00PNH_2: 0.5TPABr:12.00Et_3H	180	12	
Ferrierite (FER)	Pyridine (Py)	1.50SiO_2: 8.40H_2O: 1.40HF: 0.60n-C_3H_9N: 16.00 Py	180	5	
Ferrierite (FER)		1.50SiO_2: 8.00H_2O: 2.00HF: 4.00n-$C_5H_{13}N$: 16.00 Py	180	45	[58]
Ferrierite (FER)		1.50SiO_2: 8.40H_2O: 2.00HF: 0.60n-$C_4H_{11}N$: 16.00 Py	180	20	
Sodalite	Ethylene Glycol (EG)	1.00 SiO_2: 1.50NaOH: 20.00EG: 0.00 H_2O: 0.00NH_4F	180	28	
		1.00 SiO_2: 1.50NaOH: 20.00EG: 0.20 H_2O: 0.00NH_4F	180	21	[57]
		1.00 SiO_2: 1.50NaOH: 20.00EG: 25.00 H_2O: 0.00NH_4F	180	1	
Ferrierite (FER)	Pyridine (Py)	1.50SiO_2: 8.00H_2O: 2.00HF: 4.00n-$C_3H_7NH_2$:16.00 Py	180	12	
Ferrierite (FER)	Pyridine (Py)	1.50SiO_2: 8.00H_2O: 2.00HF: 4.00n-$C_4H_9NH_2$:16.00 Py	180	20	[59]
Ferrierite (FER)	Pyridine (Py)	1.50SiO_2: 8.00H_2O: 2.00HF: 4.00n-$C_{20}H_{11}NH_2$:16.00 Py	180	45	

Abbreviations for reagents: TPABr: Tetrapropylammonium bromide; TMABr: Tetramethylammonium bromide; Et_3N: Triethylamine; P_2O_5: Phosphoric acid; $H_2N(CH_2)_6NH_2$: Hexane-1,6-diamine; $C(CH_2OH)_4$: pentaerythritol; HF: Hydrofluric Acid;

2.4. APPLICATIONS OF LTL

The potential applications of LTL can be divided into two main areas: use of LTL as catalysts and host-guest materials for antenna receptors**.**

2.4.1. LTL as Catalysts

Treacy[13] reported the performance of Platinum (Pt) particles on K-LTL (KL) support. The results established a strong correlation between the morphology of LTL and the Pt dispersion. It was concluded that the use of short channels would allowed to have high catalytic activity, the reduction of the deactivation rate of Pt/KL system, and the decrease of blockages due to the formation of Pt clusters in the LTL channels.

Trakarnroek *et al*[9] investigated the effect of varying the morphology and the channel effect of Pt clusters supported on LTL for the aromatization of *n*-octane. Their results suggested that better catalytic performances for the reaction of *n*-octane would be achieved if the crystals have a low aspect ratio (i.e. length/diameter). Most importantly the morphology of LTL crystals could resemble a coin like shape. This would be preferable because it could shorten the diffusion path of the reactant when they would come in contact with Pt clusters. In other words, the yield of desired products would be achieved without reactants being transformed into undesired products or secondary reactions.

Fukunaga *et al*[76] studied the aromatization of C_6 paraffin to benzene using halogen-modified Pt/KL catalyst. Their results were compared with those using conventional Pt/KL and Pt/Al_2O_3 catalysts. It was observed that the modified catalyst achieved higher yield, high selectivity and a longer catalyst lifetime. On the other hand, Huo *et al*[35] reported the synthesis of mesoporous LTL which was applied in the reduction of sulphur content in hydro-desulfurization (HDS) of FCC unit. Their results showed a satisfactory desulfurization when compared to the values attained using conventional LTL and a mesoporous metallosilicate, Al-MSU-2.

2.4.2. LTL as Host Materials

There has been a considerable interest in developing artificial antenna systems that can absorb and transfer solar energy for useful chemical energy. One of the strategies is based on use LTL crystals

as the host material, where their one dimensional pores are filled with electronically non-interacting dye molecules.[42] The principle is based on the study of natural photosynthesis, where the chlorophyll molecules absorb and transport solar energy which is subsequently used to convert carbon dioxide into organic compounds.

It has been observed that the successful implementation of the antenna system is correlated to the size and the shape of LTL crystals.[38,77] A crystal with a short length along *c*-direction would allow a fast transfer of the energy to the dye molecules and would avoid the transformation of the energy into other processes before it is collected. The challenges observed in this system are the synthesis of oriented layers of LTL crystals, and the transfer of energy to the energy storage, which can be a semiconductor. Figure 2.8 illustrates a prototype of an antenna sensitized solar cell using the one dimensional pores of LTL crystals as the host material. The blue and green dyes represent donor molecules that absorb the light and transport the electronic excitation energy to the red dye. This acts as the acceptor molecule. The red dye is intercepted by a grey die which is fixed at the end of the LTL channel to transfer the energy to the semiconductor. The different dyes are used to ensure directional energy transfer.[78,79]

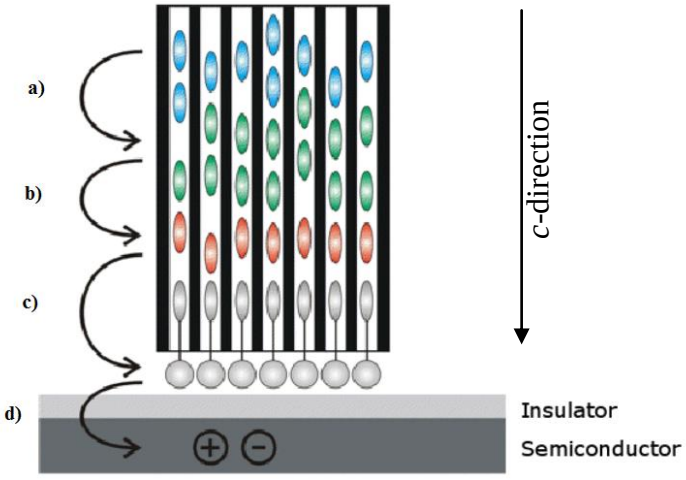

Figure 2.8. Antenna sensitized solar cell. The energy is transferred from point a) to point d).[42,79]

2.5. ISOMORPHOUS SUBSTITUTION IN ZEOLITES

Zeolites are formed by tetrahedra of Si^{4+} and Al^{3+}. Though, it is possible to substitute them by other types of elements (e.g., B^{3+}, Ge^{4+}, Fe^{3+}), which share similar ion radii and coordination. This replacement of heteroatoms in zeolite frameworks is known as isomorphous substitution.[2,61] The

isomorphous substitution results in a contraction or expansion of the cell dimensions and shifts in the lattice vibration.[61]

Moreover, the incorporation of different heteroatoms may change the acidity of the framework structure. For instance, divalent ions (e.g., Zn^{2+}, Be^{2+})[2] creates two negative charges in the framework, while trivalent ions (e.g. Ga^{3+}, Fe^{3+})[80,81] lead to one negative charge which may change Brønsted acid sites. On the other hand, the substitution of tetravalent ions (e.g. Ge^{4+})[82] maintains the charge acidity of the zeolite framework. Figure 2.9 illustrates a general schematic molecular model of a zeolite framework where Si^{4+} is isomorphously substituted by Ge^{4+}.

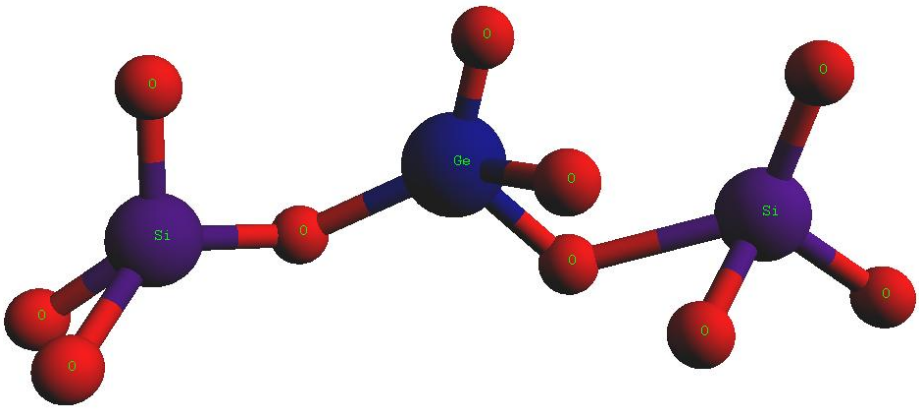

Figure 2.9. Schematic molecular representation of the T-O-T bonds (where T= Si or Ge) formed between tetrahedral. The molecular representation was constructed using ArgusLab software.

The connection of oxygen atoms among the different heteroatoms, shown in Figure 2.9 permits the formation of the pores and cavities of different zeolites species. This bond known as T-O-T (where, T = Si or Ge) possesses an angle between 140–165°. The angle of this bond is reasonably flexible when compared to the O-T-O bond angle (i.e., 109°) formed by the tetrahedra.[22] The deflection of the T-O-T angle is essential for the formation of the different zeolite frameworks. Additionally, the distance between the T-O bonds is varied depending on atom pairs. Table 2.8 illustrates different bonds lengths of various atomic pairs.[22] The present study focuses on the isomorphous substitution of Ge^{4+} in zeolites. Thus, the following information will center on this element. However, an extensive review on different heteroatoms substitutions is presented by Nagy *et al*.[83]

There are two main motivations for substituting Ge into zeolite structures. The first motivation emerges from the need to adjust their properties (i.e., redox catalytic properties, shape selectivity) towards targeted applications.[17,84-87] The second motivation is based on the use of Ge atoms to discover

novel zeolitic frameworks.[88] For instance, Corma's lab[89] discovered that the substitution of Ge in zeolite syntheses is indispensable towards the formation of a new type of zeolite framework referred as ITQ (i.e., ITQ-13, ITQ-22, ITQ-24), which otherwise are impossible to attain.

Table 2.8. Bond Length of Different Atomic Pairs[22]

Atomic Pair	Bond Length d (T-O), Å
Si-O	1.58-1.64
Al-O	1.70-1.73
B-O	1.44-1.52
P-O	1.52
Be-O	1.58
Li-O	1.96
Ge-O	1.73-1.76
Ga-O	1.84-1.92
Zn-O	1.95

From the studies conducted in ITQ-series zeolites, it has been observed that germanium increases the average T-O bond distance and decreases the T-O-T angle (where T = Ge or Si).[90] Thus, the double four-membered rings (D4Rs) of these zeolites are stabilized. Additionally, studies[91] have reported that Ge atoms are situated in the D4Rs. Similar results have been found in other types of zeolites possessing D4Rs in their framework when Si is substituted by Ge, such as zeolite Beta, zeolite A.[92,93]

Li *et al*[94] investigated the thermochemistry of $(Ge_xSi_{1-x})O_2$ in ITQ-7, polymorph c and zeolite Beta to observe the relationship between the germanium content and the framework stability. Their results showed that zeolite Beta is only stable when low germanium content is used while ITQ-7 is stable at a moderate content of Ge atoms and polymorph c showed the highest uptake of germanium to hold its stability.

More interestingly, the isomorphous substitution of Si by Ge atoms has also been conducted in zeolites that do not possess D4R units. MFI[95], FAU[88] and SOD[70,96] framework structures have been utilized to observe the effect of germanium substitution. Thus, the following review on the synthesis of germanium-containing zeolites will focus on two different types of zeolites: zeolites not possessing D4R units in their framework and zeolites possessing D4R units.

2.5.1. Ge-ZSM-5 Zeolites

ZSM-5 exhibits a MFI structure in which consists of aluminum and silicon atoms. SEM analyses show that ZSM-5 crystals possesses a twinned hexagonal-like or coffin shape[97]. It is known that Silicalite-1 demonstrates analogous MFI structure without including any Al atom in its framework.[82] A number of studies have been reported for the germanium substitution in the ZSM-5 and Silicalite-1.[21,95,98]

In 1989, Gabelica *et al*[99] reported the Ge incorporation in MFI framework. In their study, a precursor solution was prepared in fluoride media using MFI seeds and tetrapropylammonium (Pr_4N^+) as the structure directing agent. The hydrothermal synthesis was carried out at 180 °C for 15 hours. The Ge source was germanium chloride ($GeCl_4$). PXRD analyses showed an orthorhombic phase for the zeolite. However, after the samples were cooled down, the phase shifted to a monoclinic phase. Furthermore, Gabelica *et al* observed a direct relation between the incorporation of Ge atoms and the media (e.g basic or acidic) of the precursor solution. At a basic media, germanates was formed, which restricts Ge incorporation into the MFI framework. According to the authors' study, the precipitation may be avoided using short chains of alkyl amines to decrease the pH to 10, as well as the use of fluoride ions which may assist to reduce the effect of OH ions in the reaction media.

Kosslick and Fricke[100] investigated the germanium substitution of ZSM-5 framework by changing the Si/Ge ratio in the starting gel from 11, 4 and 3/2. The Ge-ZSM-5 samples were synthesized for 18 hours at 443 K using germanium chloride ($GeCl_4$), hydrofluoric acid (HF) and tetrapropylammonium ions as the organic structure directing agent. The resulting samples were characterized using XRD, SEM, Magic Angle Spinning Nuclear Magnetic Resonance (MAS-NMR), IR, Raman spectroscopy and n-hexane adsorption. A high crystallinity was observed from the XRD analyses of the first two samples. However, it was observed that the sample with a Si/Ge ratio of 3/2 presented traces of alpha-quartz and a decrease in the crystallinity, compared to the other two samples. The morphology of the samples was significantly varied when the Ge content was increased.

The increase of Ge content in the solution led to a change of zeolite crystal morphology from a hexagonal-like thin twinned shape (pellet) to spherical crystals. Based on analyses using various characterization techniques, such as MAS-NMR, IR and Raman spectroscopy, it was found that the Ge-ZSM-5 framework is mainly composed of Si-O-Si and Si-O-Ge connections. The angles in the former bridge were less affected by the incorporation of Ge; whereas the results suggested that the oxygen

bridging angle of Si-O-Ge connections were affected in order to allow the incorporation of Ge atoms. The Ge-O-Ge bridges were not observed in any of the applied techniques applied.

Tuan *et al*[101] studied the substitution of Al, Fe, B and Ge in ZSM-5, with the aim to improve the separation performance of MFI-type membranes. The precursor solution was in alkali-free form. Silica (Ludox® AS-40), a template (TPAOH), water and germanium ethoxide ($Ge(C_2H_5O)_4$) sources were utilized to prepare Ge-ZSM-5. The initial Si/Ge ratio was maintained at 100. The chemical analysis showed a Si/Ge = 220, indicating the low incorporation of Ge in the zeolite framework. The gas separation performances of isomorphous substituted membranes were tested against a silicalite-1 membrane using n -C_4H_{10}/H_2 mixtures. It was found that the separation selectivity strongly depended on the substituted cations. At room temperature, the selectivity increased in the following order: Fe< silicalite-1~Ge<Al< B-ZSM-5. Thus, it was demonstrated the efficacy of the isomorphous substitution in ZSM-5 membranes.

Maschmeyer's lab[95] developed different synthesis approaches in order to incorporate multiple heteroatoms (i.e, Ge and Al) in ZSM-5 simultaneously. These were formulated to understand how the Ge and Al contents, the nature of Al and Ge sources, the amount of water and the pH were affecting the isomorphous substitution in ZSM-5. The hydrothermal syntheses (i.e., 170 °C for 4 days) were conducted in 6 x 4 matrix blocks of small 3 mL Teflon-lined stainless steel autoclave (SSA). Two of the three synthesis approaches utilized fluoride media while the other one was only composed of the Si (Ludox® HS-40), Ge (GeO_2 source), Al (Al_2O_3 source) and a template source (TPAOH). In the latter synthesis approach, the results showed a decreased in the crystallinity as well as the appearance of additional phases (GeO_2) while Ge content was increased. Moreover, elemental analyses showed that no Al was incorporated and Ge was partially incorporated in the zeolite framework.

For the synthesis approaches using fluoride media, different sources for Ge and Al were evaluated. The synthesis approach, using Na metagermanate as the Ge source, and $NaAlO_2$ as the Al source, showed a decreased in the crystallinity of the zeolite framework and the appearance of additional phases while increasing the Ge content. Moreover, the incorporation of both heteroatoms in the framework was successful. The last synthesis approach, using $GeCl_4$, $NaAlO_2$ for the corresponding Ge and Al sources, lead to the successful isomorphous substitution of both Ge and Al atoms in ZSM-5. The crystallinity did not decrease as the Ge content increased. Furthermore, the formation of additional phases was not observed in this synthesis approach. Based on these results, it is noticed that the

successful substitution is greatly linked to the initial sources and conditions utilized in the precursor solution.

The last synthesis approach was selected to carry out studies in a larger scale (i.e., 40 ml Teflon-lined SSA). Six experiments were conducted. The Ge/(Ge+Si) was varied from 0-0.25 and the (Ge+Si)/Al was kept constant to 29.5. The results showed that Ge content was increased while the Ge/(Ge+Si) ratio increased. However, this increment of Ge and Al content in the zeolites was lower than expected. For instance, when the ratio of Ge/(Ge+Si) in the precursor solution was set as 0.05, the final ratios of Ge/(Ge+Si) and (Ge+Si)/Al in the final product became 0.03 and 53, respectively. The morphology of the Ge,Al-ZSM-5 crystals varied from elongated single crystals to a spherical aggregates while the Ge content was increased. Using FTIR technique, the authors confirmed Ge incorporation in the zeolite framework. Moreover, PXRD and nitrogen physisorption analyses showed that the Ge incorporation leads to changes in the transition phase from monoclinic to orthorhombic, the expansion of the unit cell, the increment of the surface area and the generation of mesopores and macropores.

One year later, Maschmeyer's lab[17] reported a catalytic study of Ge-ZSM-5 and Ge-Silicalite-1 on the dehydration reaction of 2-propanol. A number of Ge- substituted zeolites were synthesized in order to assess the effect of Ge content on that reaction. The Al content was kept to a ratio of 29.5.[95] Their results showed that, the final content (Ge/(Ge+Si) = 0.04) becomes closer to that of the mixture when a lower Ge content was added to the initial mixture (Ge/(Ge+Si) = 0.05). However, a higher increase of Ge content in the initial mixture (Ge/(Ge+Si) = 0.20) lead to a remarkably low incorporation (Ge/(Ge+Si) = 0.09) in the final zeolite framework. Moreover, it was observed that Al incorporation was enhanced as Ge content increased, which is consistent with previous reports.[95]

On the other hand, the Ge-Silicalite-1 zeolites presented a better incorporation of Ge atoms when compared to Ge-ZSM-5. For instance, at an initial Ge/(Ge+Si) ratio of 0.05 in the zeolite precursor solution, the ratio of the final product remained the same. In terms of their catalytic performance, it was observed that deactivation rate appeared in a much lower extent on Ge-ZSM-5 than ZSM-5. This may be due to the formation of mesopores in Ge-ZSM-5.

In 2006, Cheng *et al*[102] reported the effect of the Ge content and the type of Ge source (i.e Germanium oxide (GeO_2) and germanium ethoxide ($Ge(OC_2H_5)_4$) in the growth rate of Ge-Silicalite-1.

The synthesis of Ge-Silicalite-1 was conducted in alkaline media at 368 K during 7 days. The Si/Ge ratio in the precursor solution was varied from 100, 50, 25 and 15. It is worthwhile to comment that this study used a low Ge content (i.e, 0.0251 g for Si/Ge=100). Due to the low amount of Ge used, the resulting samples did not present a morphological change. Moreover, the PXRD patterns showed that the Ge-Silicalite-1 only present an orthorhombic phase. The particle size of Ge-Silicalite-1 slightly increased as the Si/Ge was increased regardless of the Ge sources.

The resulting samples were analyzed using XRF. This showed that not all Ge was incorporated into the framework. Additionally, XRF shows that the amount incorporated in the zeolite framework greatly varied depending on the Ge source used. For instance, when the precursor solution was synthesized using GeO_2, with an initial ratio of Si/Ge equal to 25, the XRF result of the final product showed a Si/Ge_{xrf} ratio of 47. On the other hand, when $Ge(OC_2H_5)_4$ was used in the precursor solution with an initial ratio of Si/Ge equal to 25, the XRF result of the final product showed a Si/Ge_{xrf} ratio of 83. The effect of the growth rate in Ge-silicalite-1 was analyzed using in situ small-angle X-ray scattering (SAXS). It was found that the growth rate of Ge-silicalite-1 was enhanced when compared to the growth rate of pure silicalite-1. Based on this result, the authors suggest that Ge acts as a promoter to increase the growth rate of the zeolite. ^{29}Si solution NMR was also conducted to analyze if the low incorporation of Ge into the zeolite framework was due to a change in the speciation of the mixture. However, this analysis did not show any significant shifting variations when the spectrum was compared to a pure silica solution.

Cheng *et al* expanded their previous work,[102] based on the study of Ge-Silicalite-1, to study the effect of Al and Ge incorporation in Silicalite-1.[98] Germanium oxide (GeO_2), aluminum triethoxide ($Al(OC_2H_5)_3$), a template (TPAOH), silica and water sources were used to synthesize Ge,Al-Silicalite-1. The hydrothermal synthesis was carried out for 7 days at 368 K. The Si/(Al+Ge) ratio was varied from 100, 75, 50 to 25. For each Si/(Al+Ge) the Ge/Al ratio was varied from 1 to 4. PXRD, XRF, nitrogen adsorption and SAXS were used to characterize the resulting samples. PXRD analyses showed that differences were only observable when the heteroatom content was increased. For instance, for a Si/(Al+Ge) equal to 50 and 25, the resulting peaks were broaden according to PXRD. Moreover, an increase of Al content lead to a decrease in crystallinity. The use of FTIR and nitrogen adsorption confirmed the results observed in PXRD analyses.

XRF showed Ge incorporation was enhanced with the presence of Al. Moreover, at a higher Ge/Al and Si/(Al+Ge) ratios, the Ge/Si ratios became closer to that of the initial mixture. For instance, with an initial ratio of Si/(Al+Ge) equal to 50, a ratio of Ge/Al equal to 4 and a ratio of Si/Ge equal to 0.0165 led to a final Si/Ge ratio of 0.0111, when compared to a Si/(Al+Ge) ratio of 50, Ge/Al ratio of 1 and Si/Ge ratio of 0.103, yielding a final Si/Ge ratio of 0.0112. Similar results were observed when the maximum Ge incorporation (Si/(Al+Ge) = 25) was implemented in this study. Based on these results, the authors identify that the presence of Al increases the uptake of Ge in the Ge,Al-ZSM-5 framework. Based on SAXS analyses, it was found that Al in the precursor solution decreases the growth rate of silicalite-1 while the presence of Ge increases the growth rate.

Shantz's group reported the synthesis and characterization of Ge-ZSM-5 in alkaline media.[97] The alkaline media was incorporated into the precursor solution in order to mimic the conditions that may be encountered, if the syntheses are conducted at an industrial scale. Three different zeolites (i.e., Ge-ZSM-5, Ge-Silicalite-1, and ZSM-5) were synthesized via hydrothermal synthesis under rotary conditions at 160 °C for 3 days. Germanium oxide (GeO_2), a template (TPAOH), Silica (Ludox® AS-40), sodium aluminate ($NaAlO_2$) and sodium hydroxide (NaOH) were used to synthesize Ge-ZSM-5 and ZSM-5. Silicalite-1 was synthesized without the addition of $NaAlO_2$. The three different zeolites were also synthesized using glacial acetic acid in order to adjust the pH of the precursor solution. To test the incorporation of germanium in the ZSM-5 framework, the Si/Ge ratio was varied from 10, 25 and 50. For each Si/Ge ratio, the Si/Al ratio was varied by 10, 25, 50 and 100. In the case of Ge-Silicalite-1, only the Si/Ge ratio was varied. After syntheses, the resulting materials were ion exchanged in order to have zeolites in a pure Na-exchanged form.

The resulting samples were characterized via PXRD, SEM, nitrogen adsorption, XRF and X-ray photoelectron spectroscopy (XPS), among others. PXRD analyses indicated that the materials possessed a monoclinic phase. The diffractograms of the different resulting materials did not show any amorphous or crystallinity impurity. Based on SEM analyses, the morphology of the crystals was not varied. However, the decrease in acidity of the solution led to form larger crystals. Moreover, some of the crystals presented small particles on their surface. The small particles were not observed after the resulting samples were ion exchanged. Nitrogen adsorption analyses were conducted to two different Ge-ZSM-5 (Si/Ge = 10, Si/Ge = 50) samples. Results showed a significant reduction in the accessibility of the micropore volume before ion exchange. This led the authors speculate that there was a formation of a layer in the surface of the crystals, which may be of Ge nature.

XRF and XPS analyses were conducted to study the bulk and surface composition of the Ge content of the zeolite crystals. XRF showed, for the ion-exchanged samples, that the extent of Ge incorporation increased when using higher Si/Ge ratios. The incorporation was also enhanced using higher Si/Al ratios. XPS analyses confirmed the surface enrichment by Ge, consistent with the results analyzed by the nitrogen adsorption as well as SEM images. Moreover, XPS showed that there is reduction of Al content near the surface.

2.5.2. ITQ-7 Zeolites

Corma's lab successfully synthesized a large-pore tridimensional zeolite composed exclusively of silica, named ITQ-7(Instituto de Tecnología Química). In order to employ ITQ-7 as catalyst, it is required to change the framework acidity. According to the authors, the direct incorporation of Al atoms into ITQ-7 inhibited the growth and crystallization of ITQ-7 crystals, yielding only amorphous materials. Thus, one of the approaches developed by Corma's lab was the use of Ge and B atoms in order to facilitate the incorporation of Al atoms in ITQ-7.[103] For the case of the isomorphous substitution of Si by Ge, Ge-ITQ-7 and Al-Ge-ITQ-7 were synthesized and compared with pure silica ITQ-7. The hydrothermal synthesis was conducted under static conditions at 423 K for 7 days. The precursor solution was prepared in fluoride media. A silica source, TEOS, Ge source, 1,3,3-trimethyl-6-azonium-tricyclo[3.2.1.$4^{6,6}$]dodecane hydroxide ($C_{14}H_{26}NOH$) as a SDA and water source were used to synthesize the different zeolites.

PXRD analyses were conducted to pure silica ITQ-7, Ge-ITQ-7 and Al-Ge-ITQ-7 samples. None of the patterns showed presence of amorphous materials. Moreover, it was observed that the intensity of the peaks increased in the following order: Al-Ge-ITQ-7<Ge-ITQ-7<pure silica ITQ-7. SEM analyses were only reported for pure silica ITQ-7 and Ge-ITQ-7. SEM showed that the crystal size was greatly reduced when Ge was substituted in the framework as compared to the pure silica ITQ-7 crystals. The catalytic cracking of *n*-hexane was applied for B-Al-ITQ-7, Al-Ge-ITQ-7 and compared to zeolite Beta. The acidity of the framework was assessed. It was found that the conversion increased in the following order: Al-Ge-ITQ-7<B-Al-ITQ-7<Beta. The different analyses utilized by the authors showed that Ge can be incorporated into the ITQ-7 framework without inhibiting the material crystallinity. Moreover, Ge incorporation permits the incorporation of Al atoms, allowing modifying the acidity of the framework.

In a similar study, Corma's lab also attempted to introduce Ti atoms in ITQ-7. However the Ti-ITQ-7 zeolites presented a low Ti incorporation as well as affecting the zeolite growth. In order to facilitate the incorporation of Ti atoms in ITQ-7, the authors decided to use Ge atoms in the precursor solution.[104] Pure silica ITQ-7 and Ti-Ge-ITQ-7 were synthesized via hydrothermal synthesis under static conditions at 150 °C. The precursor solution was prepared in fluoride media. A silica source, TEOS, Ge source, 1,3,3-trimethyl-6-azonium-tricyclo[3.2.1.$4^{6,6}$]dodecane hydroxide ($C_{14}H_{26}NOH$ or SDA) and water source were used to synthesize the different zeolites.

PXRD analyses were conducted to a pure silica ITQ-7 and to the Ti-Ge-ITQ-7 zeolites. The latter zeolite presented peak shifting to higher *d*-values when compared with the pure silica ITQ-7 sample. This phenomenon also indicated an expansion of the unit cell volume due to the Ge incorporation in ITQ-7. Moreover, upon Ge incorporation, the synthesis time was severely decreased when compared to pure silica ITQ-7. A crystalline material was attained only after 12 hours. It was also noted that the incorporation of Ti was enhanced due to the presence of Ge. The resulting Ti-Ge-ITQ-7 samples presented a smaller crystal size (< 1 μm) when compared to the size of pure silica ITQ-7 zeolites (1-2 μm). The authors speculated that this reduction in crystal size may be to the presence of larger number of nuclei generated by Ge.

In 2002, Corma's lab conducted a thorough study to comprehend the effect and role of Ge atoms in the ITQ-7 framework.[90] Pure silica ITQ-7 and Ge-ITQ-7 were synthesized using hydrothermal synthesis under static conditions at 150 °C. The precursor solution was prepared in fluoride media. A silica source, TEOS, Ge source, 1,3,3-trimethyl-6-azonium-tricyclo[3.2.1.$4^{6,6}$]dodecane hydroxide ($C_{14}H_{26}NOH$ or SDA) and water source were used to synthesize the different zeolites. It is noteworthy to mention that the isomorphous substitution of Si by Ge in ITQ-7 allowed decreasing the synthesis duration from 7 days to less than 12 hours when a Si/Ge = 5 was used. An increase in the Si/Ge ratio led to a slight increase in the synthesis duration.

PXRD analyses were carried out to pure silica ITQ-7 and Ge-ITQ-7 zeolites, to observe any differences among the materials. Both patterns showed the attainment of high crystalline materials. Moreover, amorphous or impurities materials were not observed in any of the PXRD patterns. However, the broadening of the peak width was observed in the PXRD pattern of Ge-ITQ-7. The authors assumed that the broadening was attributed to the presence of smaller crystal size when

compared with the crystal size of pure silica ITQ-7. SEM images confirmed their assumptions, shown in Figure 2.10.

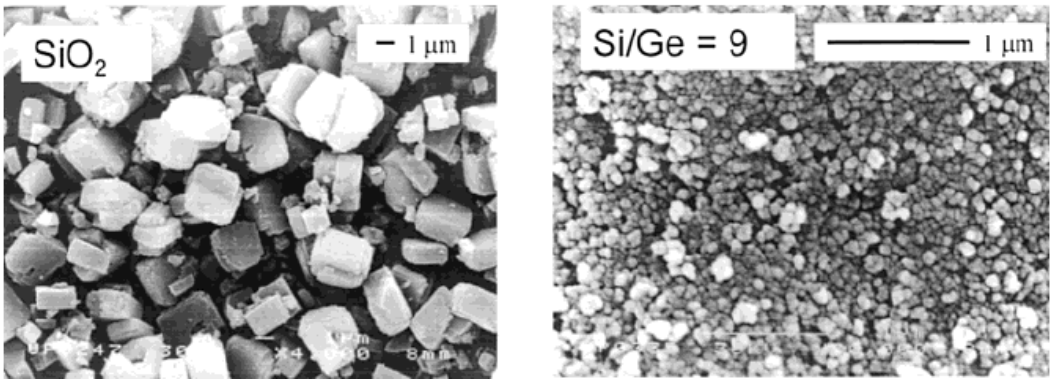

Figure 2.10. SEM images of pure silica ITQ-7 (left) and Ge-ITQ-7 (right)[90]

Nitrogen adsorption was also implemented to observe the differences between pure silica ITQ-7 and Ge-ITQ-7. From this analysis, it was found that Ge-ITQ-7 presented a large surface area (651 m^2/g) when compare with the pure silica ITQ-7 (543 m^2/g). FTIR spectra analyses were conducted to study the Ge-ITQ-7 framework. This technique allowed examining the presence of Si-O-Ge and Ge-O-Ge in the ITQ-7 framework. Using ^{19}F and ^{29}Si MAS-NMR the authors inferred that the incorporation of Ge into the ITQ-7 framework may be located in the D4Rs. The authors proposed that the crystallization rate in ITQ-7 was enhanced due to this preference of Ge in D4Rs.

In 2005, Leiva *et al*[105] presented a study of the synthesis of pure silica ITQ-7. The study was mainly motivated to find a new structure directing agent that could replace the previous used in the initial reports,[90,103,104] which was discontinued by the commercial suppliers. Pure silica ITQ-7, Ge-ITQ-7, and Ge,Al-ITQ-7 were synthesized under static conditions at different temperatures and different synthesis durations. The precursor solution was prepared in fluoride media. A silica source, TEOS, Ge source, N-butyl-N-cyclohexyl-pyrrolidinium cation (BCHP) as the SDA, water source and ammonium fluoride (NH_4F), were used to synthesize the zeolites.

The resulting samples were characterized using PXRD, IR, MAS-NMR, among others. The synthesis of Ge-ITQ-7 using the new SDA led to the attainment of high crystalline material. No extra peaks or the presence of amorphous materials were detected in the diffractograms. However, the authors observed that the decreased intensity of certain peaks in the different diffractograms may be interpreted as the presence of intergrowths in the resulting sample. This may be attributed to the

decrease of the Ge content in the solid. Moreover, as the Ge content increased, it was observed an expansion of the unit cell volume. Two phenomena were observed when the IR spectrum was implemented. First, the ratio between the asymmetric modes of the Si-O-Si vibration decreased as the Ge content increased. Second, it was found the appearance of vibration bands in the Ge-ITQ-7 which were not observed in pure silica ITQ-7. These vibrations were attributed from Si-O-Ge linkages.

^{19}F MAS NMR spectra confirmed the location of fluoride ions within D4Rs. In Ge-ITQ-7 zeolites, it has been observed that Ge atoms are preferentially located in those secondary building units.[90] Thus, this analysis technique allows to indirectly assessing the Ge content. In the case of Ge,Al-ITQ-7, it was observed a fine crystallinity of the resulting samples from PXRD analyses. Furthermore, based on the elemental analysis, a lower incorporation of Al was observed when compared with the Al content in the precursor solution. However, the Ge content in the precursor solution and in the as-synthesized zeolite were practically equal. ^{27}Al-MAS-NMR spectroscopy confirmed the incorporation of Al into the Ge,Al-ITQ-7 samples. With this study the authors illustrate how sensitive the attainment of the desired zeolite phase is and how the fluoride media and the presence of D4R units allow for a higher incorporation of Ge in the ITQ-7 framework.

CHAPTER 3
MATERIALS AND METHODS

This chapter presents the chemicals and the equipment used, as well as the experimental procedure followed to obtain the resulting materials. Moreover, this chapter is divided into three sections. First, the synthesis of LTL using co-solvents will be described, where the materials and the experimental setup are defined. Second, the materials and the experimental setup for the study of the isomorphous substitution of Si by Ge are reported. Lastly, a description of the different analytical techniques used to characterize the resulting sample is described as well.

3.1. SYNTHESIS OF LTL USING CO-SOLVENTS

3.1.1. Materials

The chemicals used for the hydrothermal synthesis are listed in Table 3.1. All materials were used as received.

Table 3.1. Materials used for the synthesis of LTL

Materials	Manufacturer/Supplier
Aluminum sulphate octadecahydrate $Al_2(SO_4)_3 18H_2O$	Aldrich
Potassium hydroxide KOH	Baker
Ludox® HS-40	Sigma
$C_2H_6O_2$ (> 99.9%,)	Alfa Aesar
$C_4H_{10}O_3$ (> 99.9%,)	Alfa Aesar
$C_6H_{14}O_4$ (> 99.9%,)	Alfa Aesar

3.1.2. Experimental Procedure

The synthesis of LTL crystals were prepared based on a previous study published by Lee *et al.*[5]. For instance, to prepare a gel composition of $1Al_2O_3$: $20SiO_2$: $10.9K_2O$: 1000 H_2O: 30 $C_2H_6O_2$, initially, the alumina-potassium solution was prepared by dissolving 2.01 g of aluminum sulphate octadecahydrate ($Al_2(SO_4)_3 18H_2O$) and 3.69 g of potassium hydroxide (KOH) in 35.50 g de-ionized water and stirred for about 20 minutes The silica solution was then prepared by adding 9.05 g of Ludox® HS-40 into 13.83 g of de-ionized water. Subsequently, to the diluted silica solution, 5.62 g of $C_2H_6O_2$ (> 99.9%) were added drop by drop using a disposable pasteur pipette from VWR International (Radnor, PA; size 5 ¾") to allow a proper mixing between the diluted silica and the $C_2H_6O_2$. The mixture of silica-H_2O-$C_2H_6O_2$ was stirred for 15 minutes. Finally, the silica-H_2O-$C_2H_6O_2$ solution was

slowly added in portions to the alumina-potassium solution. The mixture of the components was conducted at ambient temperature (25 °C).

The whole mixture was stirred for 16 hours (i.e., aging of the mixture) prior hydrothermal synthesis. The stirring of the final mixture allowed the formation of a partially reacted phase that forms an amorphous gel[106]. According to some studies, the formation of nuclei was also possible when the mixture was aged.[7] The stirring time was selected according to the one reported by Lee *et al.*[55] The final solution was transferred to a Teflon-lined stainless steel autoclave (Parr Instrument Model 4744, 45 mL). The crystallization synthesis was carried out at 150 ºC for 1 day, 3 days and 6 days statically.

At the end of each designated time, the autoclave was cooled down to room temperature. The product was recovered by filtration. The filter paper utilized had a diameter of 55 mm, purchased from VWR (Whatman™ Grade 3). The filtration step required the use of copious amounts of de-ionized water until the pH dropped to a neutral value (i.e., pH =7). The pH was measured using pH-indicator strips purchased from VWR International Inc. (EMD Millipore, Universal Range). It is worth to mention that, the total amount of de-ionized water required to reach the pH neutral value depended on the co-solvent and the amount used. For instance, 2 to 4 liters of de-ionized water were required for the filtration when the samples were synthesized using either 30 or 80 moles of $C_2H_6O_2$ or $C_4H_{10}O_3$. On the other hand, a sample synthesized with 30 or 80 moles of TEG required the use of approximately 6 liters of de-ionized water. Finally, the resulting sample was placed on a weighing paper by VWR (West Chester, PA; size 4 x 4 inches), to allow the evaporation at room temperature of de-ionized water coming from the filtration stage. The sample was left to dry for 3 days. Figure 3.1 illustrates the schematic diagram for the hydrothermal synthesis of LTL.

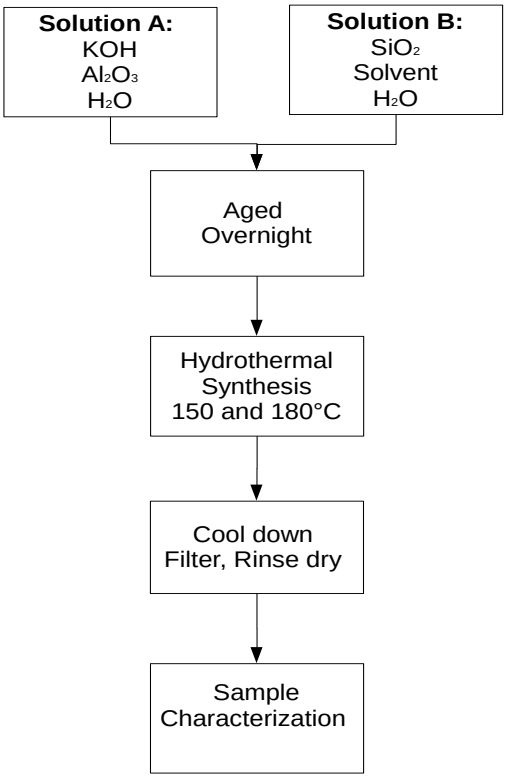

Figure 3.1. Schematic diagram for the hydrothermal synthesis of LTL

3.2. SYNTHESIS OF Ge-Zeolite L USING CO-SOLVENTS

The isomorphous substitution of Si by Ge in LTL framework was conducted via hydrothermal synthesis for 3 days at 150 °C. The main difference between the experimental setup from the previous section and this section lied on the modification of the addition of some of the chemicals, into the attainment of the precursor solution. The precursor solution was constituted of two different parts which have been named as solution A and Solution B.

3.2.1. Materials

The chemicals used for the hydrothermal synthesis are listed in Table 3.2. All materials were used as received.

Table 3.2. Materials used for the synthesis of Ge-Zeolite L

Materials	**Manufacturer/Supplier**
Aluminum sulphate octadecahydrate ($Al_2(SO_4)_3 18H_2O$)	Aldrich
Potassium hydroxide (KOH)	Baker
Ludox® HS-40	Sigma
GeO_2 (99.9999%)	Alfa Aesar
C$_6H_{14}O_4$ (> 99.9%,)	Alfa Aesar

3.2.2. Experimental Procedure

3.2.2.1. First Synthesis Procedure (M1)

Figure 3.2 shows the first synthesis procedure (M1). This was constituted by the combination of two individual parts. The first part named Solution A consisted of water, potassium and alumina source. The second part known as Solution B was comprised of water, silica source and the TEG-Ge sonicated solution. Prior to the preparation of Solution B, the TEG-Ge solution was sonicated in a Bransonic® ultrasonic cleaner model 3510R-DTH by Branson Ultrasonics Corp. (Danbury, CT) separately for 45 minutes. This time was selected as the time where 0.2 mol of GeO_2 are completely suspended in TEG. Solution B was stirred for 20 minutes and finally added to Solution A.

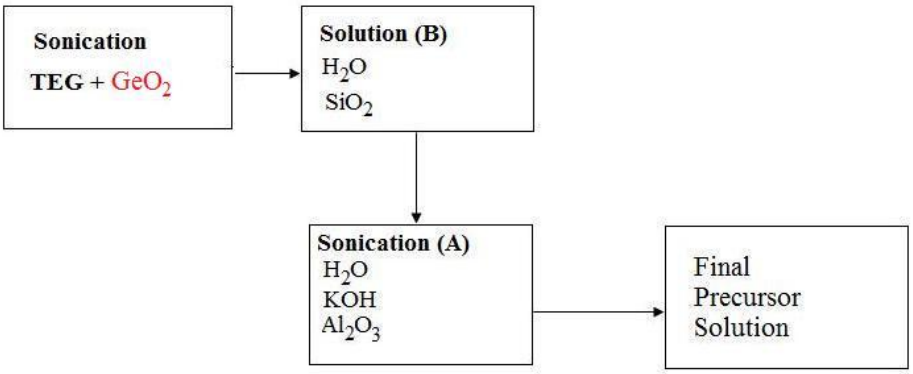

Figure 3.2. Schematic diagram of M1

3.2.2.2. Second Synthesis Procedure (M2)

Figure 3.3 illustrates the second synthesis procedure (M2) developed to study the effect of the Ge source and the mineraliser agent (KOH). According to the literature,[97,102] KOH was able to dissolve the GeO_2 powder. This procedure consisted of adding the Ge source in Solution A after water and potassium source were dissolved. The alumina source was added after 20 minutes to allow a close contact between the potassium and the Ge source. Solution B consisted of water, silica and TEG. After 20 minutes, Solution B was finally added to Solution A to obtain the final precursor solution.

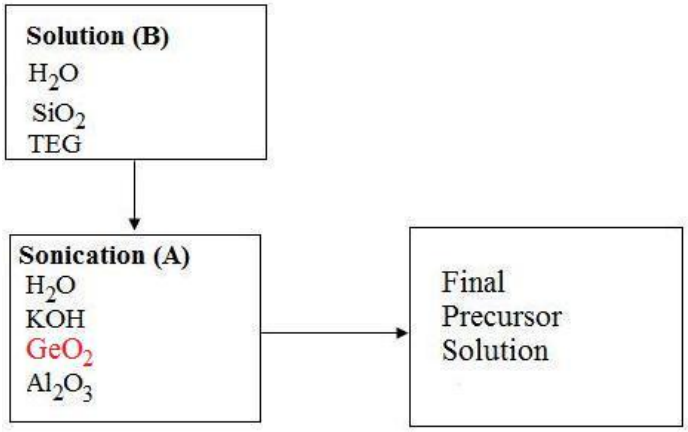

Figure 3.3. Schematic diagram of M2

3.2.2.3. Third Synthesis Procedure (M3)

Figure 3.4 depicts the third synthesis procedure (M3) formulated to study the effect that the adding sequence of the Ge source may have in the formation of the LTL phase. The changing in the adding sequence, when compared to M2, may allow observing any competition between aluminium atoms and Ge atoms for sites in the zeolite frameworks. This competition was reported when experiments were conducted in an alkaline media.[97,102] Procedure M3 consisted of adding the Ge source in Solution A after the water, potassium and alumina source were dissolved. The Ge source was added after 20 minutes to allow a close contact between the first three reactants. Solution B consists of water, silica and TEG source. After 20 minutes, Solution B was added to Solution A and thus the final precursor solution was created.

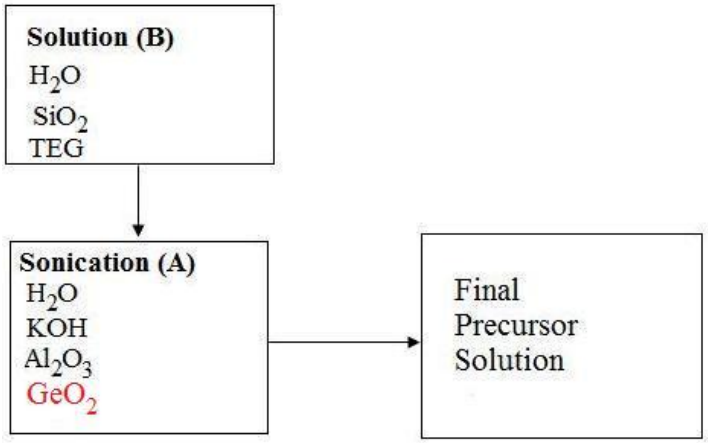

Figure 3.4. Schematic diagram of M3

3.3. ANALYTICAL TECHNIQUES

In this study, different techniques were used to characterize the samples attained from the hydrothermal synthesis, including powder X-ray diffraction (PXRD), scanning electron microscope (SEM), Fourier-transformed infrared spectroscopy (FTIR), nuclear magnetic resonance (NMR) techniques and X-ray Fluorescence Spectroscopy (XRF).

3.3.1. Powder X-Ray Diffraction (PXRD)

Powder X-ray diffraction is a routinely technique use for phase identification as well as the analysis of the material purity. It is required that the material is a crystalline solid in order to effectively use this technique. Zeolites meet this state condition. Moreover, the book *Collection of Simulated XRD powder Patterns of Zeolites*[107] provides valuable information of the different patterns of the zeolitic materials in order to compare them with the zeolite attained experimentally.[22]

In the PXRD technique, monochromatic X-rays are pointed towards a sample containing regularly spaced crystals. The crystals are constituted of parallel planes of ordered atoms. The planes reflect some of the X-ray intensity. Depending of the angle on which the X-rays are reflected (i.e, constructively interfered), they can be measured. As observed in Figure 3.5, the X-rays strike the sample at an angle θ and are reflected at the same angle. In order for the x-rays to be diffracted, the difference in the path-lengths ($2d\sin\theta$) of the rays must be an integral number of wavelengths.[108,109] Thus, the interaction between the reflected rays in the sample can be described by Bragg's law (Equation 3.1)

.

$$n\lambda = 2d\sin\theta \qquad \textbf{(3.1)}$$

where n is the order of the reflection, λ is the wavelength of the X-ray, d is the distance between planes and θ is the angle of the incident X-rays. The information attained from the PXRD is presented using a diffractogram. A diffractogram is a measure of the reflected intensity as a function of twice the angle from the surface normal of the crystal.

The sample preparation is a key step to attain reliable data. Good sample preparations guarantee that the peaks intensity was accurately related to the concentration of the sample. The preparation step consisted of grinding 0.5 grams of sample in a mortar with a pestle for 5-10 minutes until a fine powder

was obtained. The sample was collected in a 20 mL disposable scintillation vial and sent for analysis. The sample analysis was conducted at the Department of Chemistry at the University of Toronto by Dr. Serbri Petrov. Dr. Petrov conducted a second grinding. The sample was loaded in a sample holder and mounted in the sample stage. This is a small platform on the apparatus where the sample holder was placed for examination.

The powder X-ray diffractogram was measured using a Bruker D8 Advance instrument (Cu Kα1 with Ge monochrometer) by Bruker AXS (Karlsruher, Germany). The powder X-ray diffraction (PXRD) patterns were recorded in the range of $2\theta = 4 - 40^{\circ}$ with a step size of 0.03° and 25 seconds per step.

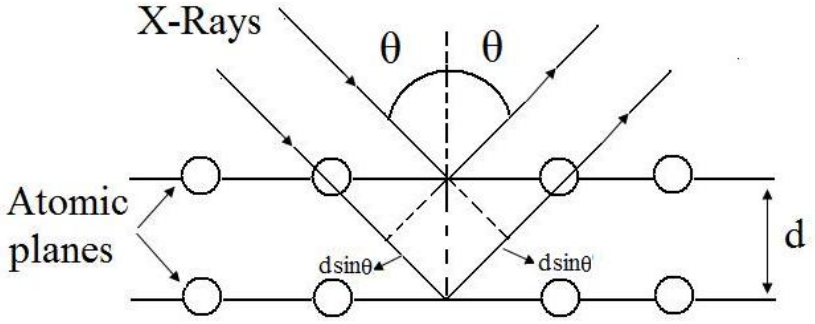

Figure 3.5. Illustration of Bragg's law.[109]

3.3.2. Scanning Electron Microscope (SEM)

SEM permits the scanning of the zeolite surface using electron beams generating high magnification and resolution. Thus, the information that was drawn from SEM images was: morphology of the LTL crystals, aspect ratio, crystal size, distribution phenomena (e.g. aggregation, intergrowth), relative roughness, amorphous phase, and unknown species were also distinguished.

Prior the SEM analyses, zeolite samples were pre-treated to ensure a proper observation of the crystals. This step consisted of adding 0.1 grams of the sample in 15 mL of ethanol (85.47% EtOH, VWR). The sample precipitated in ethanol. Then, this mixture was placed in a Bransonic® ultrasonic cleaner model 3510R-DTH by Branson Ultrasonics Corp. (Danbury, CT) for 15 minutes to allow a dispersion of the zeolite sample in ethanol and thus, forming one phase. The solution was taken from the sonicator and let it sit for 3 minutes. A small zeolite sample (< 0.5 mL) was withdrawn from the top layer of the mixture (zeolite-ethanol) using a pasteur pipette and placed in the SEM holder. This SEM

holder was provided by Mr. Qiang Li from the Department of Mechanical and Industrial Engineering at Ryerson University. The zeolite sample on the SEM holder was coated with gold and mounted in the SEM stage. Mr. Li was in charge of doing these steps, as well as, to conduct the SEM analyses.

SEM measurements were performed in a JEOL Scanning Electron Microscope (SEM), model JSM-6380 LV (Oxford Instrument, U.K). The crystals sizes were measured using the software provided by the instrument as observed in Figure 3.6. It is also worth noting that some of the crystals measurements were carried out manually using the scale bar given by the SEM image. For instance, in Figure 3.6 the scale bar is 1µm. The length and diameter of 10 different crystals were measured. The average length and diameter were recorded and the standard deviation was attained as well.

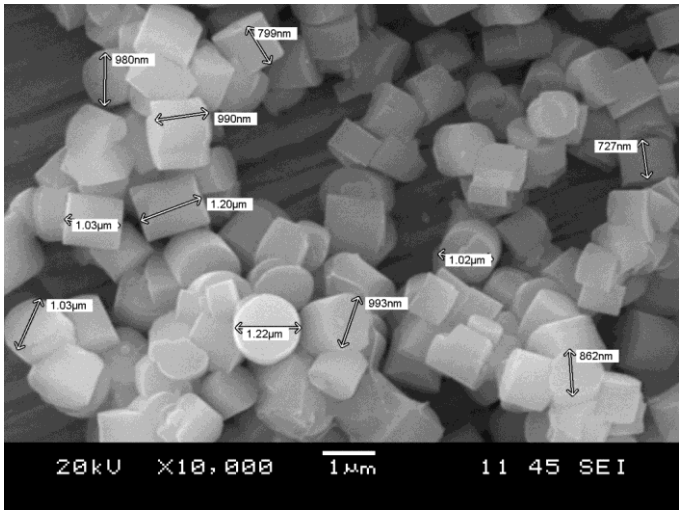

Figure 3.6. Measure of the LTL crystals conducted by the use of the SEM software. The hydrothermal synthesis was conducted for 6 days at 150 ºC using $1Al_2O_3$:$20SiO_2$:$10.9K_2O$: 950 H_2O: 80 $C_6H_{14}O_4$. The addition sequence was inverted for this sample (see Figure B.1).

3.3.3. Fourier-Transformed Infrared Spectroscopy (FTIR)

Fourier-transformed infrared analysis provides spectral information, which represents a molecular fingerprint of the material. This technique allows attaining information from the functional groups of a molecule. However, information such as the connectivity of the functional groups cannot be extracted by using this technique.[109] The infrared radiation (IR) interacts with the different functional groups in the sample where some of the IR is absorbed by the sample and the other part passes through (transmitted) the sample. Depending on the functional group, the IR is absorbed in a specific wave number range, which allows identifying the functional group in the sample.[109] The wave number assigned to a specific functional group is independent of the effect of temperature and pressure.

Moreover, zeolite L (LTL) has been studying using FTIR.[110] Table 3.3 presents the characteristic wavelength bands when using this technique.

Table 3.3 Zeolite L band assignments.[110]

Wavelength (cm^{-1})	Assignment
1200-1000	Asymmetric stretching vibrations O-(Al,Si)-O (Internal tetrahedral or external tetrahedral)
770	Symmetric stretching vibration O-(Al,Si)-O
725	Symmetric stretching vibration of "isolated" AlO_4 tetrahedral
645 sh.	Vibration of Double six membered rings (D6Rs)
608	
580 sh.	
477	Bending vibration O-(Al,Si)-O
438 sh.	Vibration of D-12 Rings (pore opening)

sh: shoulder.

The zeolite samples were prepared by mixing 5 mg with 500 mg of KBr and pressed into pellets. The instrument was prior conditioned before placing the samples by preparing a pure KBr pellet. A background spectrum of the pure KBr pellet was acquired in order to start the data acquisition. The spectrum was collected in Transmittance mode from 450 to 4000 cm^{-1}. The FTIR technique was applied to samples with the highest crystallinity of LTL shown by PXRD patterns. The FTIR patterns obtained were compared with the FTIR pattern of a pure LTL (i.e. without using any co-solvent) to observe any differences among them. FTIR measurements were performed using a Perkin Elmer Spectrum One, V3.01 spectrometer from Waltham, USA.

3.3.4. Nuclear Magnetic Resonance (NMR)

Nuclear Magnetic Resonance (NMR) is applied to determine the structure of *organic molecules* in a sample. This spectroscopic technique can only be used to study atomic nuclei having an odd number of protons or neutrons (or both). For instance, atoms such as ^{1}H, ^{13}C and ^{19}F have this particularity. The nucleus possesses a magnetic property denominated spin as well as a rotation movement in the axis, B_o, which allows the nucleus to behave as small magnet. Figure 3.7 illustrates a schematic of a spinning proton.[111,109]

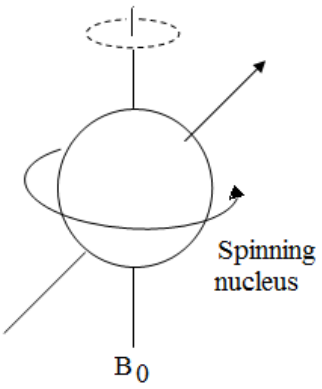

Figure 3.7. The spinning proton resembling a small magnet.[109]

In the absence of a magnetic field, the spinning nuclei are oriented randomly. However, when a sample is placed in a magnetic field as shown in Figure 3.8, the nucleus with a positive spin is oriented in the same direction as the magnetic field, in a minimum-energy state, whereas the nucleus with a negative spin is oriented in opposite direction to the magnetic field, in a higher-energy state.

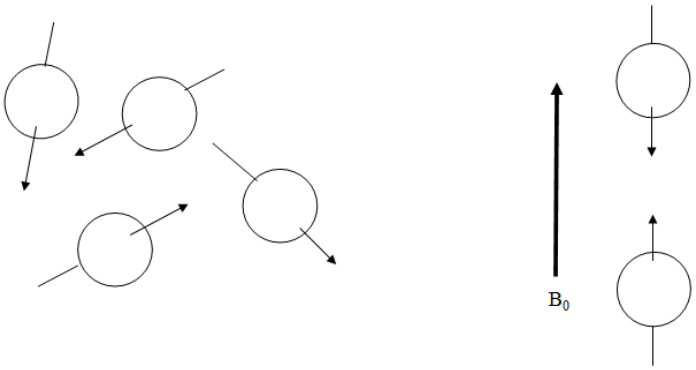

Figure 3.8. Schematic representation of nuclei with a without the presence of a magnetic field.[111] Left side: nucleus randomly oriented. Right side: nucleus oriented according to the external magnetic field applied.

The distribution of the nuclei between the two energy states is dependent on the temperature and the magnetic field strength. A diagram of a NMR spectrometer is presented in Figure 3.9. The spectrometer is composed mainly of a stable magnet, radiofrequency transmitters and power amplifiers for generation the magnetic field (B_0); a detector or probe for delivering B_0 fields to the sample and to measure the absorbed energy from the sample; a computer to receive the data from the radio frequency reception system and for processing the data.[109] The sample is loaded inside the strong magnetic field where the effects of the field in the nucleolus of every atom in the molecule is detected, and thus, permitting the analysis of the structures. The accuracy of the instrument when running different spectra is in general ± 5%.[109] The samples were analyzed in a Bruker 400 MHz Nuclear Magnetic Resonance Spectrometer by Bruker Biospin (Rheinstetten, Germany).

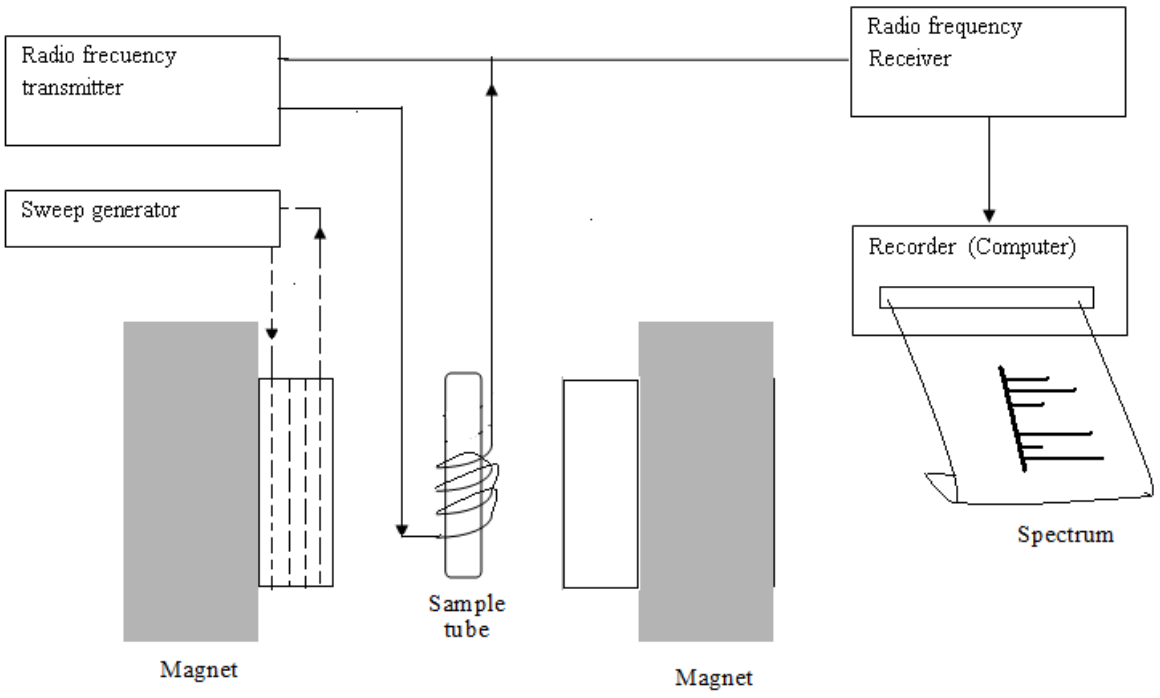

Figure 3.9. Schematic diagram of a NMR spectrometer.[111]

It is worth noting that in reality the nucleus is surrounded by electrons. These electrons partially protect the nucleus from the influence of an external magnetic field. When the external magnetic field is applied to the molecule, the electrons movements generate an induced magnetic field that opposes the external magnetic field. Due to this opposition, the strength of the external magnetic field is reduced around the nucleus. This reduction is known as *shielding*.[111] On the other hand, when a nucleus is influenced by increasing the external magnetic field, then the strength of the external magnetic field requires to be reduced. This phenomenon is known as *deshielding*. As a result, the different types of nucleus in a molecule have different resonant frequencies. These differences are known as chemical shift. The chemical shift (δ), shown in Equation (3.2, is defined as the difference between the nucleus resonant frequency (ν_{sample}) in a chemical environment and the reference nucleus frequency ($\nu_{\text{reference}}$), divided by the spectrometer frequency.

$$\delta = \frac{\nu_{\text{sample}} - \nu_{\text{reference}}}{\nu_{\text{spectrometer}}} \qquad \textbf{(3.2)}$$

The chemical shift range is expressed in parts per million (ppm). Table 3.4 presents a characteristic chemical shift ranges for ^{1}H and ^{13}C. The chemical shifts are acquired by using tetramethyl silane (TMS) as the reference compound. Moreover, Figure 3.10 shows a general

illustration for proton shift values. Highly shielded protons appear at the right region of the chart that is usually denominated as high field. Deshielded protons appear at the left region of the chart which is denominated as low field.

Table 3.4 Chemical shifts regions for ^{1}H and ^{13}C.[111]

Compounds types	**^{1}H (ppm)**	**^{13}C (ppm)**
alkanes	0.5-1.3	5-35
R-CH_2-NR_2	2-3	42-70
R-CH_2-SR	2-3	20-40
R-CH_2-PR_3	2.2-3.2	50-75
R-CH_2-OH	3.5-4.5	50-75
R-CH_2-NO_2	4-4.6	70-85
R-CH_2-F	4.2-5	70-80
R-CH_2-Cl	3-4	25-50
R-CH_2-Br	2.5-4	10-30
R-CH_2-I	2-4	-20-0
Alkenes	4.5-7.5	100-150
Esters	-	160-175

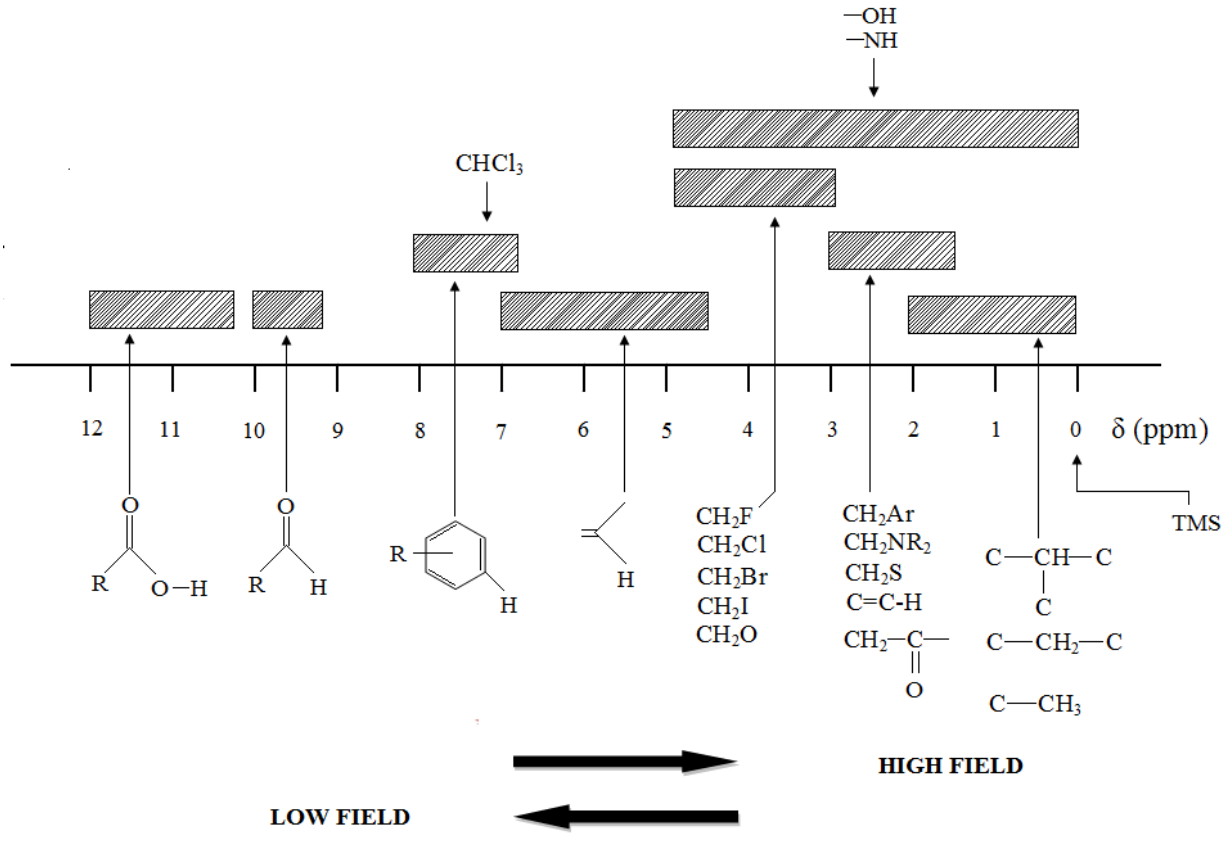

Figure 3.10. A general illustration of the ranges of chemical shift values for the most common types of protons.[112]

In order to study the gel mixture aged after 16 hours, the following series of experiments were implemented. First, ^{1}H-NMR and ^{13}C-NMR analyses were performed for each pure co-solvent. These spectra were used as the benchmarks to the aged precursor solutions. Then, ^{1}H-NMR and ^{13}C-NMR analyses were performed for each of the aged gels using different co-solvents. The ^{1}H-NMR and ^{13}C-NMR studies were conducted using different types of deuterated solvents. Deuterated water (99.98% D_2O, Aldrich) was used for the ^{1}H-NMR analyses and deuterated chloroform (99.96% $CDCl_3$, Aldrich) was used for the ^{13}C-NMR analyses. The ^{1}H-NMR and ^{13}C-NMR spectra of the pure co-solvents are found in Appendix A (i.e., Figure A.1-A.6).

According to the suggestions by Dr. Russell Viirre, from the Department of Chemistry at Ryerson University, 5.0 to 20.0 mg of each of the samples and 0.5 mL of the solvents were required to run ^{1}H-NMR and ^{13}C-NMR analyses. The samples and the solvent (i.e., D_2O or/and $CDCl_3$) were sonicated in a Bransonic® ultrasonic cleaner model 3510R-DTH by Branson Ultrasonics Corp. (Danbury, CT) to allow a proper mixture among them. In this study, I utilized 5.0 mg of the sample dissolved in 0.5 mL of the solvent. Prior to adding the mixture in the NMR tubes, it was required to ensure that the mixture was clear of solid materials. The samples analyzed in this study did not presented the formation of solid entities. Analyses using NMR require that the NMR tubes (Wilmad-LabGlass, 5 mm outer diameter) had a specific amount of the mixture, which was determined by the height of the mixture in the NMR tube. The minimum height for operable condition in the NMR instrument was 5 cm. After the NMR analyses were conducted, the NMR tubes were rinsed right away with ethanol in order to avoid any contamination of the tubes. Approximately 10 washes were required to properly clean one NMR tube.

3.3.5. X-ray Fluorescence Spectrometry (XRF)

The X-ray Fluorescence technique (XRF) is based on the knowledge that an atomic system possesses different energy levels as well as having electronic transitions between the energy levels. The XRF phenomenon can be described in two steps-processes: the removal and the transition process of electrons. In the removal process, an X-ray beam is emitted to the system. The energy is absorbed by the system which creates an excited state. This state allows removing an inner shell electron of an atom. The removal of the electron in the inner shell leaves a vacancy which is filled by an outer shell electron. This transition of the electron is known as the second step and results in a release of radiation energy i.e., X-ray photon. Thus, XRF is a measurement of the radiation energy emitted in these

electronic transitions. The intensity of the photon emission allows measuring the amount of each of the elements in the sample. The XRF process is illustrated in Figure 3.11.[109]

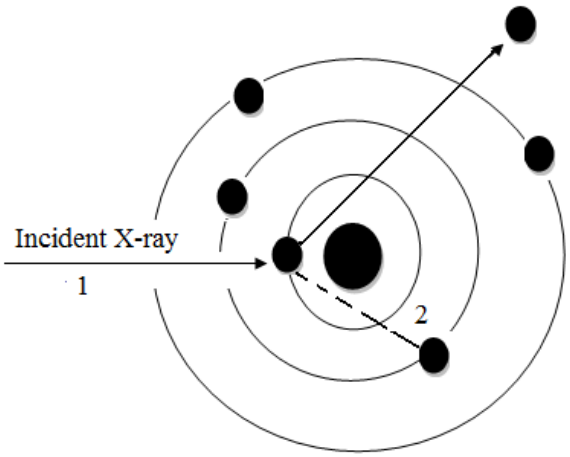

Figure 3.11. The XRF process. The numbers represent the two step-processes involved in this technique.[109]

Generally 0.8 grams of the crystalline solid was required to conduct XRF analyses. Dr. Mike Gorton, from the Department of Geology at the University of Toronto, conducted the samples preparation and analyses. The resulting samples were measured using a fully automated, Philips PW 2404 sequential spectrometer by Philips Analytical (Almelo, Netherlands). The apparatus is equipped with an automated sample changer and an end-window rhodium anode tube.

3.4. EXPERIMENTAL REPRODUCIBILITY OF ZEOLITE L (LTL)

The reproducibility of zeolite L (LTL) phase was conducted experimentally, in the following order: first, duplicating the gel composition reported by Lee *et al*: 1 Al_2O_3: 20 SiO_2: 10.9 K_2O: 1030 H_2O at 180 °C for 3 days.[55] The PXRD pattern is shown in Figure 4.1(a). It was observed the formation of LTL and impurity phases.

Second, the addition sequence of the solution A and solution B from the precursor solution was tested in order to observe if this change was influencing the attainment of LTL phase. The hydrothermal synthesis was conducted for 6 days at 150 ºC using $1Al_2O_3$:$20SiO_2$:$10.9K_2O$: 950 H_2O: 80 $C_6H_{14}O_4$. PXRD patterns showed that the change in addition sequence did not play a role in the attainment of LTL. Highly crystalline LTL phase was attained. The PXRD patterns are shown in Figure B.1

Third, the sample labeled as 80TEG-150-3 was synthesized in two occasions. The hydrothermal synthesis was conducted for 3 days at 150 ºC using $1Al_2O_3$:$20SiO_2$:$10.9K_2O$: 950 H_2O: 80 $C_6H_{14}O_4$. The PXRD analyses shown in Figure B.2 illustrate the same trend: co-existence of LTL phase and amorphous materials.

Fourth, the reproducibility of the experiments conducted with Ge was tested by repeating the sample labeled as M2-80TEG-150-0.2Ge for 3 days at 150 °C days using $1Al_2O_3$:$19.8SiO_2$:$0.2GeO_2$:10.9 K_2O:950 H_2O:80 $C_6H_{14}O_4$. Moreover, for this specific experiment, a synthesis was conducted in new Teflon sleeves to eliminate the possible seeding effect of old sleeves. According to PXRD analyses, pure LTL phase was attained without the formation of any impurities when using the new jars. Hence, the reproducibility of the experiments was confirmed. The PXRD patterns are shown in Figure B.3.

CHAPTER 4
RESULTS AND DISCUSSION

4.1. SYNTHESIS OF LTL USING CO-SOLVENTS

4.1.1. Effect of Co-Solvent Identity

Lee *et al* had demonstrated that LTL crystals with smooth hexagonal long-rod morphology can be synthesized using 1 Al_2O_3: 20 SiO_2: 10.9 K_2O: 1030 H_2O at 180 °C for 3 days.[55] Recently, our research group reported an alternative route to tune LTL morphology towards a disc-shape by incorporating ethanol (EtOH) as the co-solvent in the synthesis gel.[14] The reason for the dramatic change of crystal morphology is not clear. For systematically investigating the co-solvent effect, ethylene glycol (EG) is selected as the co-solvent identity with an extra OH group with respect to EtOH. Diethylene glycol (DEG) and triethylene glycol (TEG) are chosen as co-solvent identities with the chain length effect.

Figure 4.1 shows the powder X-ray diffraction (PXRD) patterns using an initial gel composition of $1Al_2O_3$:$20SiO_2$:$10.9K_2O$: 1000 H_2O: 30 $(OH)_2(CH_2)_{2n+2}O_n$ (n = 0,1,2) at 180 °C for 3 days. The synthesis procedure published by Lee *et al* is reproduced as the benchmark. Figure 4.1(a) shows the PXRD pattern of the benchmark LTL crystals. The LTL phase in a PXRD pattern is identified by the diffraction peaks at 2θ of 5.5°, 16.55°, 22.5°, 28.96° and 33.45°.[107] This experiment corroborates the reproducibility of the synthesis procedure published by Lee *et al.* However, it is also observed the co-existence of LTL phase with zeolite W, when the benchmark is reproduced.[14,56]

Figure 4.1(b) shows that the use of EG (30EG-180-3) in the synthesis does not lead to the formation of LTL phase. Instead, the PXRD pattern displays distinctive peaks at 2θ of 14° and 28.5° which may be attributed to cancrisilite phase[113,114] as well as the presence of zeolite W. Furthermore, when DEG (30DEG-180-3) is used, Figure 4.1(c) illustrates weak crystallinity features of LTL phase and zeolite W. In Figure 4.1(d), it is observed that the characteristic peaks of LTL become more prominent when TEG (30TEG-180-3) is utilized as the co-solvent with the presence of zeolite W. According to the PXRD patterns in Figure 4.1 (b)-(d), the use of TEG demonstrate a notable improvement towards the formation of LTL compared to the use of the other two co-solvents

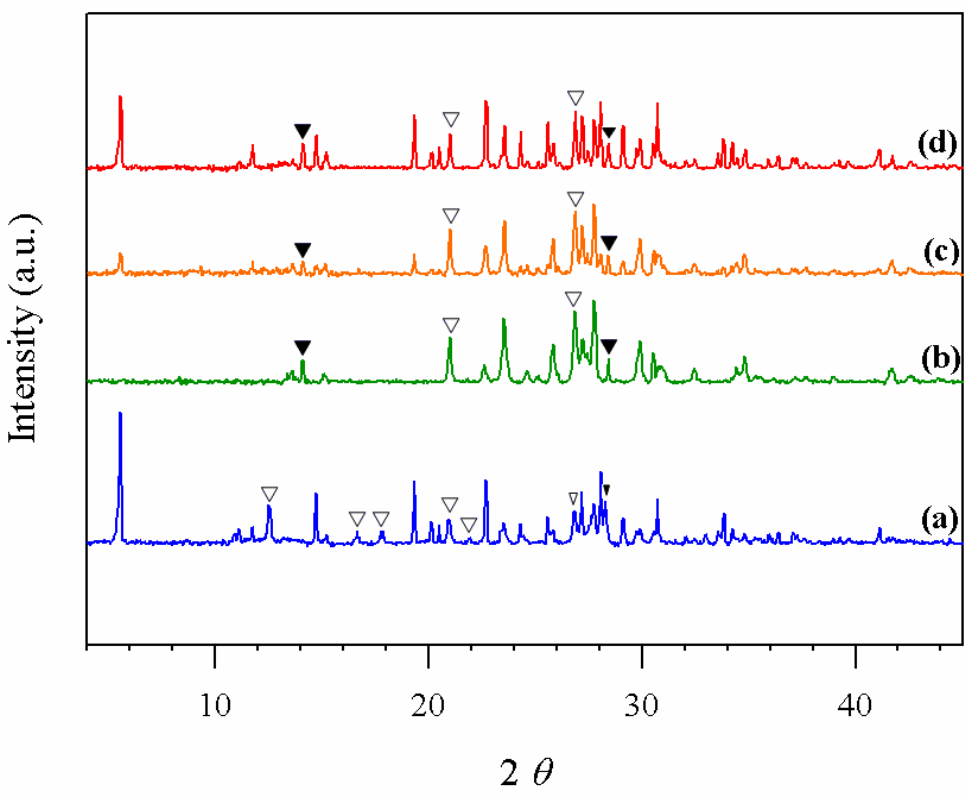

Figure 4.1. Powder XRD patterns attained at 180 °C for 3 days using $1Al_2O_3$:$20SiO_2$:$10.9K_2O$: 1000 H_2O: 30 $(OH)_2(CH_2)_{2n+2}O_n$ (n = 0,1,2). (a) pure LTL; (b) $C_2H_6O_2$, (30EG-180-3); (c) $C_4H_{10}O_3$, (30DEG-180-3); (d) $C_6H_{14}O_4$, (30TEG-180-3). The empty triangles represent peaks of zeolite W. The solid triangles represent peaks of cancrisilite.

Our previous study reported that the incorporation of co-solvents can tune the morphology of LTL crystals dramatically, depending on the concentration of co-solvents. A similar phenomenon can be observed in the current investigation. Figure 4.2 shows the SEM images of the crystalline samples using 30DEG-180-3 and 30TEG-180-3 individually at the low concentration. Figure 4.2 (a) and Figure 4.2 (b) show that LTL crystals are imbedded in cancrisilite using 30DEG-180-3. The morphologies of LTL crystals are a combination of long rods and short stubs whose dimensions in *c*-direction are about 2 μm and 1 μm respectively. This observation is similar with the published results[14]. Figure 4.2 (c) and Figure 4.2 (d) illustrate the intergrowth of short-stub LTL crystals with smooth surfaces when 30TEG-180-3 is synthesized. Figure 4.2 (c) exhibits the presence of the cancrisilite phase, consistent with the PXRD pattern in Figure 4.1 (d). However, using TEG (30TEG-180-3) as the co-solvent does facilitate the formation of LTL. It is worth noting that the cancrisilite phase should not be confused with the cancrinite cage. The cancrinite cage is the secondary unit building of LTL, whereas the cancrisilite phase is an impurity observed from the PXRD patterns. The cancrisilite phase can co-exist with the LTL phase. In Figure 4.2 (a) and (c), the yellow arrows point out to the cancrisilite phase, while the green arrows point out the LTL crystals.

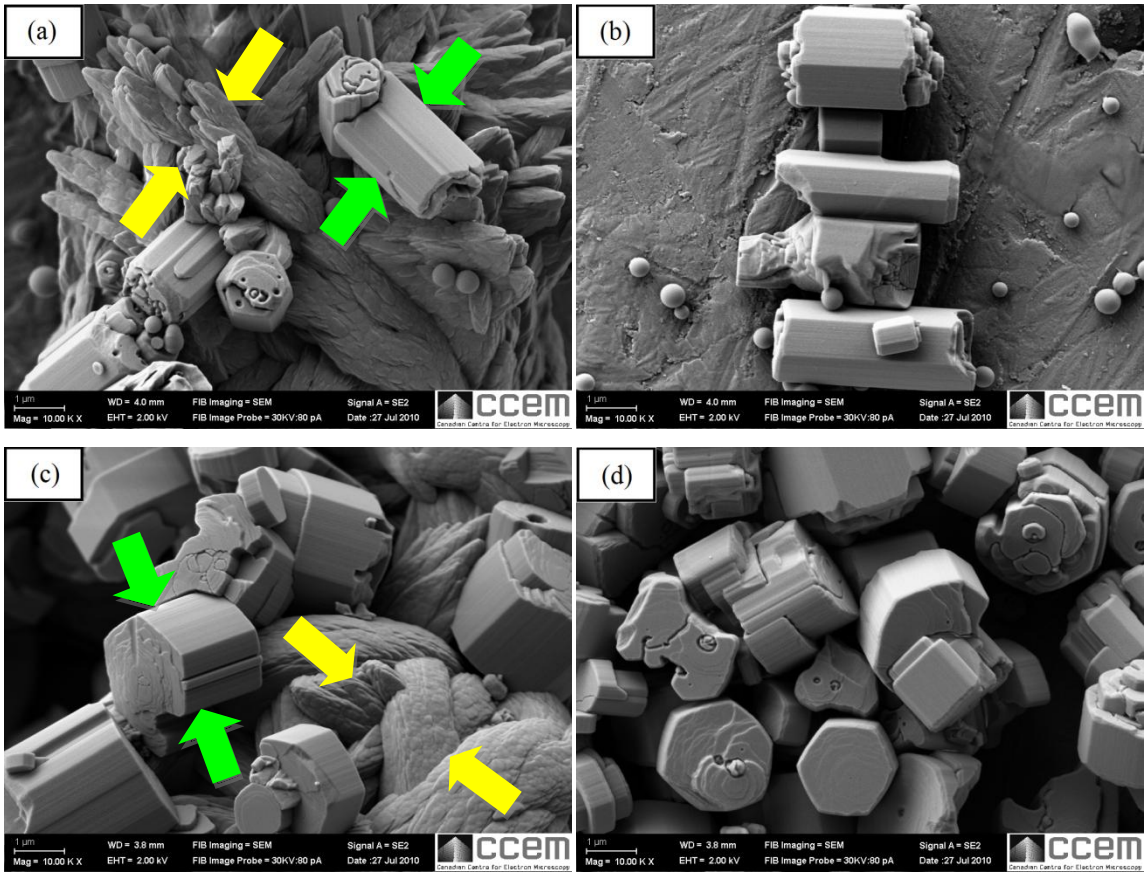

Figure 4.2. SEM images of samples prepared at 180 °C for 3 days using $1Al_2O_3$:$20SiO_2$:$10.9K_2O$: 1000 H_2O: 30 $(OH)_2(CH_2)_{2n+2}O_n$ (n = 1,2): (a)-(b) $C_4H_{10}O_3$, (30DEG-180-3); (c)-(d) $C_6H_{14}O_4$, (30TEG-180-3). The yellow arrows point out to the cancrisilite phase. The green arrows point out to the LTL crystals.

Even though the gel composition used to attain LTL crystals adopts high water content in the synthesis gel, the formation of LTL is dramatically inhibited when the co-solvents are added. It is noteworthy that the formation of LTL is facilitated by the longer backbone scaffold of co-solvent identity, i.e. TEG > DEG > EG.

Given the co-existence of LTL with cancrisilite and zeolite W, we further investigate the synthesis duration effect on LTL formation. Figure 4.3 illustrates the PXRD patterns of synthesized materials using prolonged synthesis duration. As the synthesis duration is increased from 3 days to 6 days, the formation of the cancrisilite phase becomes more obvious when EG (30EG-180-6) is used as the co-solvent (Figure 4.3(a)).The use of DEG (30DEG-180-6) leads to the formation of cancrisilite phase and weak features of LTL with a intensity of the peaks at 2θ =5.5°, 22.66°, 22.9°, 36.28°, indexed with arrows in Figure 4.3 (b). The addition of TEG, Figure 4.3 (c), shows a similar powder XRD pattern when EG is used.

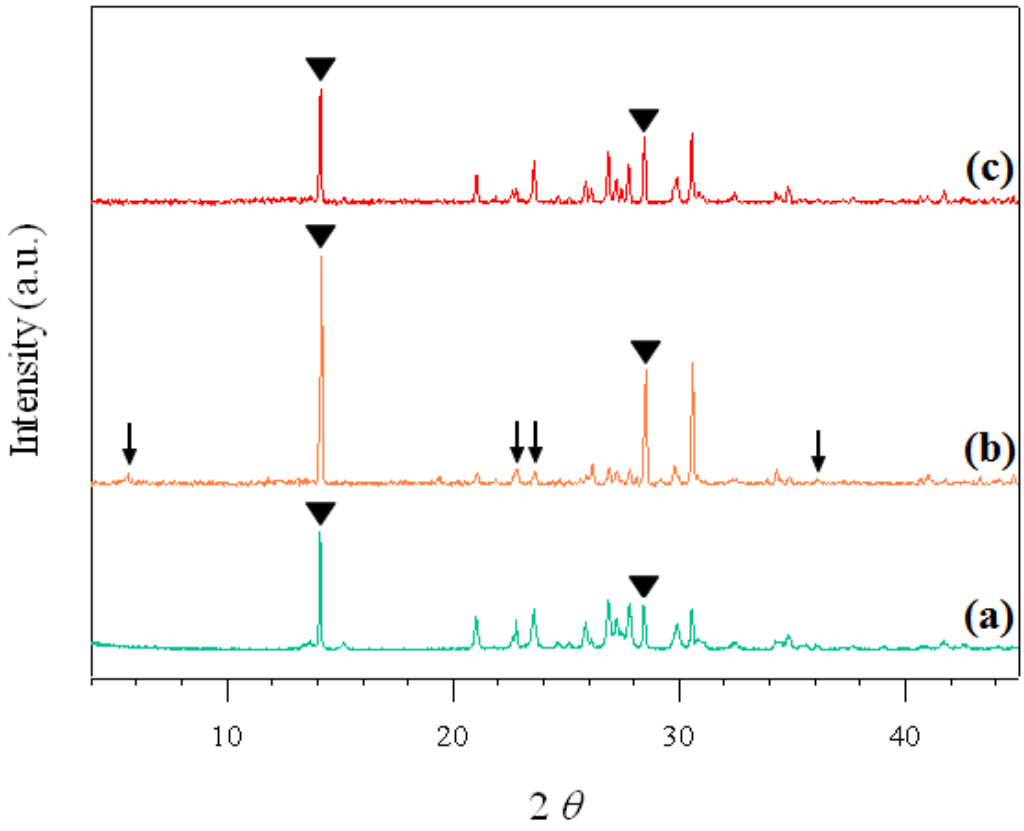

Figure 4.3. Powder XRD patterns attained at 180 °C for 6 days using $1Al_2O_3$:$20SiO_2$:$10.9K_2O$: 1000 H_2O: 30 $(OH)_2(CH_2)_{2n+2}O_n$ (n = 0,1,2). (a) $C_2H_6O_2$, (30EG-180-6); (b) $C_4H_{10}O_3$, (30DEG-180-6); (c) $C_6H_{14}O_4$, (30TEG-180-6). Arrows in spectrum (b) indicate the emerging peaks of LTL. The solid triangles indicate the peaks from cancrisilite phase.The arrows in (b) indicate the emerging of LTL phase.

In a separate study using ethanol (EtOH) as the co-solvent, we observed that the morphology of LTL crystals became more uniform when the amount of EtOH was varied from 30 to 80 moles in the synthesis gel.[14] Inspired by our previous observation, we further increase the amount of each of the co-solvents (i.e., EG, DEG and TEG) of the synthesis gels in the current study from 30 to 80 moles. The hydrothermal synthesis temperature is kept at 180 °C. The experiments are conducted for 3 days as observed in Figure 4.4.

Figure 4.4 (a) shows the PXRD pattern for the sample using 80EG-180-3. The pattern shows only the formation of cancrisilite phase. Additionally, the PXRD patterns of 80EG-180-3 and 30EG-180-3 (Figure 4.1(b)) are almost identical. The increment in the concentration leads to attain more prominent features of the cancrisilite phase. Figure 4.4 (b) illustrates the PXRD pattern attained using 80DEG-180-3. Compared with 30DEG-180-3, the formation of LTL crystals is further frustrated. However, very weak features of LTL phase can be noticed, indexed with arrows.

Figure 4.4 (c) shows the result obtained when TEG (80TEG-180-3) is utilized as the co-solvent. The PXRD pattern demonstrates the most obvious LTL features among those of the investigated co-solvents using 80 moles. Meanwhile, the crystallinity of the cancrisilite phase is further increased with increasing the concentration of TEG. The cancrisilite phase is identified at 2θ around 14° and 28.5

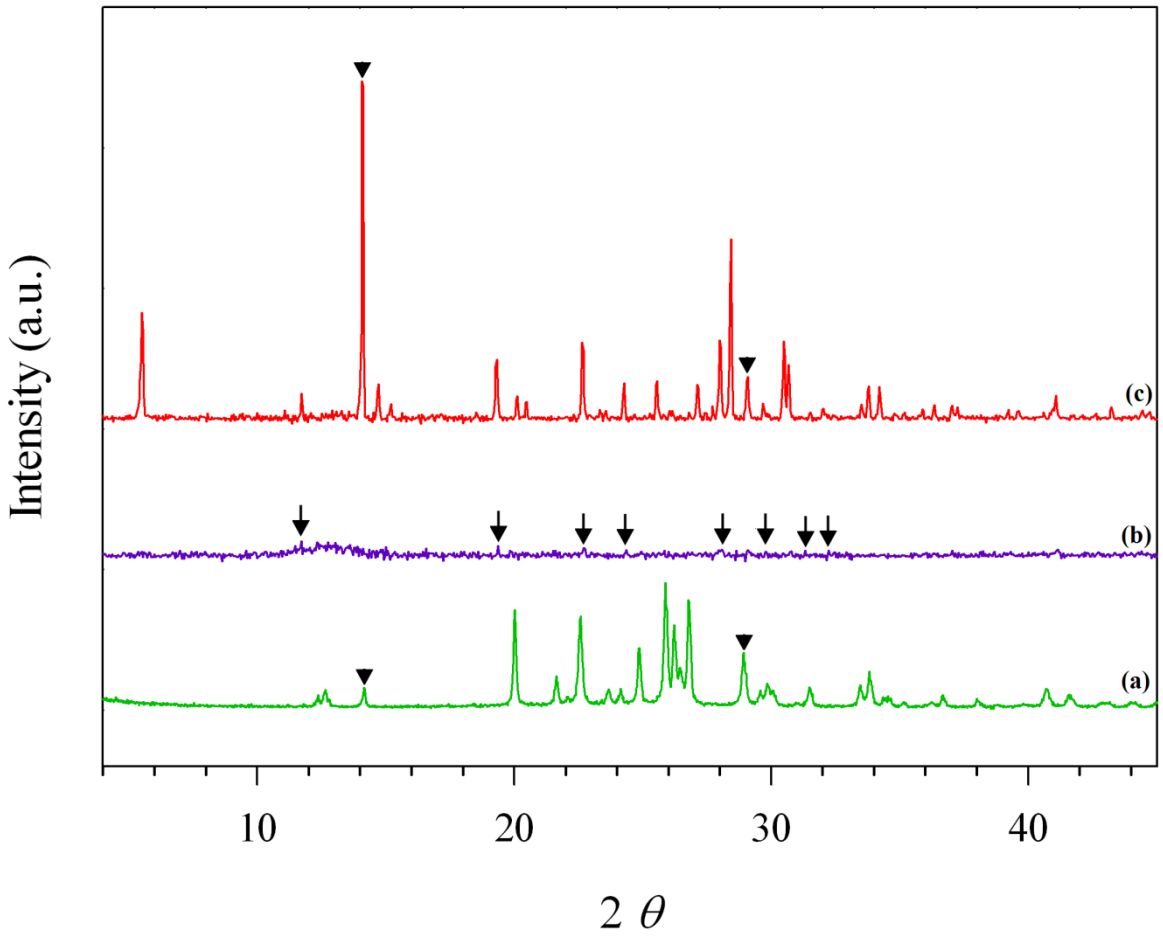

Figure 4.4. Powder XRD patterns attained at 180 °C for 3 days using $1Al_2O_3$:$20SiO_2$:$10.9K_2O$: 950 H_2O: 80 $(OH)_2(CH_2)_{2n+2}O_n$ (n = 0,1,2). (a) $C_2H_6O_2$, (80EG-180-3); (b) $C_4H_{10}O_3$, (80DEG-180-3); (c) $C_6H_{14}O_4$, (80TEG-180-3). The solid triangles represent the peaks from cancrislite phase. The arrows in (b) indicate the emerging of LTL phase.

Experiments are also prepared when the synthesis time is extended from 3 days to 6 days. Figure 4.5 (a) shows that no formation of LTL crystals could be observed using EG (80EG-180-6). The peaks around 20-30° observed during the synthesis time of 3 days remain constant when the time is increased to 6 days. Moreover, it appears that the increase of the duration synthesis time resulted in the occurrence of the peak around 14°. Thus, we may assume that the prolongation in the synthesis time leads to the formation of undesired phases.

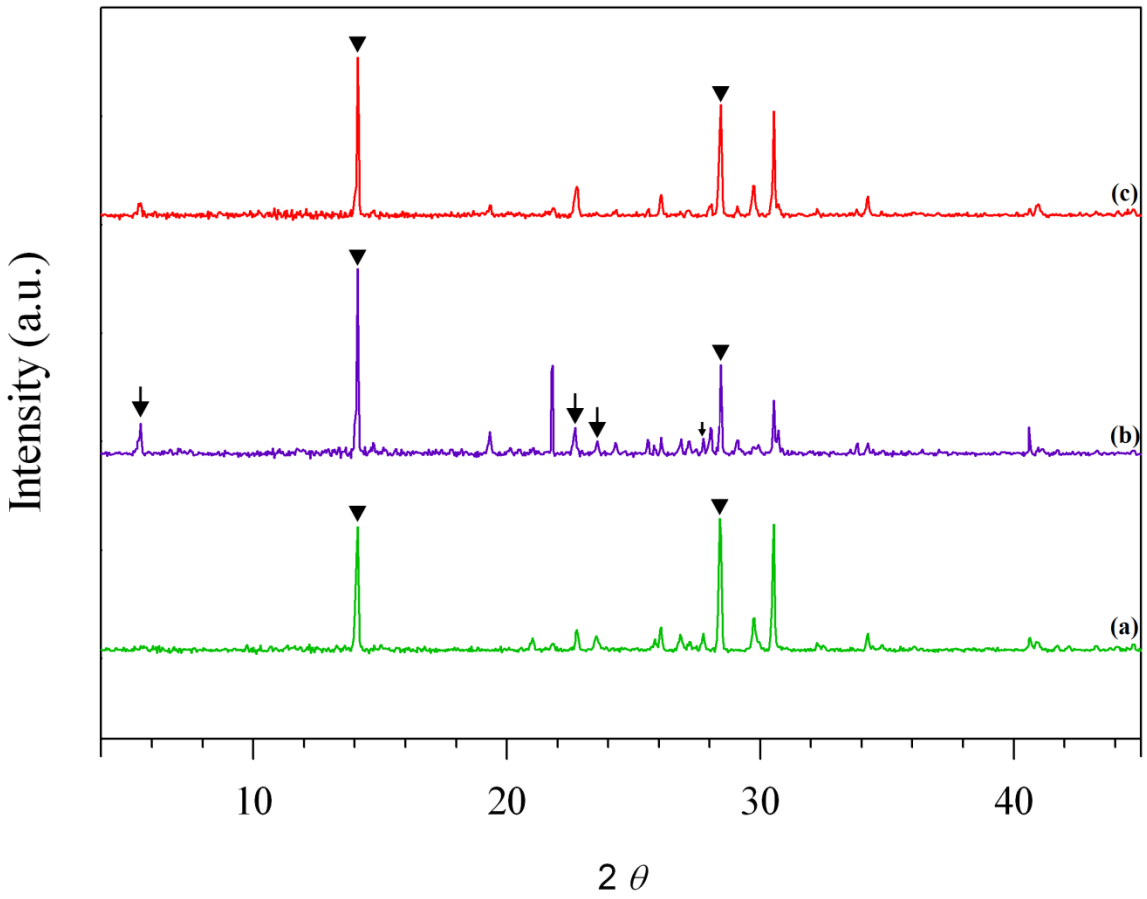

Figure 4.5. Powder XRD patterns attained at 180 °C for 6 days using $1Al_2O_3$:$20SiO_2$:$10.9K_2O$: 950 H_2O: 80 $(OH)_2(CH_2)_{2n+2}O_n$ (n = 0,1,2). (a) $C_2H_6O_2$, (80EG-180-6); (b) $C_4H_{10}O_3$, (80DEG-180-6); (c) $C_6H_{14}O_4$, (80TEG-180-6). The solid triangle represents peaks of cancrisilite. The arrows in (b) indicate the emerging of LTL phase.

4.1.2. Effect of Co-Solvents Using Lower Temperature

In order to further analyze the effect of the co-solvents, a series of experiments are conducted using a lower temperature (150 °C). The concentration (30 and 80 moles) effect is also investigated along with the synthesis duration effect (3 and 6 days) of each co-solvent.

Figure 4.6 shows the PXRD patterns for the experiments that are conducted for 3 days using 30 moles of each of the co-solvents. All the PXRD patterns demonstrate that amorphous materials are formed at 150 °C. The appearance of amorphous material is justified by the appearance of a hump between 2 θ = 10-16°. The formation of amorphous materials implies that longer synthesis duration may be required to observe the LTL phase when the temperature at 150 °C is used.

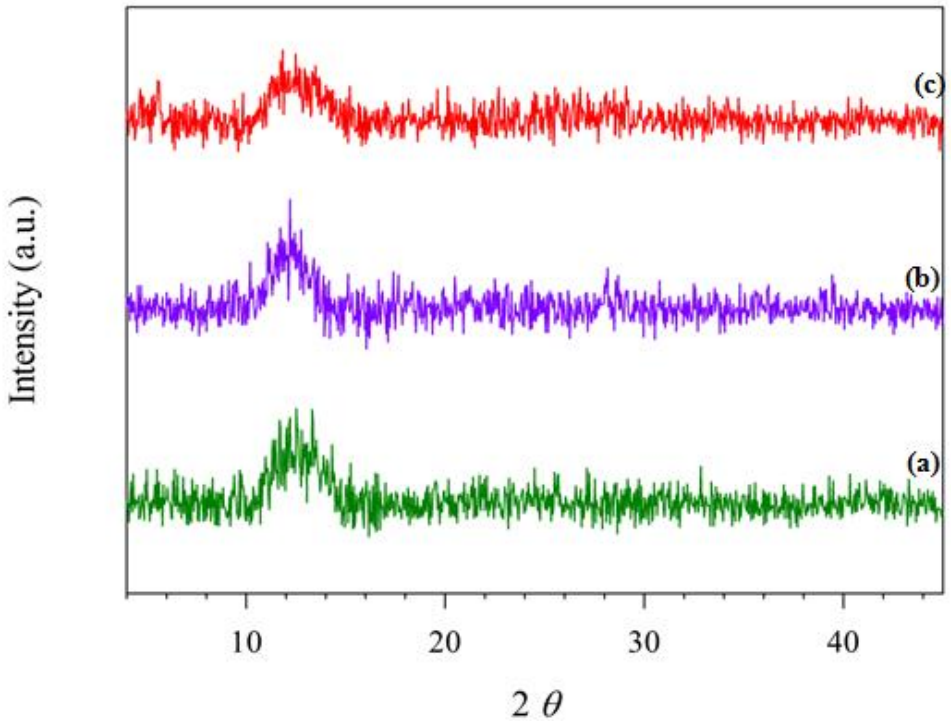

Figure 4.6. Powder XRD patterns attained at 150°C for 3 days using $1Al_2O_3$:$20SiO_2$:$10.9K_2O$: 1000 H_2O: 30 $(OH)_2(CH_2)_{2n+2}O_n$ (n = 0,1,2). (a) $C_2H_6O_2$, (30EG-150-3); (b) $C_4H_{10}O_3$, (30DEG-150-3); (c) $C_6H_{14}O_4$, (30TEG-150-3)

Figure 4.7 illustrates the PXRD patterns when the syntheses are carried out for 6 days using 30 moles of each co-solvent. PXRD patterns indicate the formation of LTL for each of the co-solvents used. Among the three types of solvents used, a higher crystallinity is attained using TEG (30TEG-150-6, Figure 4.7 (c)) with the coexistence of another impurity phase whose feature peaks at 2θ of 7.5° and 13.5°. This impurity phase may be assigned as zeolite T. The formation of this phase is facilitated using lower synthesis temperatures (<150 °C).[115,116] Samples using EG (30EG-150-6, Figure 4.7 (a)) and DEG (30DEG-150-6, Figure 4.7 (b)) show the emergence of LTL crystals with the co-existence of amorphous materials.

SEM images are taken to observe the morphology and size attained when using the different types of solvents and also to confirm the formation of amorphous and crystalline materials observed from the PXRD analyses for 30EG-150-6 and 30DEG-150-6. Figure 4.8 (a) shows the SEM image when using 30EG-150-6. It is observed a mixture of amorphous and crystalline materials, which confirmed previously made assumptions. The shape of the crystals is hexagonal and the approximate length is 3 µm and the approximate diameter is 2 µm. The morphology of the LTL crystals is in accordance with the results shown in the literature[55,77] when a higher water content was applied in their synthesis gel mixture. Figure 4.8 (b) shows the crystals attained using 30DEG-150-6. It is noted that a

mixture between a coin-like shape, a long stick-like shape, and amorphous materials. The length of the cylindrical crystals were about 1.3 µm while the diameter of the coin-like crystals were about 2 µm and one of the stick-like crystal length had a length of approximately 11 µm.

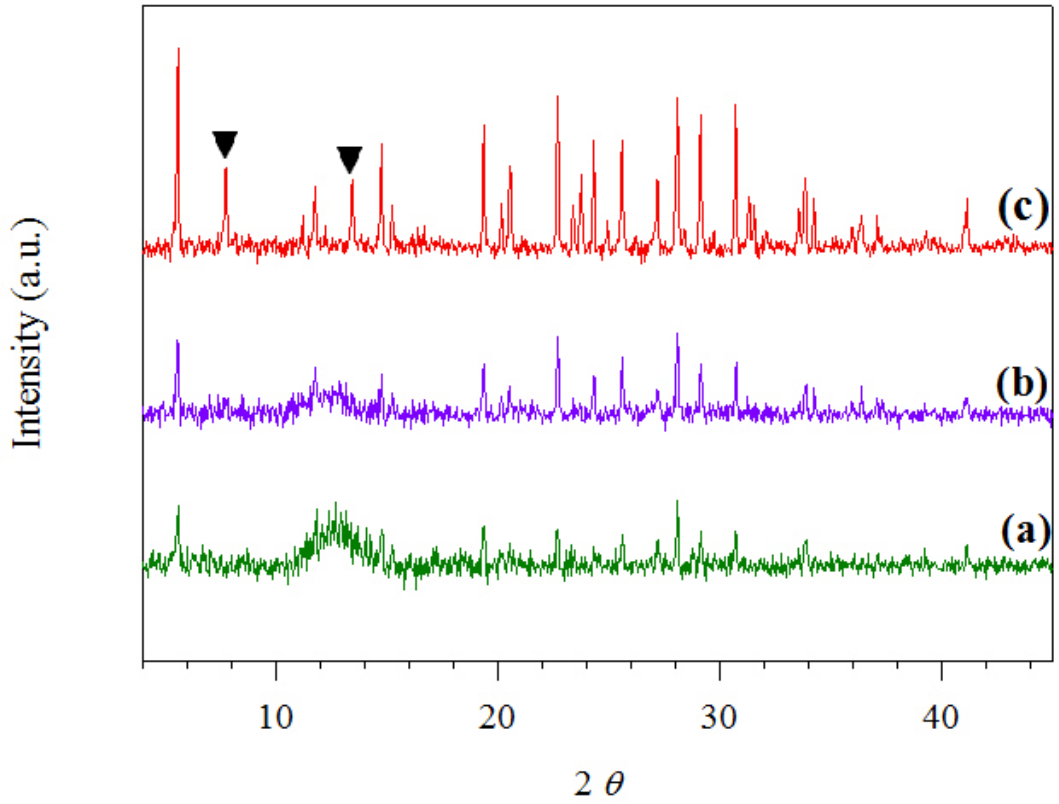

Figure 4.7. Powder XRD patterns attained at 150 °C for 6 days using $1Al_2O_3$:$20SiO_2$:$10.9K_2O$: 1000 H_2O: 30 $(OH)_2(CH_2)_{2n+2}O_n$ (n = 0,1,2). (a) $C_2H_6O_2$, (30EG-150-6); (b) $C_4H_{10}O_3$, (30DEG-150-6); (c) $C_6H_{14}O_4$, (30TEG-150-6). The solid triangles point out zeolite T phase.

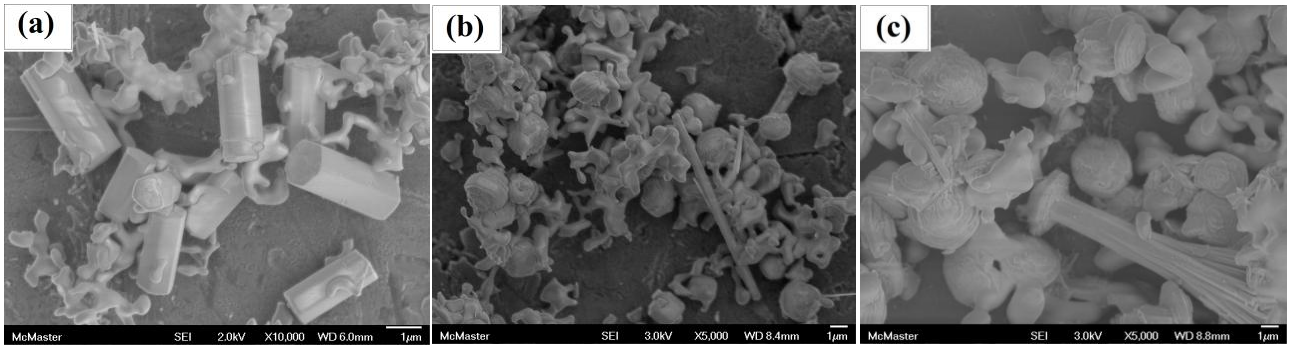

Figure 4.8. SEM images of LTL (LTL) using $1Al_2O_3$:($20SiO_2$:$10.9K_2O$:$1000H_2O$: $30(OH)_2(CH_2)_{2n+2}O_n$ (n = 0,1,2) for 6 days at 150 °C. (a) $C_2H_6O_2$, (30EG-150-6); $C_4H_{10}O_3$, (30DEG-150-6); $C_6H_{14}O_4$, (30TEG-150-6). The scale bar is 1 µm.

Figure 4.8 (c) shows the crystals morphology attained using 30TEG-150-6. It is noted a combination of single coin-like shape crystals, amorphous materials, hexagonal cylindrical shape, and bundle of narrow long crystals. The observation is interesting and my speculation is rational as follows:

first, it is known by previous studies[60,47] that the growth mechanism of LTL is favorable along the prismatic face or along the *c*-direction, where the typical shape of the crystals are long hexagonal cylinders. From Figure 4.8 (c), it can be observed a crystal constituted by two different shapes: a coin-like shape and a bundle of narrow long crystals. Thus, it appears that the pinacoidal faces of the coin-like shape crystal may have different active sites that may lead to the formation of the bundle of narrow crystals. Another possible explanation could be related to the scarcity of one of the elements in the gel composition. For instance, Lee *et al*[55] developed a series of experiments to observe the possible NaOH effect on the morphology of the crystals by reducing the amount of KOH and increasing the NaOH content. The morphology of the crystals was not severely affected (i.e, hexagonal cylindrical shape) until reduction of the molar concentration of KOH reached 6 from an initial molar concentration of 10.9 moles. Thus, attaining crystals attached to a set of narrow long crystals, only on one of the pinacoidal faces. This result could suggest that the amount of the mineralizing agent has a major effect in the nucleation and formation of the crystals, allowing the uniformity in the morphology structure of the crystals. A similar trend was observed by Larlus *et al,*[11] however, they attained tower-like structures. A particularity in their initial gel synthesis concentration was that the KOH used for this synthesis was 0.25 moles at 170 °C for 25 hours.

The length in the prismatic face of bundle of narrow long crystals of the crystals was about 10 µm, while the diameter of the coin-like shape crystals was approximately 3-3.5 µm. The SEM images in Figure 4.8 also show an intergrowth when using the different types of co-solvents. This intergrowth may due to the high content of potassium hydroxide, which is interrelated to the high pH environment. This result is in accordance with previously studies.[53,56]

It is observed from Figure 4.7 the presence of amorphous materials when 30EG-150-6 and 30DEG-150-6 is used. The appearance of amorphous materials indicates that longer synthesis duration may be required in order to attain crystalline materials. In order to confirm this assumption, an experiment was carried out for 15 days using 30DEG-150-15 (Figure 4.9 (b)). The PXRD shows a significant improvement compared to the PXRD from Figure 4.9 (a). However, it is observed the appearance of zeolite T peaks. Thus, it can be considered that when using DEG at higher concentration the attainment of pure LTL phase can be achieved between 6 to 15 days.

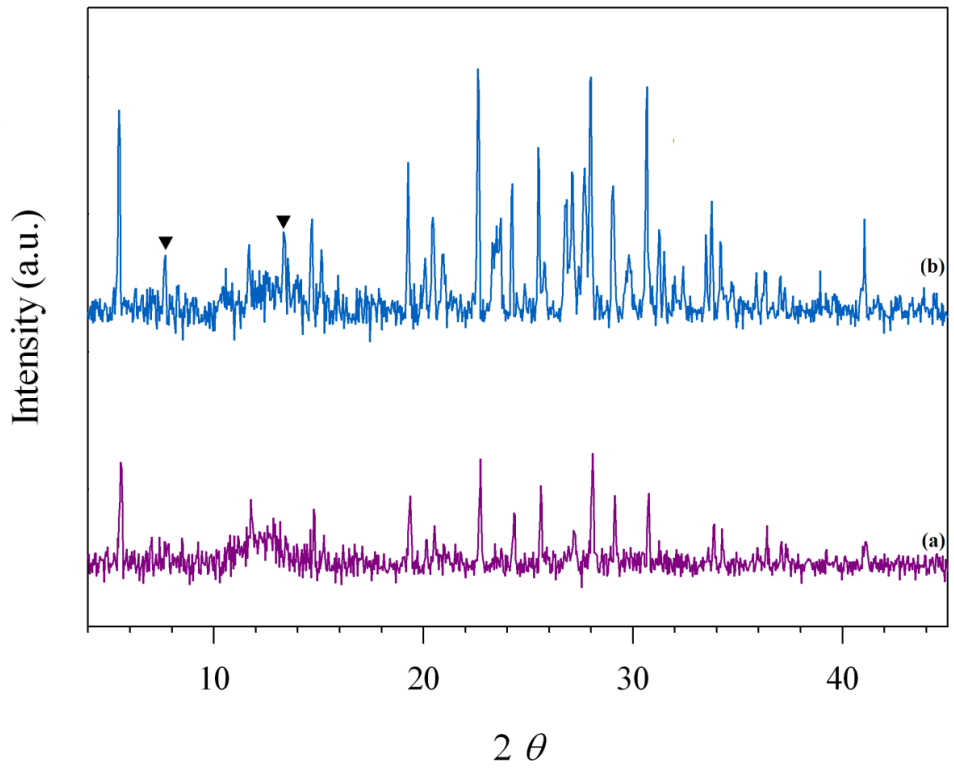

Figure 4.9. PXRD patterns attained using $1Al_2O_3$: $20SiO_2$: $10.9K_2O$: $1000H_2O$: 30 $C_4H_{10}O_3$ at 150 °C for different synthesis durations: (a) 6 days; (b) 15 days. The solid triangles points out the emerging peaks of zeolite T.

Figure 4.10 shows the SEM analysis implemented for the samples characterized in Figure 4.9. It can be observed the reduction of the amorphous materials. Moreover, it is observed two main different types of morphologies: needle-like and coin-like shape. The length in the pinacoidal face of needle-shape crystals varied between 8.98 to 22 µm, while the diameter of the coin-like shape crystals was approximately 2.73-3.45 µm.

Since the attainability of LTL phase was not pure when 30 moles of each of the co-solvents was implemented, we decide to conduct a series of experiments where the amount of each co-solvent is increased from 30 to 80 moles. The synthesis duration is also varied from 3 days to 6 days and the PXRD patterns are shown in Figure 4.11 and Figure 4.12, respectively.

Figure 4.11 shows that the characteristic peaks of LTL phase only start to emerge when the co-solvent used is TEG (80TEG-150-3, Figure 4.11 (c)). However, the amorphous phase is still dominant in Figure 4.11 (c).

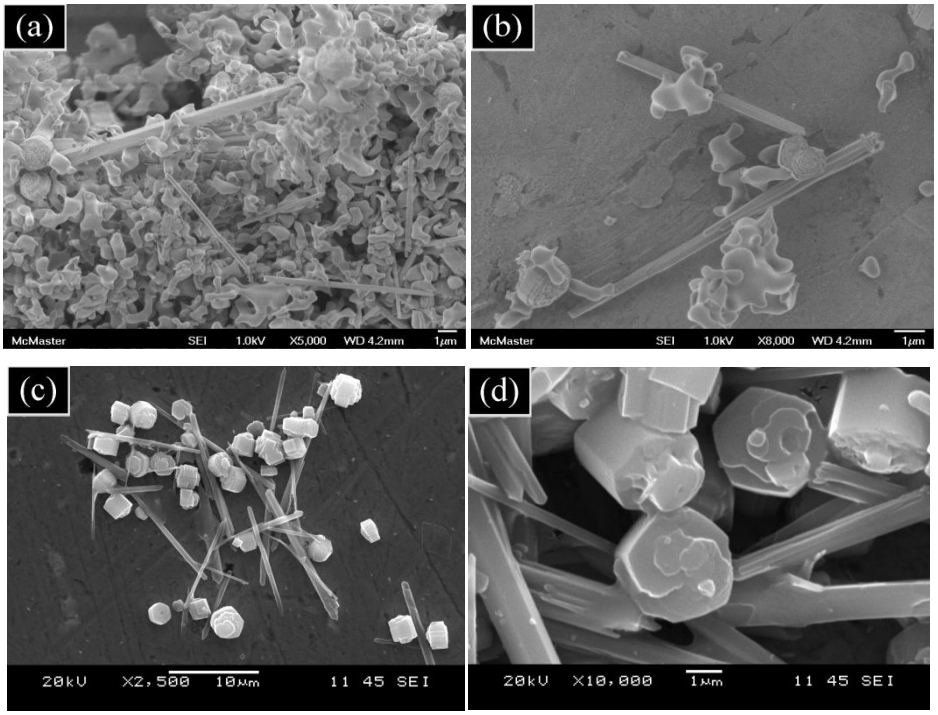

Figure 4.10. SEM image of Zeolite L (LTL) using $1Al_2O_3$:$20SiO_2$:$10.9K_2O$:$1000H_2O$: 30 $C_4H_{10}O_3$ for 6 days 150 °C for different synthesis durations: (a)-(b) 6 days; (c)-(d) 15 days**.**

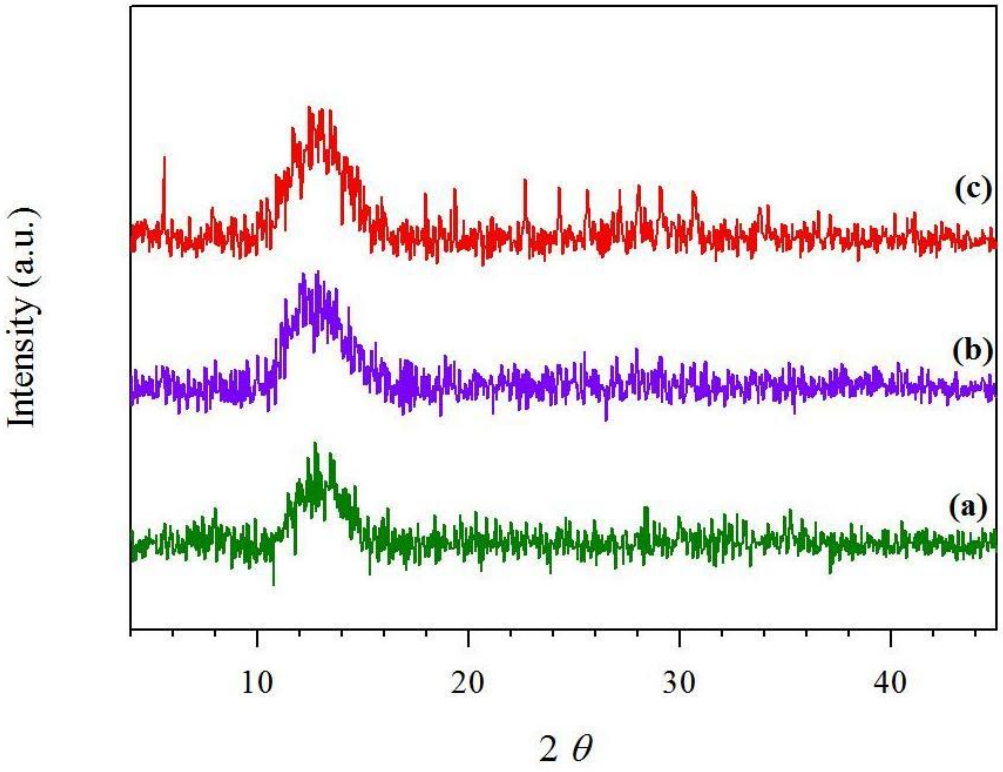

Figure 4.11. PXRD patterns attained using different types of co-solvents at 150 °C for 3 days using $1Al_2O_3$:$20SiO_2$:$10.9K_2O$: 950 H_2O: 80 $(OH)_2(CH_2)_{2n+2}O_n$ (n = 0,1,2). (a) $C_2H_6O_2$, (80EG-150-3); (b) $C_4H_{10}O_3$, (80DEG-150-3); (c) $C_6H_{14}O_4$, (80TEG-150-3).

On the other hand, the uses of EG (80EG-150-3) and DEG (80DEG-150-3) do not lead to the formation of LTL phase; only amorphous phase is observed. Comparing the results of co-solvent concentration effect (Figure 4.7 and Figure 4.11), we still observe that TEG behaves as the best co-solvent identity to induce the formation of LTL. By using the TEG identity, it is noted that the use of higher concentration favours the formation of LTL phase under the specific conditions (3 days at 150 °C). It can also be expected that, if the synthesis duration is prolonged to 6 days, then a stronger LTL phase should be observed when TEG is used.

Figure 4.12 shows the PXRD patterns for each co-solvent used when the synthesis duration is increased from 3 days to 6 days. The temperature is maintained at 150° C and 80 moles is used for each co-solvent. The results from these experiments corroborated the assumption that the formation of LTL phase is facilitated by the use of higher concentration of co-solvents in the synthesis gel. This trend has also been reported by Huang *et al*[117] when they utilized EtOH as the co-solvent to synthesize sodalite. Figure 4.12 (c), shows that a strong LTL phase is only attained when TEG (80TEG-150-6) is used. Moreover, Figure 4.12 (a) and Figure 4.12 (b) illustrate the results attained using EG (80EG-150-6) and DEG (80DEG-150-6), respectively. It can be observed that the formation of LTL phase is emerging with the co-existence of zeolite T when 80EG-150-6 is used as the co-solvent. It is interesting to notice that LTL features are weak using 80DEG-150-6 as the co-solvent under the elongated synthesis duration.

Figure 4.13 shows the SEM image of the sample which exhibits a high crystallinity. It can be observed that the morphology of LTL is dramatically changed compared to Figure 4.8 (c) where the amount of co-solvent has a major effect in the changing of morphology of the LTL. The morphology observed from Figure 4.13 is a cylinder-like structure. The dimension of the pinacoidal plane is about 1.5 to 1.8 µm in diameter, and that of the prismatic plane is about 1.5 to 1.8 µm, yielding an aspect ratio (prismatic/pinacoidal) of about 1.0. Both surfaces exhibit smooth surfaces, which is consistent with results.[55,38]

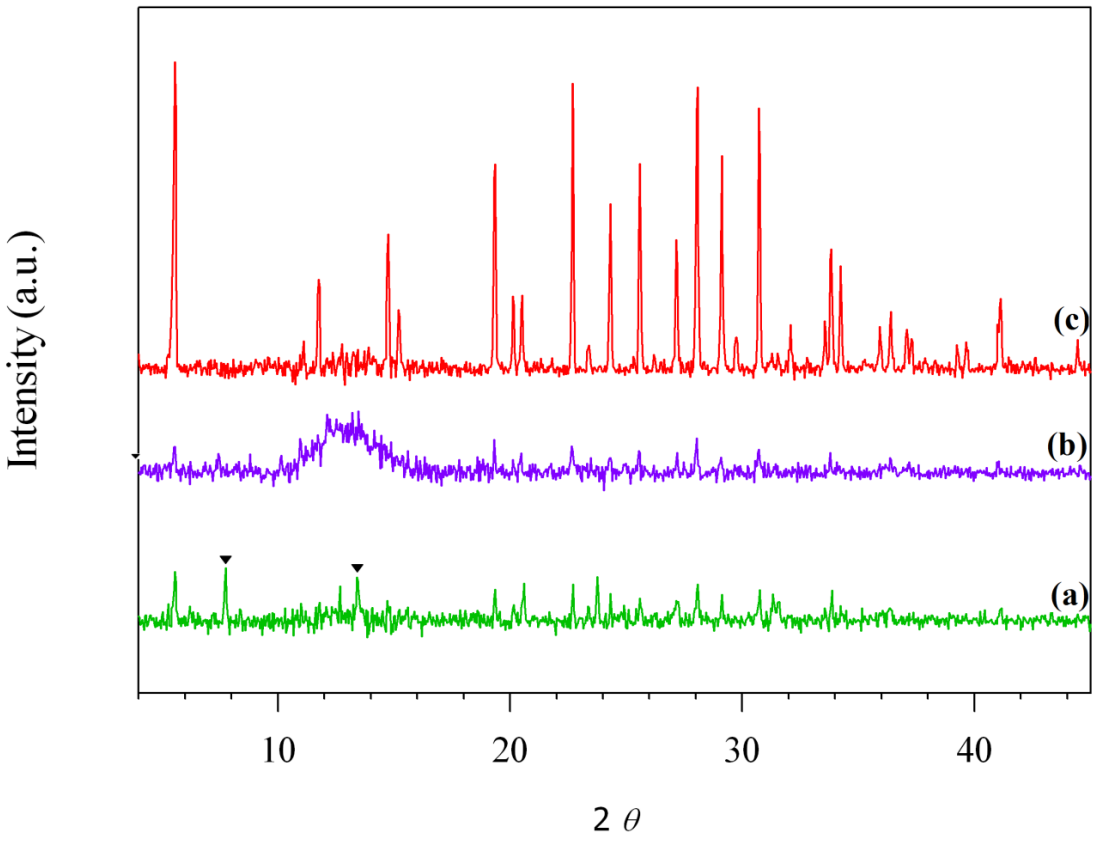

Figure 4.12. Powder XRD patterns attained at 150 °C for 6 days using $1Al_2O_3$:$20SiO_2$:$10.9K_2O$: 950 H_2O: 80 $(OH)_2(CH_2)_{2n+2}O_n$ (n = 0,1,2). (a) $C_2H_6O_2$, (80EG-150-6); (b) $C_4H_{10}O_3$, (80DEG-150-6); (c) $C_6H_{14}O_4$, (80TEG-150-6). The solid triangles represent the starting growth of zeolite T.

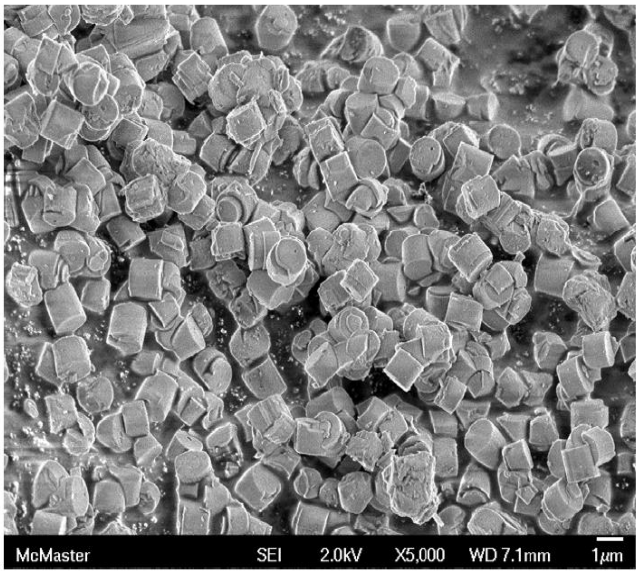

Figure 4.13. The SEM image of LTL (LTL) using $1Al_2O_3$:$20SiO_2$:$10.9K_2O$:$950H_2O$: $80C_6H_{14}O_4$ for 6 days at 150 °C.

From the analysis conducted to the co-solvent identity we can depict that when 30EG-150-6 is utilized for the syntheses of LTL, it is observed that LTL can be synthesized without the co-existence of zeolite T phase. However, the formation of LTL is accompanied with the presence of an amorphous material. An increase in the EG (80EG-150-6) concentration, leads to a favourable formation of the LTL phase. However, zeolite T phase is also formed when a higher concentration of EG is used.

Moreover, when the temperature is increased from 150° C to 180° C using 30EG-180-3 or 30EG-180-6, the formation of LTL phase is not observed. Instead, the interaction between the two parameters (i.e., temperature and concentration of co-solvent) results in the formation a cancrisilite phase. The increase of concentration, 80EG-180-3 or 80EG-180-6, have had the same outcome.

When 30DEG-150-6 is synthesized, a weak LTL phase is observed. Moreover, it is noted that the increase of the temperature from 150 °C to 180 °C allows for a decrease in the synthesis duration, resulting in the formation of a weak LTL phase after 3 days (30DEG-180-3). However, the PXRD diffractograms show a weak peak of LTL and the starting growth of the cancrisilite crystalline phase at 2 θ = 14° and 28.5°. The increase of temperature from 150 °C to 180 °C using 80DEG-180-3 does not lead to the formation of LTL phase. The increase of the synthesis duration to 6 days yielded the formation of weak LTL phase and the cancrisilite phase. The results attained using low and higher concentrations for DEG when the temperature is 180 °C suggest that, when DEG is used as the co-solvent, it is preferable to use lower concentration at a higher temperature in order to attain LTL phase.

When TEG is used at lower concentration (30TEG-180-3), the use of higher temperature (180 °C) leads to the appearance of LTL with cancrisilite phase around 2 θ = 14° and 28.5°. A further increase in the synthesis time (30TEG-180-6) does not lead to the formation of the LTL phase, instead only the cancrisilite material is formed with an increment of intensity of the peak around 2 θ = 14°. When lower synthesis temperature is implemented (150 °C), LTL is formed as well as zeolite T with characteristic peaks around 2 θ = 7.8° and 13.5° when 30TEG-150-3 is synthesized.

When TEG is applied at a higher concentration, the temperature effect can be observed in the formation of cancrisilite material and in the fast crystallization rate when higher temperature is implemented (180 °C). One can also speculate that the appearance of the cancrisilite phase can be treated as an indirect measure of the optimum synthesis conditions for the formation of LTL phase. To corroborate this assumption, a synthesis for 2 days is carried out to observe if a higher crystalline phase

LTL may be attained. Figure 4.14 shows the PXRD patterns for the synthesis of LTL conducted at 180 °C for different reaction times of 1, 2 and 3 days using 80 moles of TEG. The arrows in Figure 4.14 (a) show the emerging peaks of LTL. Figure 4.14 (b) shows that a high crystalline LTL phase can be obtained within 2 days. The formation of the cancrisilite material (2 θ = 14° and 28.5°) is minimized under the applied synthesis conditions. It can also be noted that the formation of LTL phase is facilitated using lower temperature (150 °C) when a higher concentration of TEG (80TEG-150-6) is used.

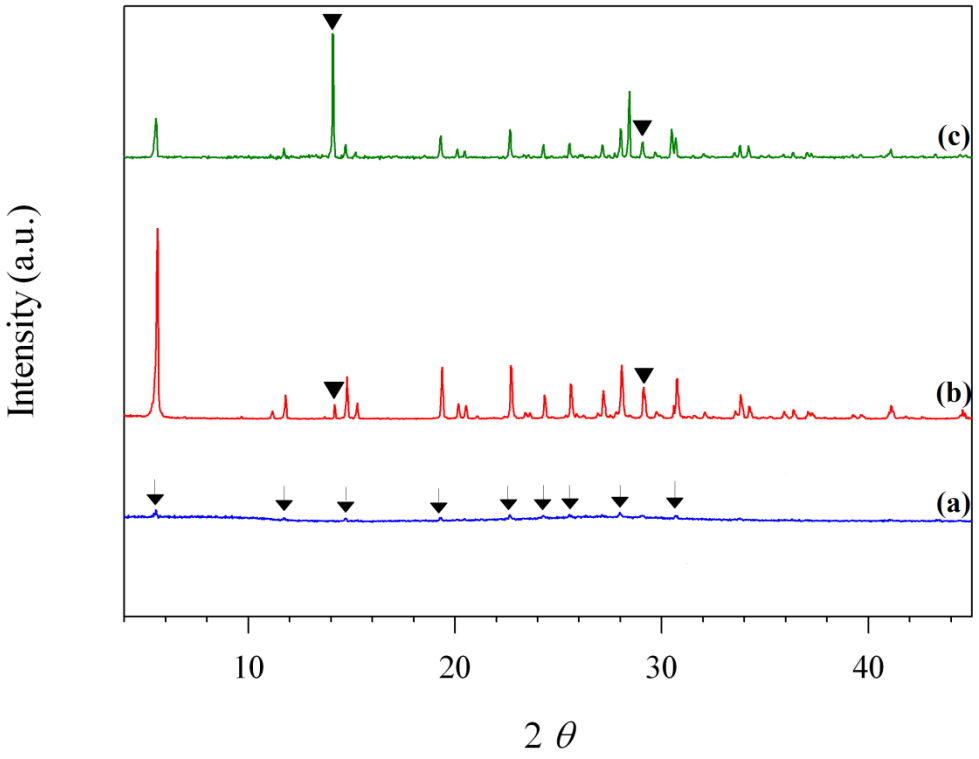

Figure 4.14. PXRD patterns attained using $1Al_2O_3$:$20SiO_2$:$10.9K_2O$:$950H_2O$: $80C_6H_{14}O_4$ at 180 °C for different synthesis durations: (a) 1 day, (b) 2 days, (c)3 days. The arrows are pointing the emerging peaks of LTL. The solid triangles represent the emerging peaks of cancrisilite.

4.1.3. Synthesis Temperature Effect

The effect of temperature on the synthesis of LTL has been reported by several researchers.[56,57,77] It has been concluded that temperature plays a major role on the synthesis of LTL. Thus, we will describe how the change in temperature has influenced the co-solvent identity and LTL morphology.

It is observed that the increase of the temperature from 150 °C to 180 °C leads to a higher crystallization rate to form LTL phase when TEG used as the co-solvent. This phenomenon may be

understood from the nucleation theory perspective.[2,118] Initially the gel mixture is aged at room temperature. A partially reacted phase is formed.[106] Moreover, based on literature suggestions[7], nuclei are also formed during the aging of the gel mixture. However, the nuclei do not possess the sufficient energy required to start the nucleation process to form the final zeolite structure. The use of temperatures above 100 °C allows overcoming this energetic barrier to form zeolite frameworks. The overcoming of the energetic barrier usually takes place in a specific period of time which is denominated as the induction period. This can take hours or even days. Experimental studies show that the induction time decreases while increasing the synthesis temperature.[119,120] The nucleation process starts after the induction time, and the appearance of a supersaturated solution. The supersaturated solution is the driving force for the nucleation process and the crystallization process (i.e., starting of the crystal growth) of zeolites.[2] It is also worth noting that the supersaturation not only depends on the synthesis temperature, but on the different ratios of the species present in the gel mixture.[118] The crystallization finalizes when the nutrients (i.e., chemical species present in the gel mixture) are depleted.[2]

Extrapolating the aforementioned concepts into the results attained in this study, PXRD results show the presence of LTL phase with amorphous materials after 3 days of hydrothermal synthesis at 150 °C using TEG (80TEG-150-3). Thus, it may be considered that 3 days is the induction period required to form LTL phase when using this synthesis temperature. On the other hand, the use of 180 °C decreases this induction time. This statement can be illustrated by the sample of 80TEG-180-1, on which the PXRD pattern shows the attainment of LTL with the presence of amorphous materials (Figure 4.14 (a)) after 1 day. Moreover, it is noteworthy that the formation of LTL using the procedure by Lee *et al*[55] only allows the attainment of LTL after 3 days of hydrothermal synthesis at a temperature of 180 °C. Thus, the application of TEG as the co-solvent to synthesize LTL using 180 °C can shorten the induction time and thus the crystallization time from 3 days to 1 day. Moreover, Ko and Ahn[121] observed that the increase of synthesis temperature from 100 and 170 °C allowed decreasing the induction time to form LTL phase and thus enhancing the crystallization rate. It is worth noting that the thorough study of the crystallization mechanism of LTL is out of the scope of this work.

Interestingly, the appearance of impurity phases can be observed for each temperature applied to the hydrothermal synthesis of LTL using co-solvents. For instance, when the temperature of 150 °C is applied, we notice the appearance of zeolite T phase featuring the diffraction peaks around 7.5° and 13.5°. Whereas, when the temperature is increased to 180 °C, a different impurity appears based on the

PXRD diffractogram around 14° and 28.5°, which is determined to be cancrisilite phase. The appearance of impurity phases has also been reported by Ban *et al.*[56] Although they could not identify them, the phenomena strongly indicate that the appearance of this peaks are a function of the temperature and is independent of the type of co-solvent used.

The effect of temperature on the morphology of LTL crystals is manifested in the attainment of homogeneous structures when using lower temperature. The increase in temperature from 150 °C to 180 °C leads to the deformation of the structure, as well as the non-uniformity of the length the crystals.

4.1.4. Synthesis Duration Effect

The PXRD patterns in Figure 4.15 shows the evolution of the different phases (i.e., cancrisilite and LTL) when varying the synthesis duration. The synthesis conditions such as temperature and amount of co-solvent are kept at 180 °C and 30 moles, respectively. It is observed that the change in the synthesis duration when EG is used only results in the formation of amorphous material after 1 day (Figure 4.15 (I), (a)) and the appearance of cancrisilite after 3 and 6 days (Figure 4.15 (I), (b-c)).

The use of DEG exhibits the formation of amorphous materials after 1 day (Figure **4.15** (II), (a)). The prolongation of the synthesis duration to 3 days (Figure 4.15 (II), (b)) leads to the formation of LTL and cancrisilite phase. When the synthesis durations is prolonged to 6 days (Figure 4.15 (II), (c)), it is observed the detriment of the LTL phase and an intensification of the cancrisilite phase (2 θ= 14° and 28.5°). Comparing the synthesis durations when TEG is used, it is observed that the hydrothermal synthesis conducted for 3 days allow attaining LTL and cancrisilite phase (Figure 4.15 (III), (b)). A reduction of the synthesis duration to 1 day (Figure 4.15 (III), (a)) produces amorphous material while prolonged synthesis duration (6 days) results in the total inhibition of LTL and the appearance of cancrisilite phase as shown in Figure 4.15 (III), (c).

Figure 4.16 (a) shows the morphology of the crystal that appears to be the cancrisilite phase from the PXRD pattern observed in Figure 4.15 ((I),(c)). Figure 4.16 (b) and Figure 4.16 (c) illustrate how a cylindrical structure of LTL is attained with the presence of cancrisilite phase when the gel is synthesized using 30DEG-180-3 (Figure 4.15 (II), (b)) and 30TEG-180-3 (Figure 4.15 (III), (b)), respectively.

Figure 4.17 illustrates the change in concentration from 30 to 80 moles and the variation of the synthesis duration for all the co-solvents used. TEG is the only co-solvent which shows a positive interaction when using higher temperature to form LTL phase. Moreover, Figure 4.17 (II), (c) shows a starting growth of LTL phase, when DEG is used after 6 days. Figure 4.18 shows the SEM images that shows the attainment of LTL phase according to the PXRD patterns from Figure 4.17 Comparing Figure 4.16 with Figure 4.18, it can be observed that the increment of the concentration lead to better crystalline structures of LTL when DEG and TEG are used respectively. Based on the results attained in Figure 4.15 and Figure 4.17, it is corroborated the metastability of the phases, which also confirms that the Ostwald mechanism is also observed in this system. Thus, when using 180 °C and the synthesis duration is prolonged, the cancrisilite phase is the most stable phase.

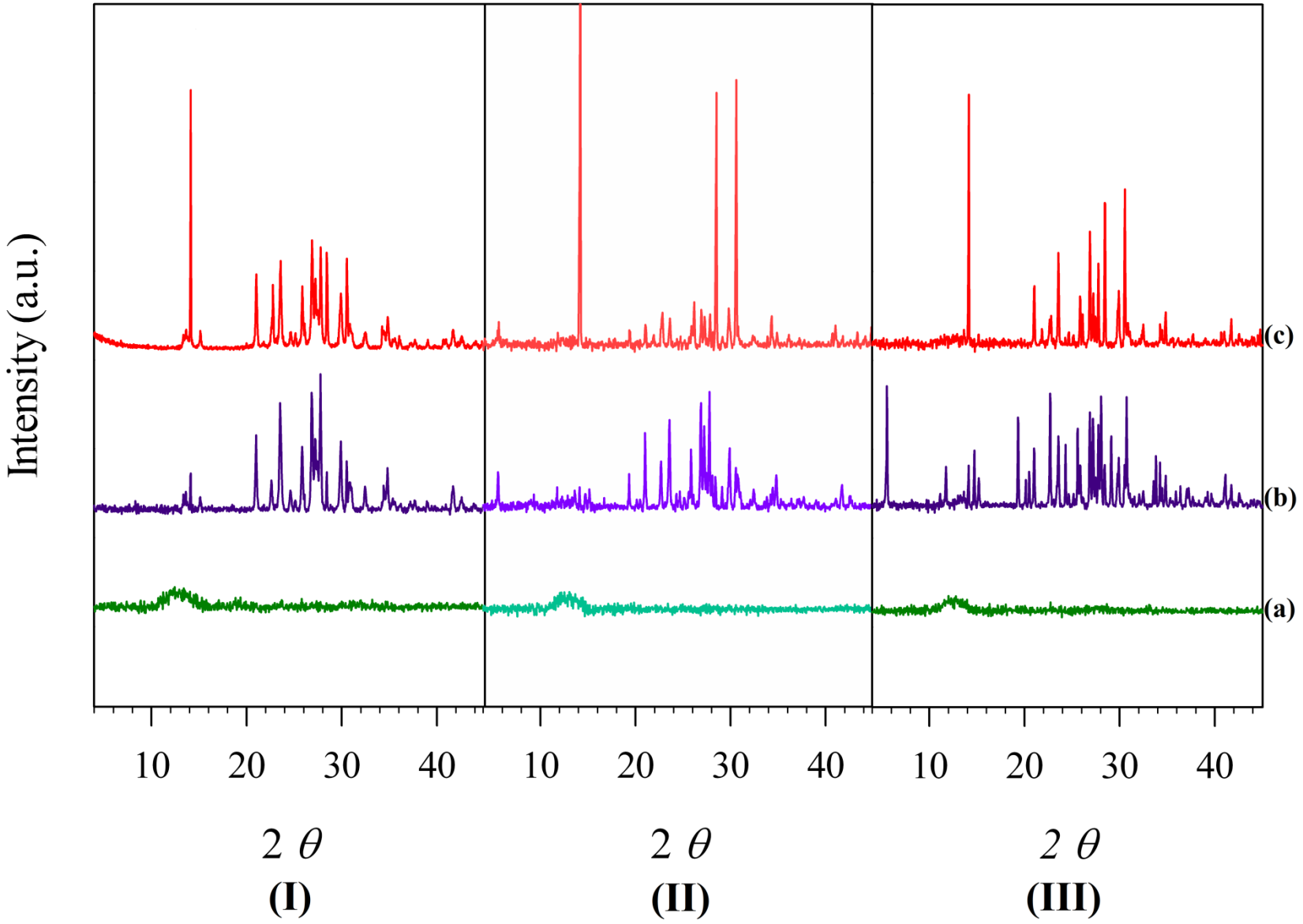

Figure 4.15. PXRD patterns at 180 °C using $1Al_2O_3$:$20SiO_2$:$10.9K_2O$: 1000 H_2O: $30(OH)_2(CH_2)_{2n+2}O_n$ (n = 0,1,2). (I) $C_2H_6O_2$; (II) $C_4H_{10}O_3$; (III) $C_6H_{14}O_4$. where (a), (b) and (c) represents 1, 3 and 6 days respectively

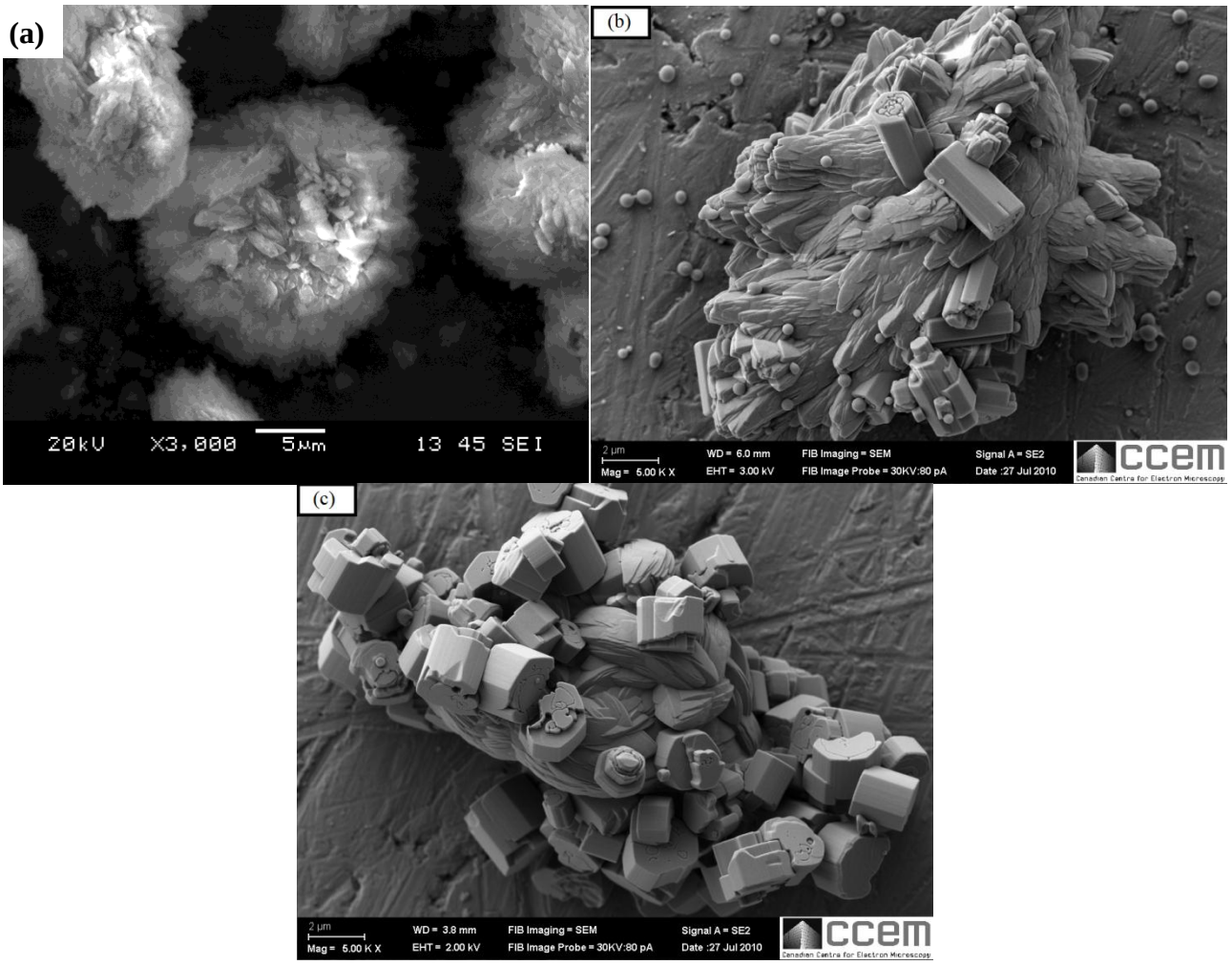

Figure 4.16. SEM images of zeolite L and cancrisilite material using $1Al_2O_3$:$20SiO_2$:$10.9K_2O$: 1000 H_2O: 30 $(OH)_2(CH_2)_{2n+2}O_n$ (n = 0,1,2) at 180 °C (a) $C_2H_6O_2$, (30EG-180-6); (b) $C_4H_{10}O_3$,(30DEG-180- 3); (c) $C_6H_{14}O_4$, (30TEG-180-3).

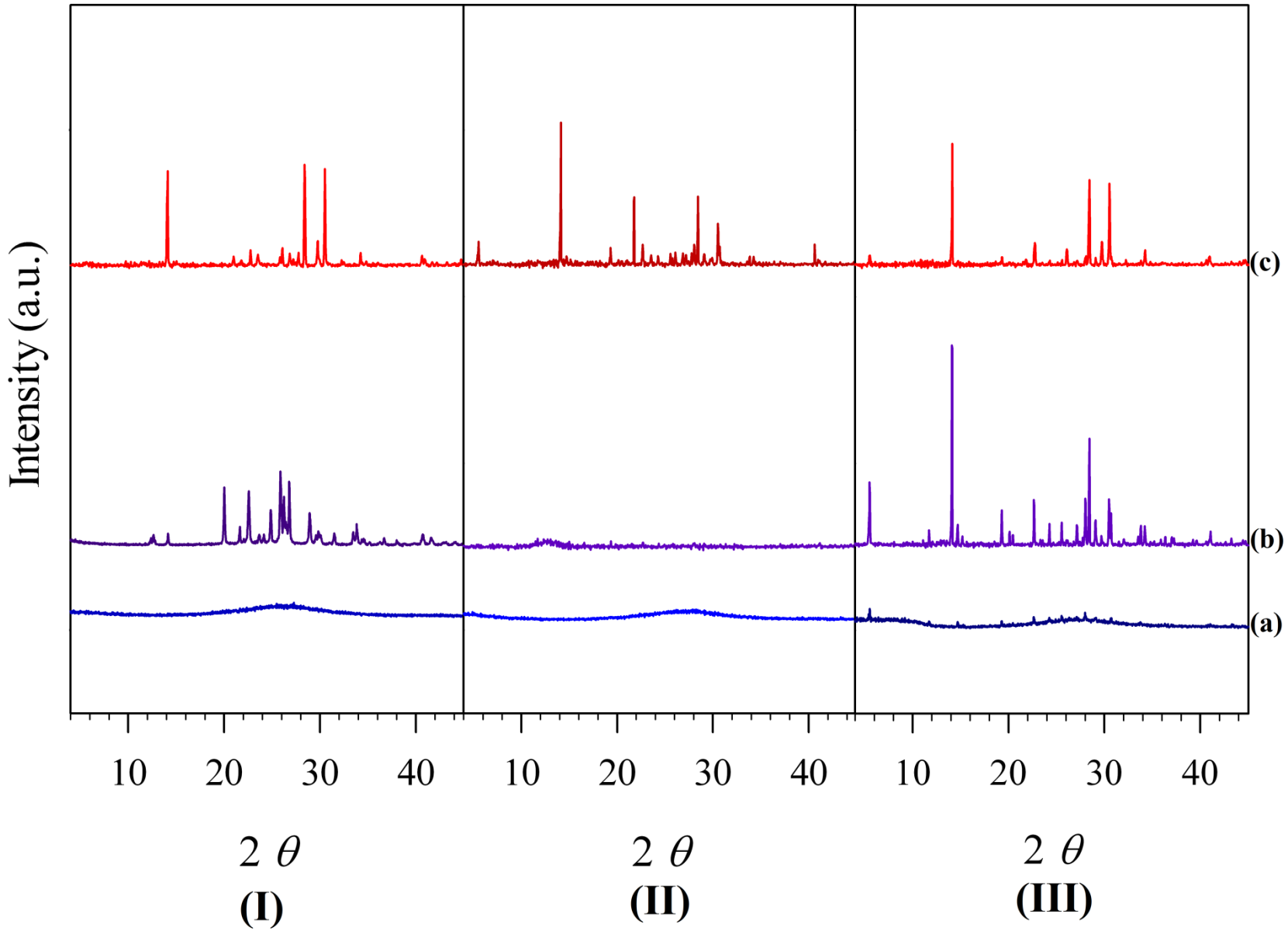

Figure 4.17. PXRD patterns at 180 °C using $1Al_2O_3$:$20SiO_2$:$10.9K_2O$: 950 H_2O: 80 $(OH)_2(CH_2)_{2n+2}O_n$ (n = 0,1,2). (I) $C_2H_6O_2$; (II) $C_4H_{10}O_3$; (III) $C_6H_{14}O_{4..}$ where (a), (b) and (c) represents 1, 3 and 6 days, respectively.

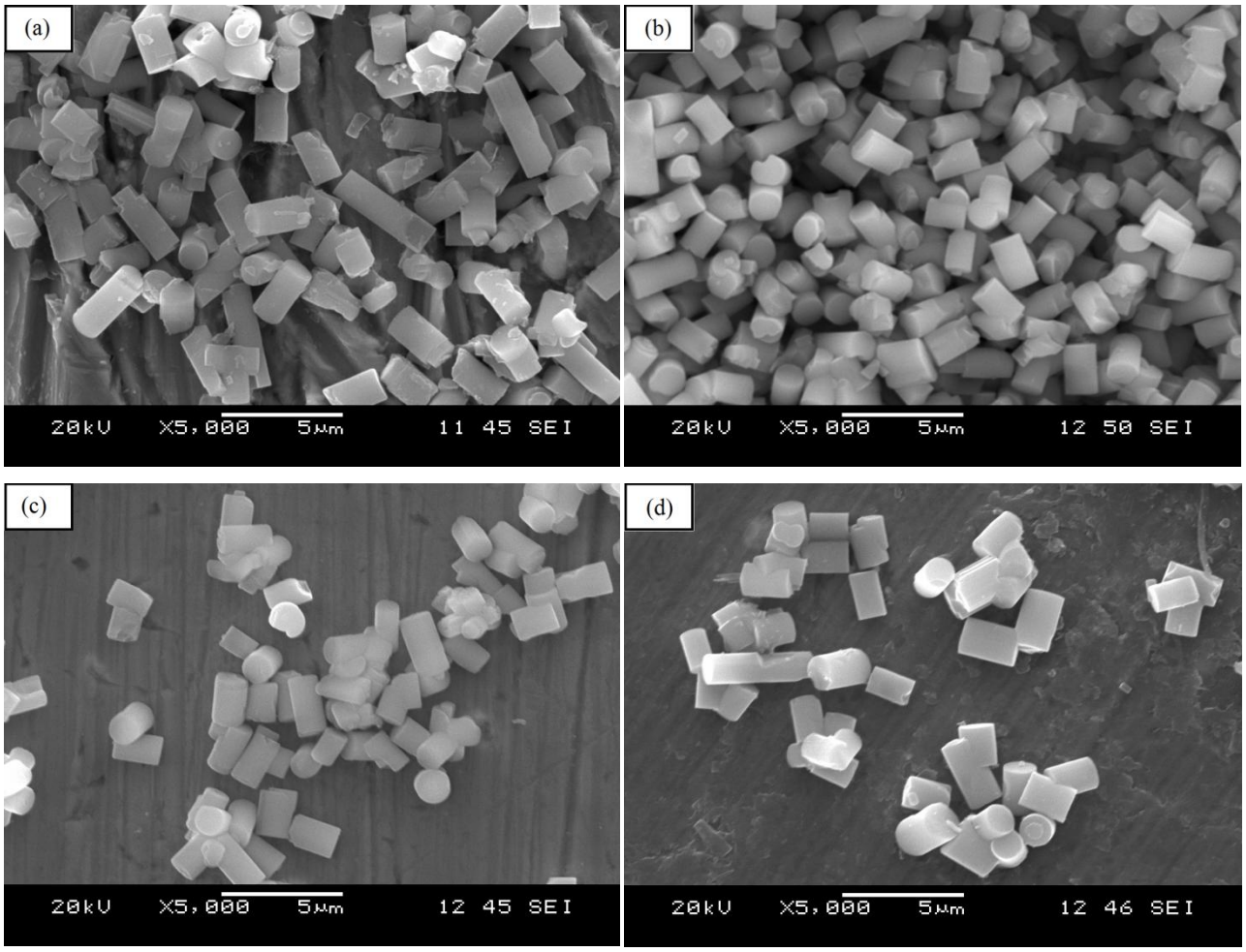

Figure 4.18. SEM images of LTL crystals using $1Al_2O_3$:$20SiO_2$:$10.9K_2O$: 950 H_2O: 80 $(OH)_2(CH_2)_{2n+2}O_n$ (n = 0,1,2) at 180 °C. (a) $C_6H_{14}O_4$, (80TEG-180-2); (b) $C_6H_{14}O_4$, (80TEG-180-3); (c) $C_6H_{14}O_4$, (80TEG-180-6); (d) $C_4H_{10}O_3$, (80DEG-180-6)

4.1.5. Effect of Aging Time

The aging of the synthesis gel mixture at room temperature prior to the hydrothermal synthesis is often used to tailor the size of zeolite crystals.[11,122] Moreover, the effect of aging has also been studied to reduce the formation of undesired phases, particularly in the synthesis of zeolite Y.[123] Since strong characteristic peaks of LTL and the formation of cancrisilite phase are observed in the PXRD patterns after 3 days when 80 moles of TEG are used and the hydrothermal syntheses are carried out at 180 °C. We have focused our efforts to analyze the effect of aging time while maintaining the synthesis duration, temperature, and co-solvent concentration constant in order to determine if the aging time contributes to the reduction of the cancrisilite phase.

Figure 4.19 shows the PXRD patterns for products whose aging time is varied from 16, 17.5, 22, 32, and 72 hours. According to Figure 4.19, increasing the aging time significantly amplifies and narrows the intensity of the characteristic peak of LTL around 2 θ = 5.5º compared to the one prepared with the standard aging time of 16 hours. A further examination of the PXRD patterns also reveals that the peak intensity (2θ =14°) of the cancrisilite phase decreases only when the aging time is 22 hours (Figure 4.19 (c)). It is not clear why the peak becomes more prominent when the aging time is further increased. We may assume that there is a workable range where the aging time for the specific gel composition would suppress the formation of the cancrisilite phase under thermal synthesis conditions. It is proposed the range is between 17.5 < 22 < 32 hours.

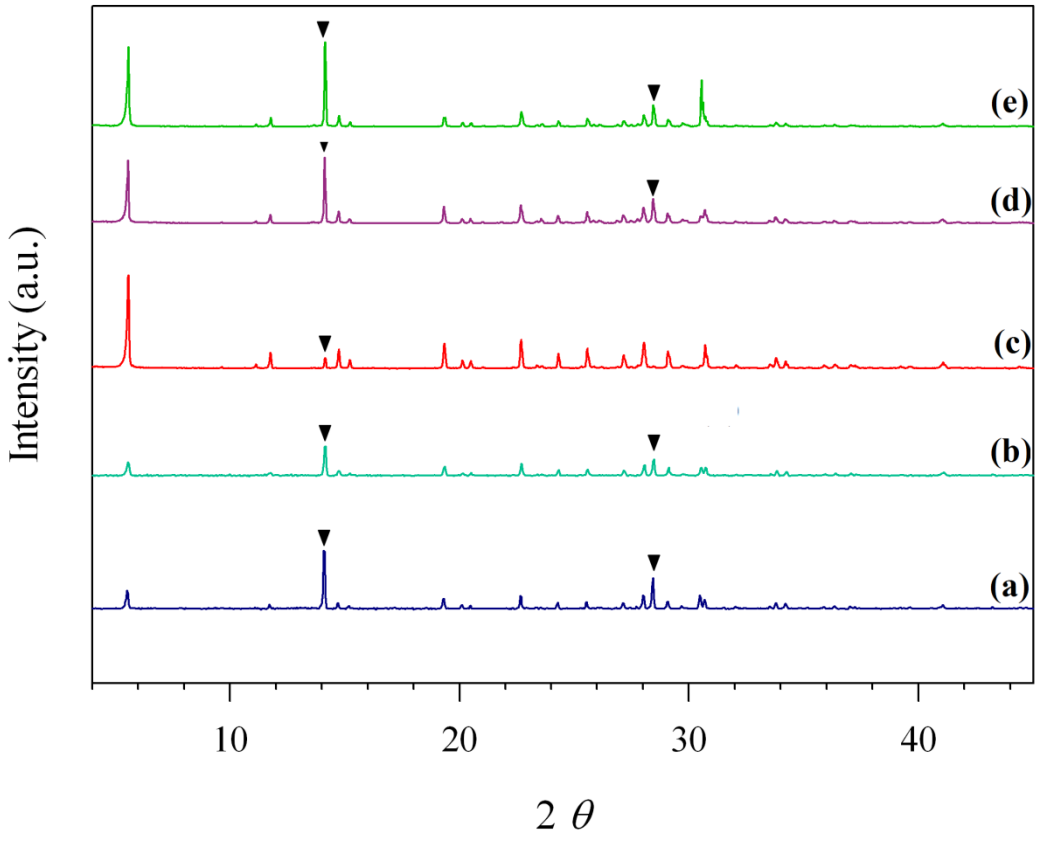

Figure 4.19. PXRD patterns of Zeolite L synthesized at 180 ºC for 3 days using $1Al_2O_3$:$20SiO_2$:$10.9K_2O$: 950 H_2O: 80 $C_6H_{14}O_4$. (a) aging time for 16 hours;, (b) aging time for 17.5 hours, (c) aging time for 22 hours; (d) aging time for 32 hours; (e) aging time for 72 hours. The solid triangles points out the emerging peak of cancrisilite phase.

Figure 4.20 shows SEM analyses conducted to the PXRD patterns from Figure 4.19. It can be observed well-defined LTL crystals using 80TEG-180-3 when the aging of the gel has been varied for all the samples. It is observed that the morphology of the LTL in all the samples have a cylindrical form. Table 4.1 contains the summary of the dimensions of the prismatic plane and the pinacoidal face for all

the samples. It can be noted that there is a reduction of the size of the pinacoidal face from 1.3 to 0.92 µm. However, the prismatic face only shows this trend for the sample aged up to 22 hours. When the sample is aged for 32 hours, the prismatic face dimension is increased again (1.74 µm). A further aging of the gel (72 hours) leads to further decrease on the prismatic face dimension of around 1.53 µm.

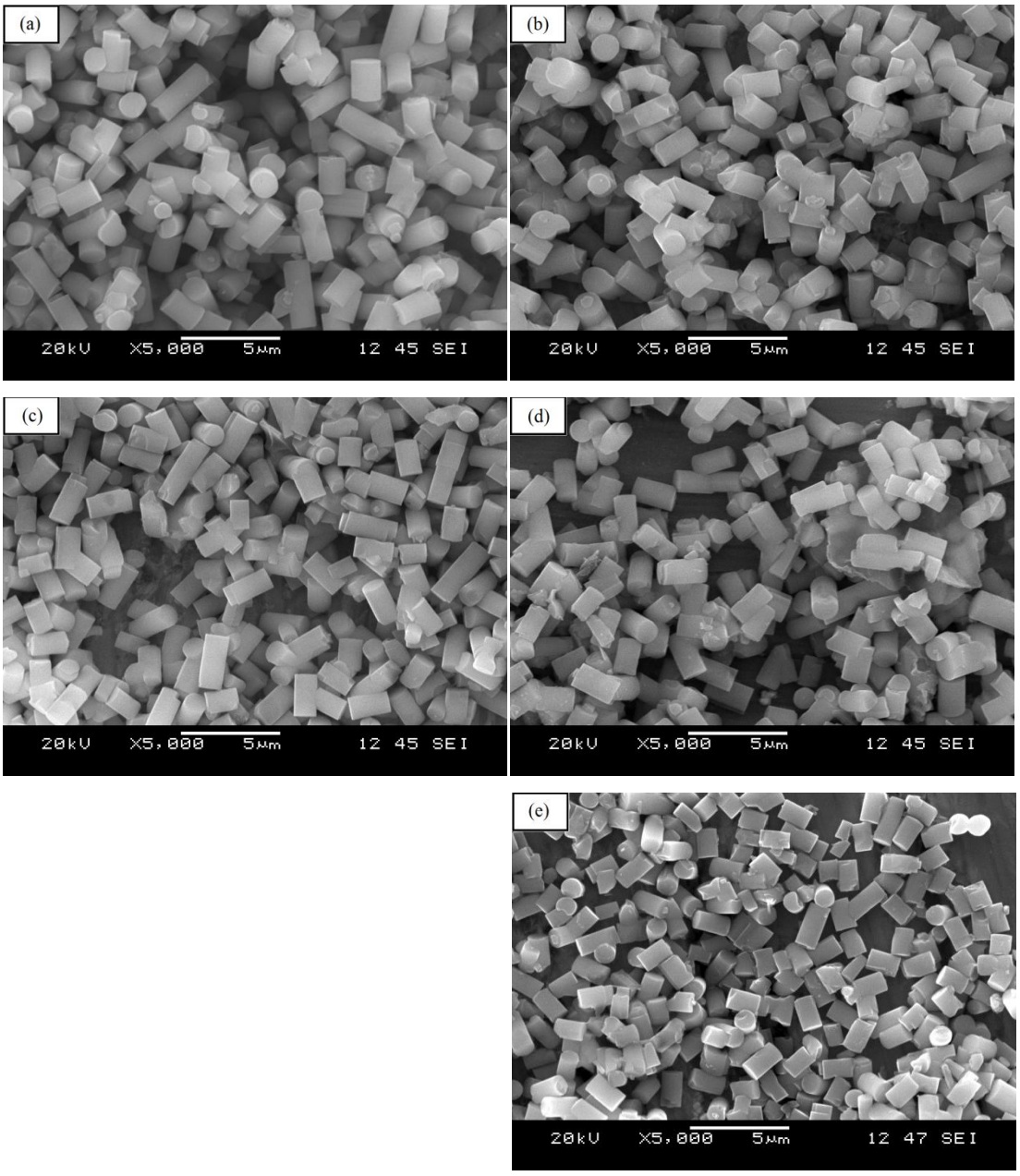

Figure 4.20. SEM images of LTL crystals using $1Al_2O_3$:$20SiO_2$:$10.9K_2O$: 950 H_2O: 80 $C_6H_{14}O_4$ at 180 °C for 3 days. (a) aged for 16 hours; (b) aged for 17.5 hours; (c) aged for 22 hours; (d) aged for 32 hours; (e) aged for 72 hours.

Table 4.1. Summary of dimensions of LTL crystals attained using different aging time

Figure 4.20	(a)	(b)	(c)	(d)	(e)
Prismatic face (μm)	2.00± 0.73	1.98±0.18	1.54±0.36	1.74± 0.14	1.53±0.58
Pinacoidal face (μm)	1.30± 0.10	1.16±0.10	1.11±0.06	1.10±0.04	0.92±0.04
Aspect Ratio	1.53	1.7	1.38	1.59	1.66

4.1.6. NMR Analyses

The PXRD patterns indicate that a strong LTL phase is attained using a high concentration of co-solvents at 150 ºC for 6 days. Therefore, it is expected that a higher temperature (180 ºC) will assist in the formation of LTL phase at a shorter synthesis duration when higher concentration (80 moles) of any of the co-solvents are utilized. However, the aforementioned assumption is only correct when TEG is used.

The ability of TEG to assist in the formation of LTL makes us question why this phenomenon is occurring. Moreover, why have similar results not been observed with the other two co-solvents? The only visible difference among the three co-solvents is the change in the colour of all the TEG samples from a milky white to an opaque beige colour after the solution is aged for 16 hours. Meanwhile, the colour for the EG samples remains milky white after the aging time (16 hours) and the colour of DEG only turns to a very light beige colour under the same condition. Thus, the change in the colour of TEG precursor solution prior to the hydrothermal synthesis may be an indication that the chemical structure of the TEG has possibly been changed during the aging process. To corroborate this assumption, it is decided to analyze the aged gel mixtures prepared with the three co-solvents using ^{1}H-NMR and ^{13}C-NMR spectroscopy techniques. Figure 4.21 shows the structure of each co-solvent. The results attained from ^{1}H-NMR and ^{13}C-NMR analyses are listed in Table 4.2 to Table 4.6. The ^{1}H-NMR and ^{13}C-NMR spectra of the pure co-solvents are found in Appendix A (i.e., Figure A.1-A.6).

Figure 4.22, Figure 4.23, and Figure 4.24 show the ^{1}H-NMR analyses for aged precursor solution containing EG, DEG, and TEG, respectively. Table 4.2, Table 4.3 and Table 4.4 compare resonance signals between the benchmark and the aged sample. In Table 4.2, it can be observed that the EG molecule shows a difference in the resonance of about 0.04 ppm. This phenomenon may be attributed to accuracy of the machine which lies in a range of ± 5%.[109]

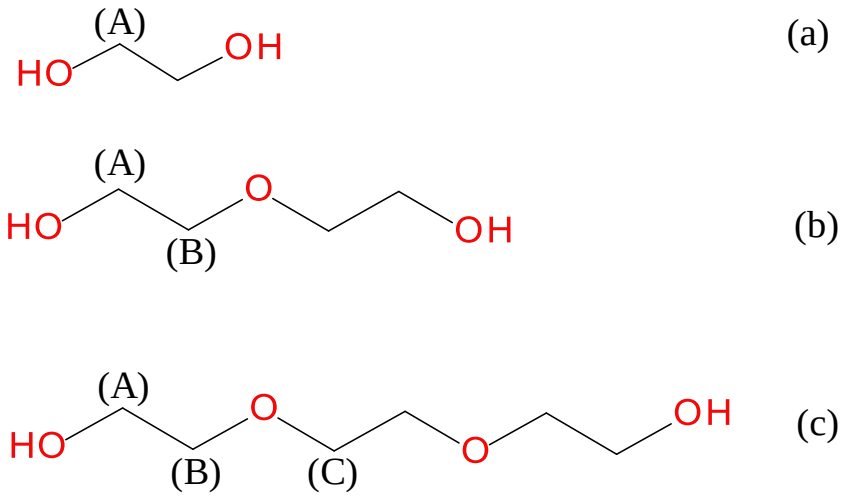

Figure 4.21. Molecular structure of each co-solvents. (a) EG; (b) DEG; (c) TEG

Table 4.3 presents the summary for the chemical shifting acquired when ^{1}H-NMR measurement is conducted to the aged precursor solution containing DEG. There is a difference of 0.02 ppm between the spectra. However, the accuracy of the ^{1}H-NMR measurement lies in the range of ± 5%.[109] Therefore, this change in 0.02 ppm is not accounted as the deshielded effect.

Table 4.4 shows the comparison of resonance signals between the benchmark and the aged sample. It is observed that no chemical shifting can be observed. These values indicate that the structure of TEG molecules has been maintained after the 16 hours of aging of the gel.

Table 4.2. Summary of chemical shifting in ^{1}H-NMR spectrum for EG molecule

	Benchmark Sample (ppm)	**Aged Sample (ppm)**
(A)	3.61	3.65

Table 4.3. Summary of chemical shifting in ^{1}H-NMR spectrum for DEG molecule

	Benchmark Sample (ppm)	**Aged Sample (ppm)**
(A)	3.710	3.710
(B)	3.615	3.613

Table 4.4. Summary of chemical shifting in ^{1}H-NMR spectrum for TEG molecule

	Benchmark Sample (ppm)	**Aged Sample (ppm)**
(A)	3.730	3.727
(B)	3.700	3.699
(C)	3.610	3.610

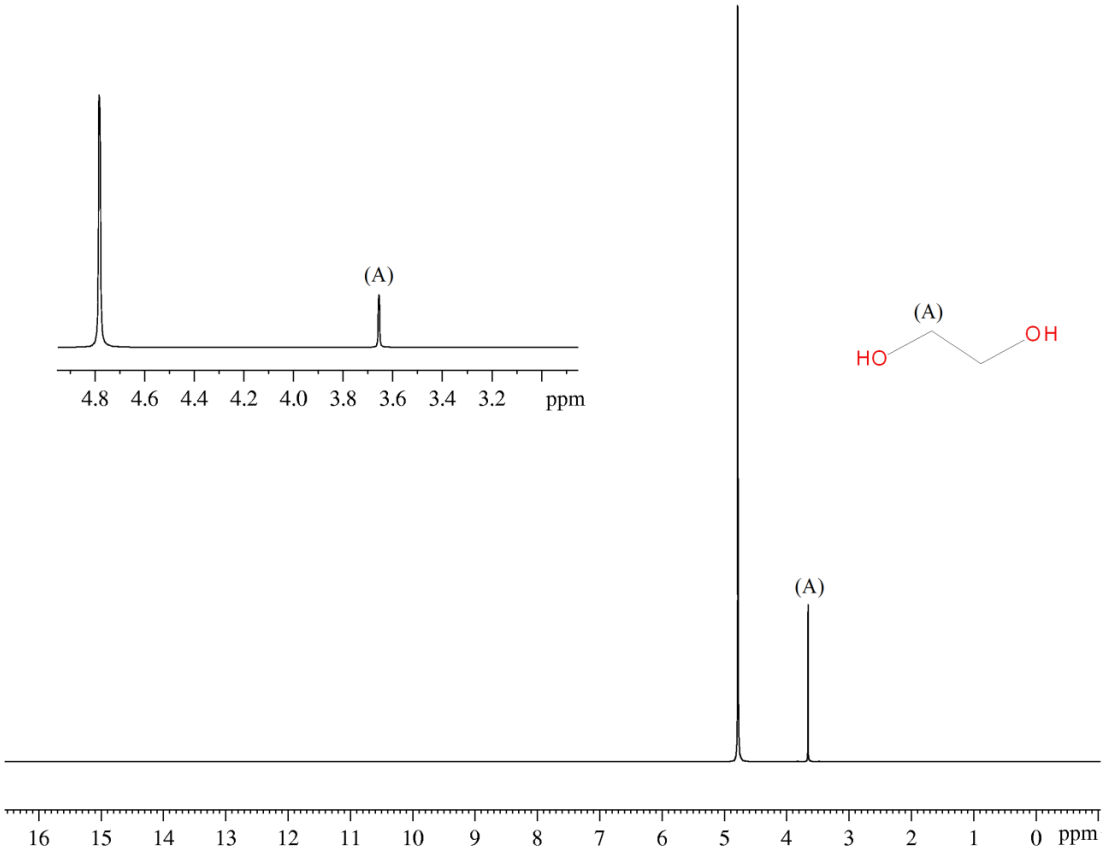

Figure 4.22. ^{1}H-NMR spectrum for the EG-contained precursor solution aged for 16 hours (D_2O, 400 MHz)

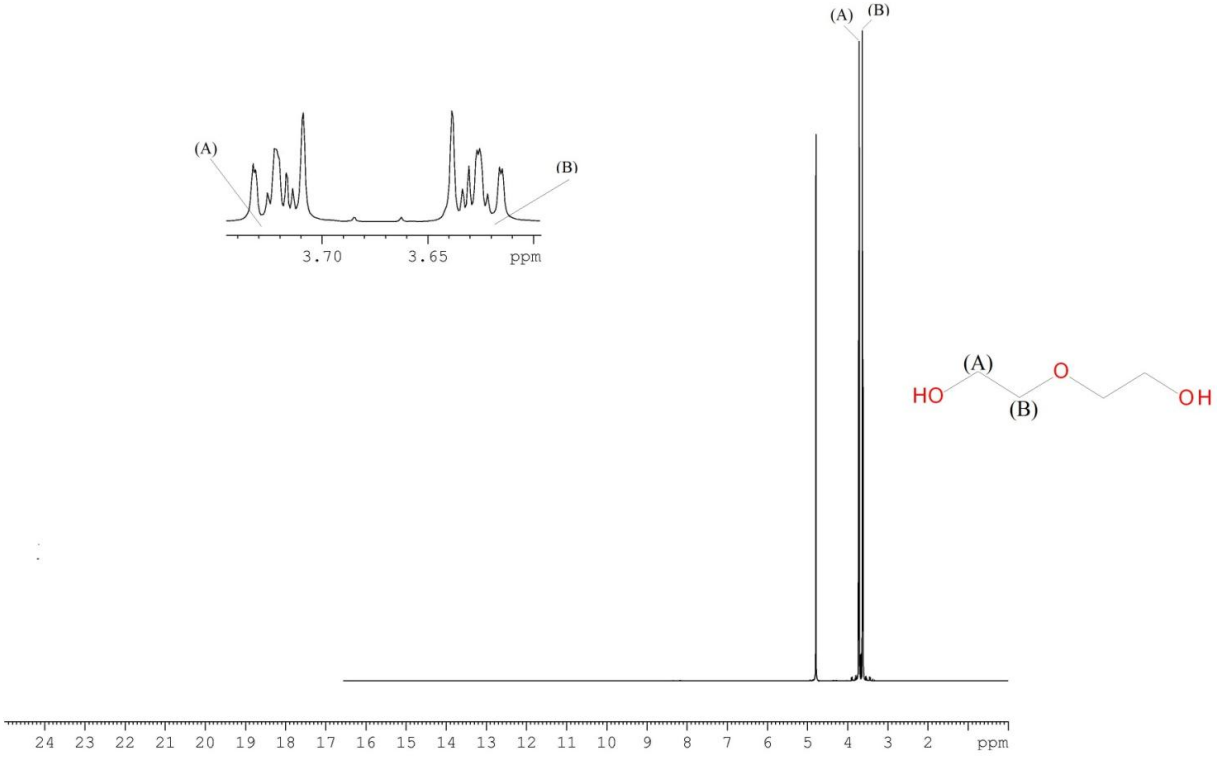

Figure 4.23. ^{1}H-NMR spectrum for DEG-contained precursor solution aged for 16 hours (D_2O, 400 MHz).

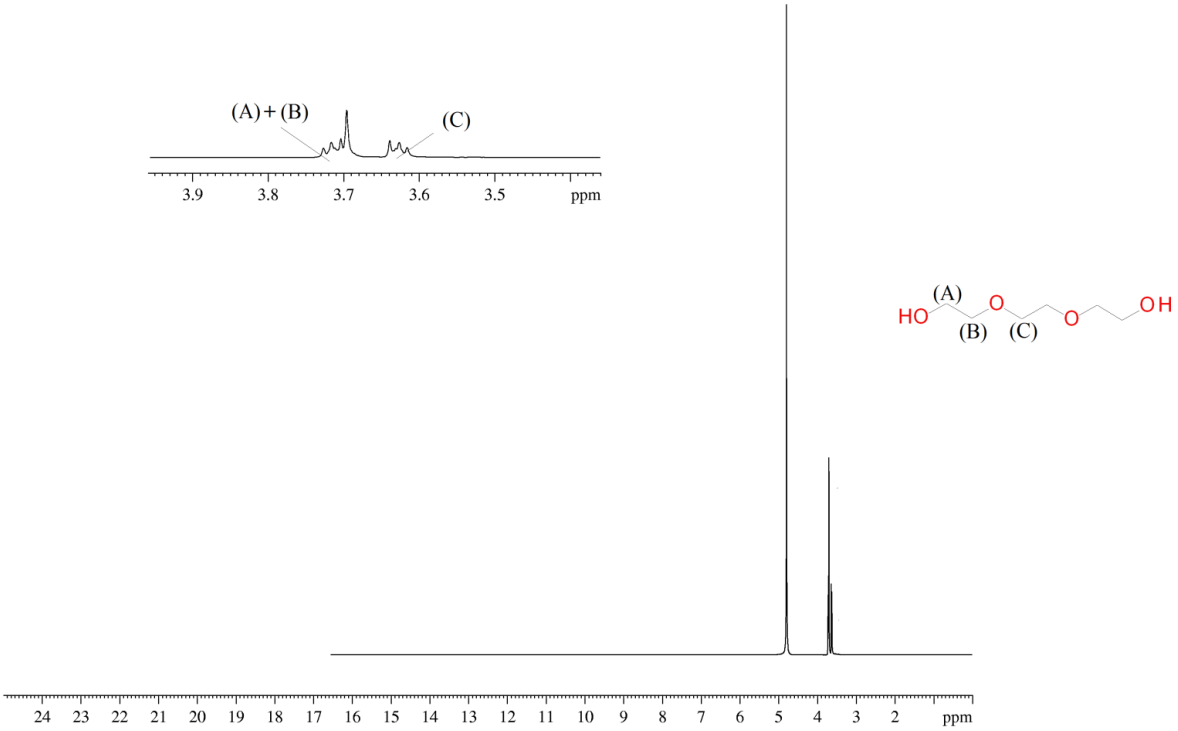

Figure 4.24. ^{1}H-NMR spectrum for TEG-contained precursor solution aged for 16 hours (D_2O, 400 MHz)

Figure A.4, Figure A.5, and Figure A.6 show ^{13}C-NMR spectra of pure EG, DEG, and TEG correspondingly. The resonance values obtained from these spectra are used as the benchmark for those samples aged at room temperature for 16 hours. Table 4.5 shows the summary of resonance signals in each spectrum.

Table 4.5. Summary of resonance signals in ^{13}C-NMR spectra of pure EG, DEG, and TEG

	EG	**DEG**	**TEG**
(A)	63.224	71.886	72.307
(B)		60.869	69.930
(C)			60.960

Table 4.6 shows the summary of resonance signals obtained when the precursor solutions containing each corresponding co-solvent are aged. The DEG molecule has the most significant shifting effect when the resonance signals are compared with the pure co-solvent listed in Table 4.5. This phenomena may be attributed to the entrapment of the DEG molecule, where similar results have been reported by Ossenkamp *et al*,[124] when molecules containing alcohol groups were in contact with precipitated silica and followed a subsequent reaction among them (i.e., esterification of silanols). The ^{13}C-NMR spectra showed an increase in the chemical shift of anchored alcohol groups on silica surface

when compared to physisorbed alcohol groups. Moreover, a similar downfield shifting of resonance signals can be observed in TEG ^{13}C-NMR spectrum. The ^{13}C-NMR spectra of aged gel precursor solutions containing co-solvents are shown in Figure 4.25, Figure 4.26 and Figure 4.27.

Table 4.6. Summary of resonance signals in ^{13}C-NMR spectra of EG-, DEG-, and TEG-contained zeolite precursor solutions

	EG	**DEG**	**TEG**
(A)	63.625	71.310	72.653
(B)		61.810	70.290
(C)			61.586

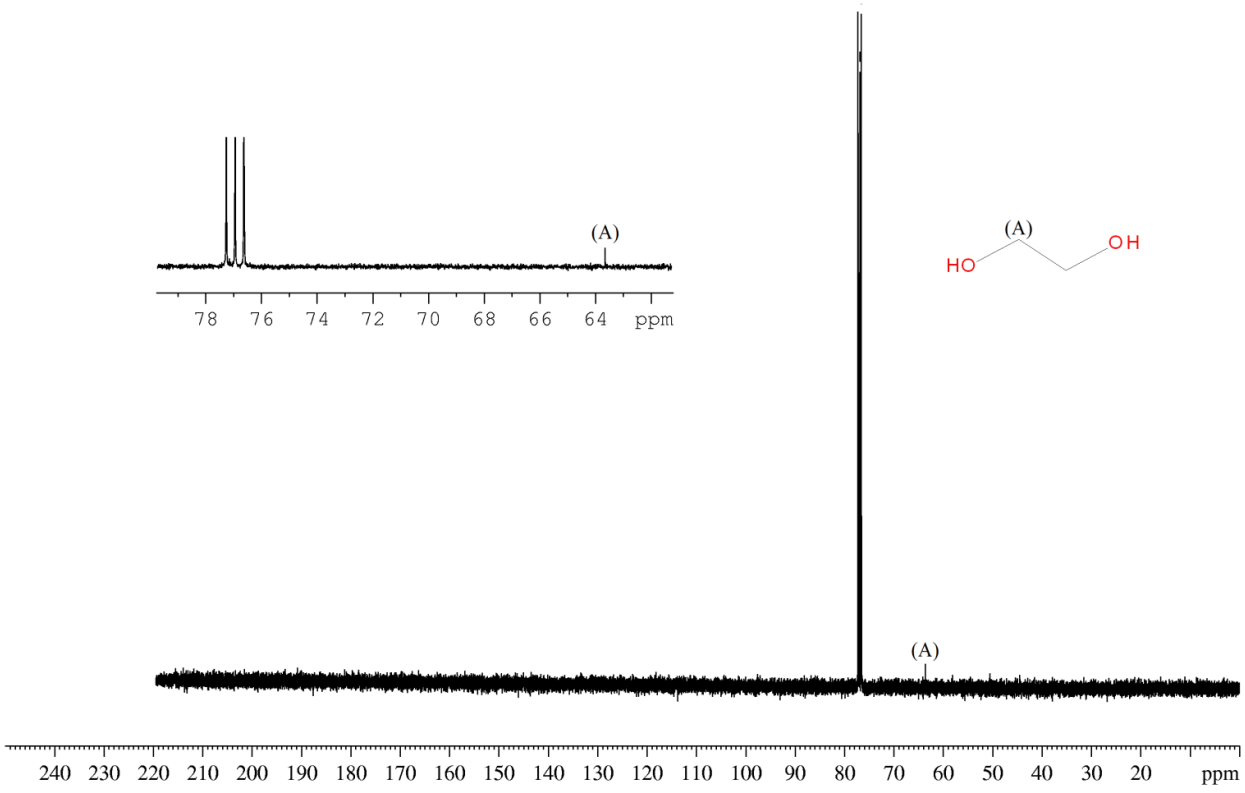

Figure 4.25. ^{13}C-NMR spectrum for the aged precursor solution containing EG ($CDCl_3$, 400 MHz)

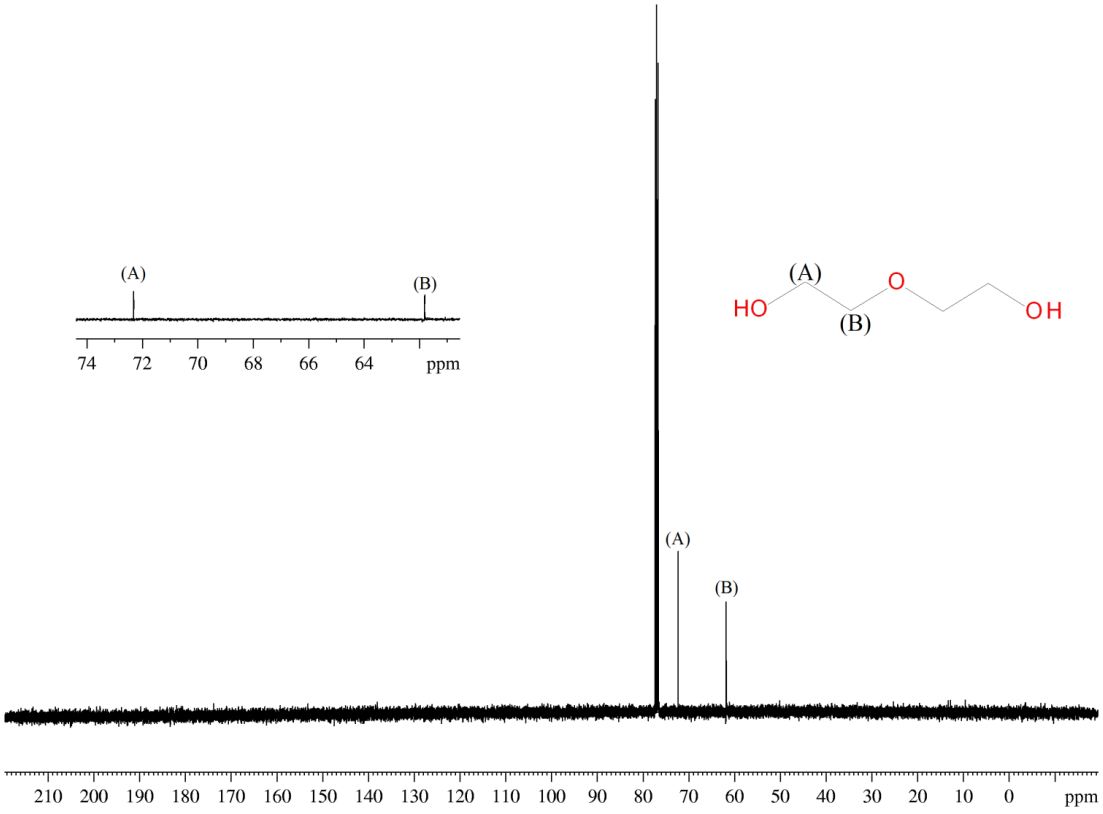

Figure 4.26. ^{13}C-NMR spectrum for the aged precursor solution containing DEG (CDCl3, 400 MHz)

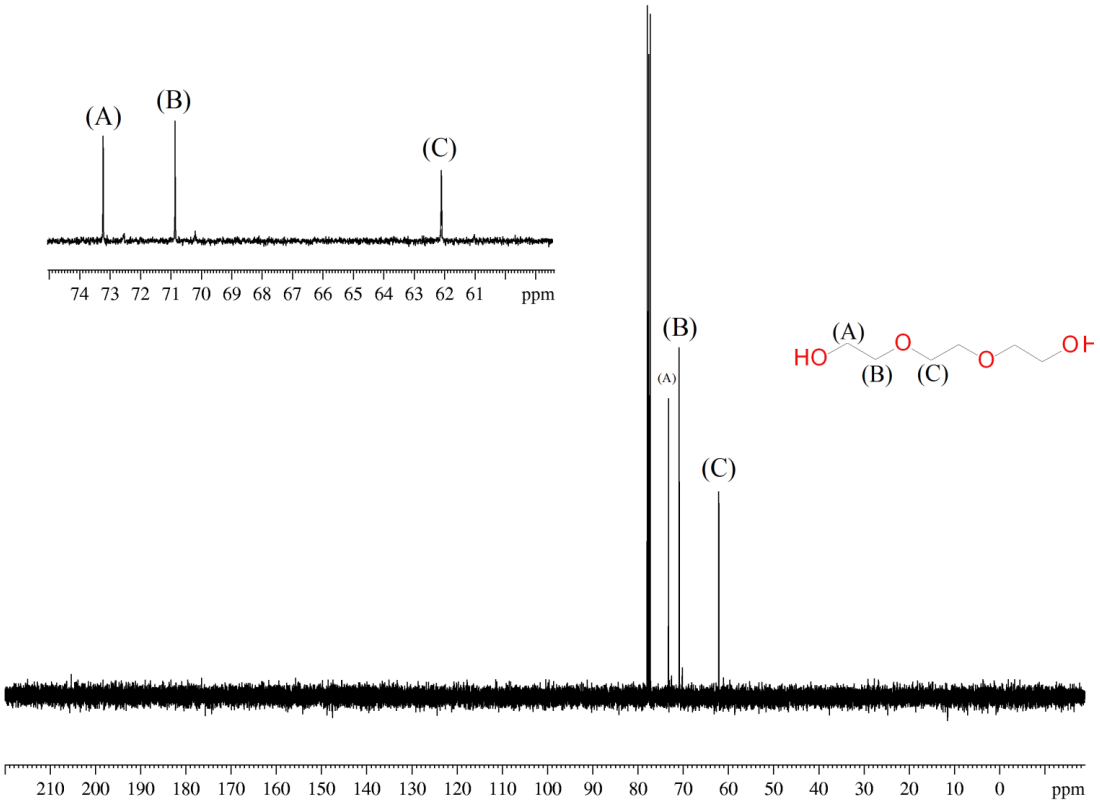

Figure 4.27. ^{13}C-NMR spectrum for the aged precursor solution containing TEG ($CDCl_3$, 400 MHz)

4.1.7. FTIR Spectra Analyses

Figure 4.28 illustrates the FTIR spectra conducted to LTL samples that show high crystallinity in their powder XRD patterns without the formation of impurity phases. However, for comparison purposes, it is decided to conduct a measurement on one of the samples that show high crystallinity, as well as the formation of the impurity phase. Figure 4.28 (a) represents the benchmarked LTL crystals. Figure 4.28 (b) represents LTL attained when 30TEG-150-6, while Figure 4.28 (c) illustrates the FTIR spectra for LTL attained using 80TEG-150-6.

In Figure 4.28 (a), it is observed a peak at 461 cm^{-1}. This is assigned to the Si-O bending vibration of LTL framework.[125] However, the peak at 461 cm^{-1} is not noticed in Figure 4.28 (b) and (c), which may indicate that the Si-O bending vibration is stabilized by the incorporation of TEG molecules. The peaks at 616 cm^{-1} and 584 cm^{-1} are attributed to the vibration of D6Rs in LTL framework. The peak at 484 cm^{-1} is assigned to the bending of O–(Si,Al)–O from LTL framework.[110] The peaks at 777 $cm^{-1}$and 726 cm^{-1} correspond to LTL framework. The former belongs to the symmetric stretching of O–(Si,Al)–O and the latter is assigned to the AlO_4^-.[126] It is observed that there is an appearance of peak around 1190 cm^{-1}, which represents the C-O bonds of ester groups as well as C-C bonds of alkane groups[127] and may be assigned to TEG molecules.

The peak at 1642 cm^{-1} is attributed to the vibration of H_2O.[126] The humps at 3604 cm^{-1} and 3474 cm^{-1} are attributed to the O-H stretching. Finally several peaks are observed around 2800 to 3000 cm^{-1} in Figure 4.28 (b) and Figure 4.28 (c) representing C-H stretching bonds. The presence of carbon and oxygen atoms can be observed in each of LTL attained using TEG.

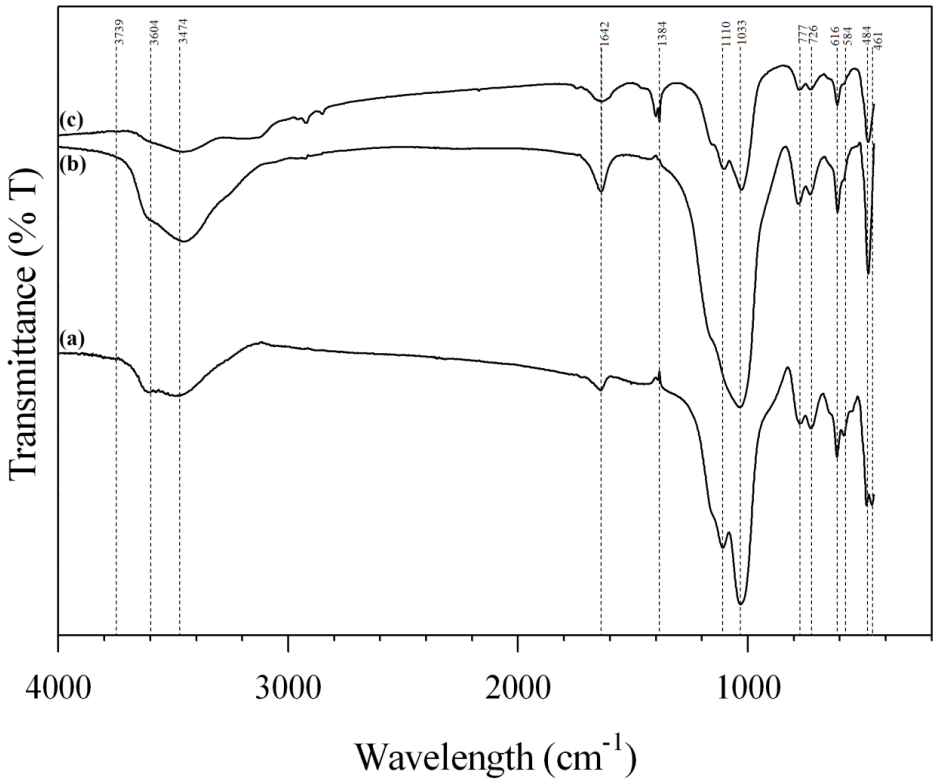

Figure 4.28. FTIR spectra of LTL crystals acquired using different synthesis conditions. (a) LTL synthesized based on the method described by Lee *et al*;[55] (b) LTL attained using 30TEG-150-6; (c) LTL attained using 80TEG-150-6.

4.2. ISOMORPHOUS SUBSTITUTION OF Si by Ge IN LTL FRAMEWORK

Prior to starting the study of the substitution of Si by Ge into LTL framework, we decide to conduct two control experiments. The first control experiment is prepared to observe if LTL phase is attained using the following synthesis composition **$1Al_2O_3$: $20SiO_2$: $10.9K_2O$: $950H_2O$** which does not include TEG. This precursor solution is treated at 150 °C for 6 days. The second control experiment is conducted to observe if LTL phase is formed when the precursor solution is synthesized by adding GeO_2 only but without the inclusion of TEG. The synthesis composition of this control experiment is **$1Al_2O_3$: $19.8SiO_2$: $0.2GeO_2$: $10.9K_2O$: $950H_2O$**. This precursor solution is heated at 150 °C for 3 days.

Figure 4.29 (a) and (b) illustrate the PXRD patterns for the two control experiments. Figure 4.29 (a) shows the formation of crystalline materials with unknown peaks between 2 θ = 20-30° and the weak presence of LTL phase when the synthesis is conducted for 6 days at 150 °C without using TEG and GeO_2. This result clearly demonstrates the importance of TEG to form LTL phase when compared with Figure 4.12, where LTL is obtained using the lower synthesis temperature.

Figure 4.29 (b) shows an amorphous material is attained at 150 °C adding GeO_2 source into the precursor solution. This PXRD pattern depicts that a successful heteroatom substitution in the LTL framework requires maintaining the material crystallinity. Thus, it is required to develop synthesis approaches that may yield a highly crystalline material, as well as being able to incorporate Ge atoms in the LTL framework.

From our previous study,[128] we observed that highly crystalline LTL phase is obtained at 150 °C for 6 days using co-solvents. Due to the good results obtained, the use of lower synthesis temperature (i.e. 150 °C) and TEG as the co-solvent in the precursor solution simultaneously are selected to carry out the development of synthesis methods, which may permit studying the incorporation of Ge in the LTL framework.

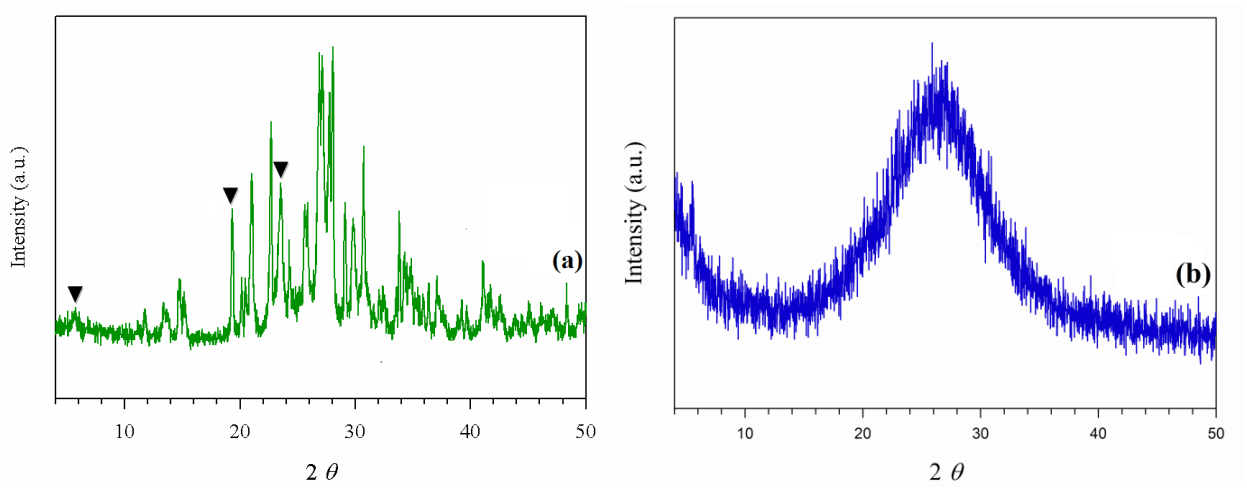

Figure 4.29. Powder XRD patterns of LTL crystals attained at 150 °C. (a) $1Al_2O_3$: $20SiO_2$: $10.9K_2O$: $950H_2O$ for 6 days (b) using $1Al_2O_3$: $19.8SiO_2$: $0.2GeO_2$: $10.9K_2O$: $950H_2O$ for 3 days. The solid triangles represent peaks of LTL.

4.2.1. First Synthesis Procedure (M1)

Figure 4.30 shows the PXRD patterns for Method 1 (M1). The aged precursor solution is synthesized at 150 °C for 3 days. To observe if the Ge content affects the crystallinity of the LTL phase, the content of Ge is gradually increased from 0.2, 0.3, 0.4 and 0.5 moles. PXRD patterns show a highly crystallised LTL material for all samples. Thus, according to PXRD analyses, the Ge content does not affect the crystallinity of the LTL phase for the specific amounts of Ge used in this experiment. Moreover, PXRD results do not show the appearance of impurities such as quartz (i.e. $2\theta = 26.6°$)[100] or GeO_2[95] in any of the resulting samples. Based on the PXRD analyses, it can be speculated that the

addition of GeO_2 increases the crystallization rate[92] and thereby permits to reduce the synthesis duration from 6 days to 3 days using 150 °C.[14]

Figure 4.31 shows the SEM images of LTL crystals attained using M1. It is observed that the crystals possess a cylindrical morphology. Moreover, the growth of the crystals along the *c*-direction increases when increasing the GeO_2 content in the samples. The increment in the crystals size has also been reported elsewhere.[100] Figure 4.31 (a) and (b) shows discrete crystals with a minor appearance of impurities on their surfaces. However, in Figure 4.31 (d), the deformation of the surface of the crystals is more pronounced than their counterparts. Moreover, it is also observed the formation of agglomerations among the cylindrical structure.

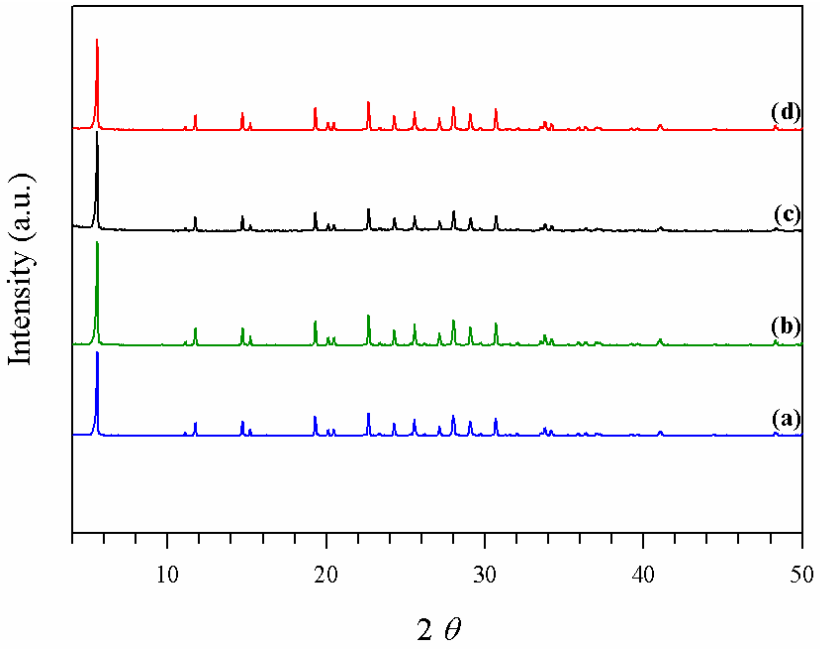

Figure 4.30. Powder XRD patterns of LTL crystals attained at 150 °C for 3 days using $1Al_2O_3$:$xSiO_2$:$yGeO_2$:10.9 K_2O:950 H_2O:80TEG. (where $x+y$ = 20, x/y = 99, 65, 49, 39). (a) x/y= 99 (M1-TEG-80-150-0.2Ge); (b) x/y= 65 (M1-80TEG-150-0.3Ge); (c) x/y = 49 (M1-80TEG -150-0.4Ge); (d) x/y= 39 (M1-80TEG -150-0.5Ge)

Table 4.7 shows a summary of the dimensions of LTL crystals. When these values are compared to the sample synthesized using 80 moles of TEG for 6 days at 150 °C, it is noticed that the aspect ratio decreases from a value of 1 to 0.66 using only 0.2 moles of Ge. The decrease in the aspect ratio may be due to the presence of Ge which allows forming much larger number of nuclei. A similar phenomena was observed in the formation of Ge-ITQ-7 crystals; where the crystal sizes have decreased from ~1-2 to <0.1 µm.[104] It is also interesting to note, that a linear relationship between the Ge content and the

increase of the length of the crystals. This may be considered as an indication of the isomorphous substitution of Si by Ge in LTL framework.

Table 4.7. Summary of dimensions of LTL crystals attained using M1

Sample ID	Diameter, D(μm)	Length, L (μm)	Aspect Ratio, L/D
M1-80TEG-150-0.2Ge	1.07 ± 0.06	0.71 ± 0.07	0.66
M1-80TEG-150-0.3Ge	1.02 ± 0.07	0.87 ± 0.19	0.85
M1-80TEG-150-0.4Ge	1.00 ± 0.09	0.88 ± 0.18	0.88
M1-80TEG-150-0.5Ge	1.14 ± 0.09	0.93 ± 0.24	0.82

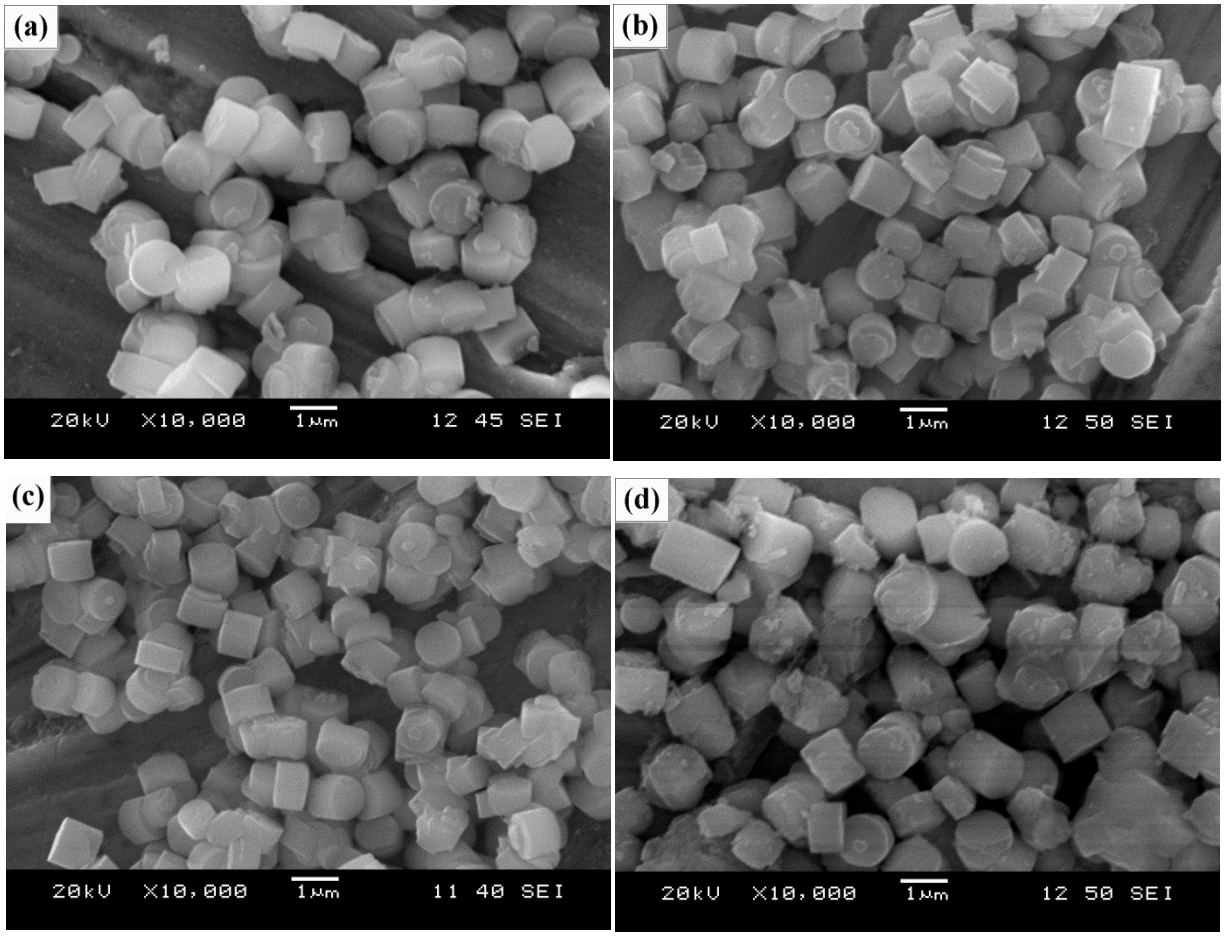

Figure 4.31. SEM images of LTL crystals attained at 150 °C for 3 days. (a) M1-80TEG-150-0.2Ge; (b) M1-80TEG-150-0.3 Ge; (c) M1-80TEG-150-0.4Ge; (d) M1-80TEG-150-0.5Ge. The scale bar is 1 μm.

4.2.2. Second Synthesis Procedure (M2)

Figure 4.32 shows the PXRD patterns of M2. When the resulting samples are synthesized at higher GeO_2 content, 0.4 and 0.5 moles (i.e., Figure 4.32 (c)-(d)), it is observed the presence of amorphous materials in the PXRD analyses. The statement is justified by the hump of their base lines

shown individually in Figure 4.33 (c) and (d). Overall, the crystallinity of LTL phase is maintained using M2 approach and with no appearance of GeO_2 peaks in any of the resulting samples.

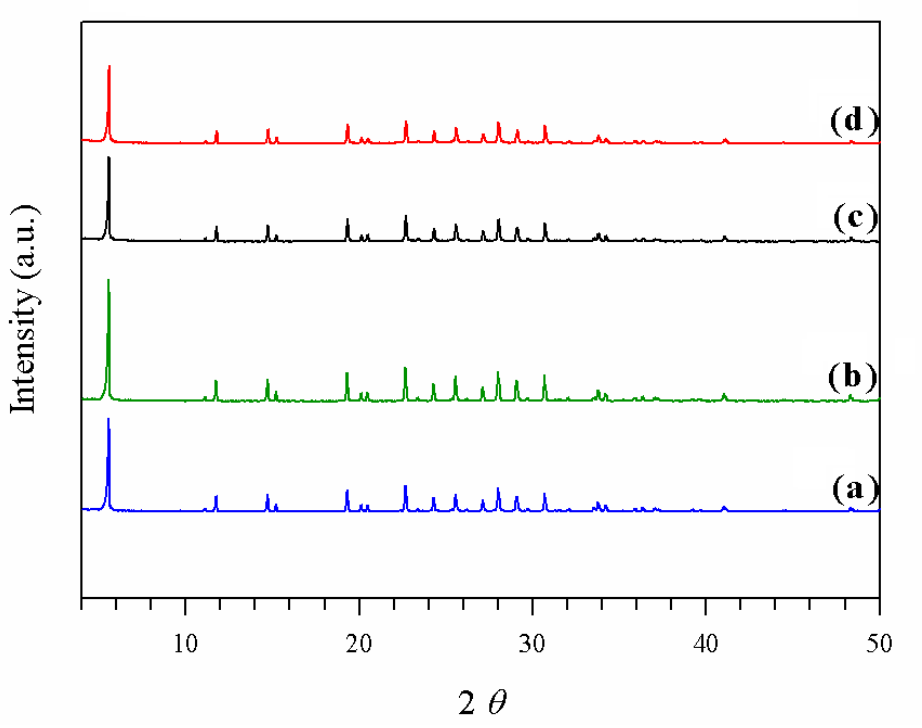

Figure 4.32. Powder XRD patterns of LTL crystals attained at 150 °C for 3 days using $1Al_2O_3$:$xSiO_2$:$yGeO_2$:10.9 K_2O:950 H_2O:80TEG. (where $x+y$ = 20, x/y = 99, 65, 49, 39); (a) x/y = 99 (M2-80TEG-150-0.2Ge); (b) x/y = 65 (M2-80TEG-150-0.3Ge); (c) x/y = 49 (M2-80TEG-150-0.4Ge); (d) x/y = 39 (M2-80TEG -150-0.5Ge).

Figure 4.34 shows the SEM images of LTL crystals using M2. It is observed that the synthesis approach did not change the morphology of LTL crystals. Figure 4.34 (a)-(c) show even surfaces for most of LTL crystals until the GeO_2 content reaches 0.4 moles. This can be observed in Figure 4.34 (d), where the crystals suffers a detriment on the surface, as well as the appearance of amorphous materials. This phenomenon is in accordance with PXRD analyses. The detriment of the surface in Figure 4.34 (d), may be attributed to the lower period of time (i.e., 20 minutes) employed to dissolve Ge and Al source. In order to validate the assumption, a sample is synthesized using a longer dissolution time (i.e., 40 minutes) to observe if the amorphous materials disappear. Figure 4.34 (e) shows discrete LTL crystals with smooth surfaces are attained after the dissolution time is elongated. Moreover, it is observed that the growth in the *c*-direction of the crystals is also increased while increasing GeO_2 content. The same effect is observed when using M1.

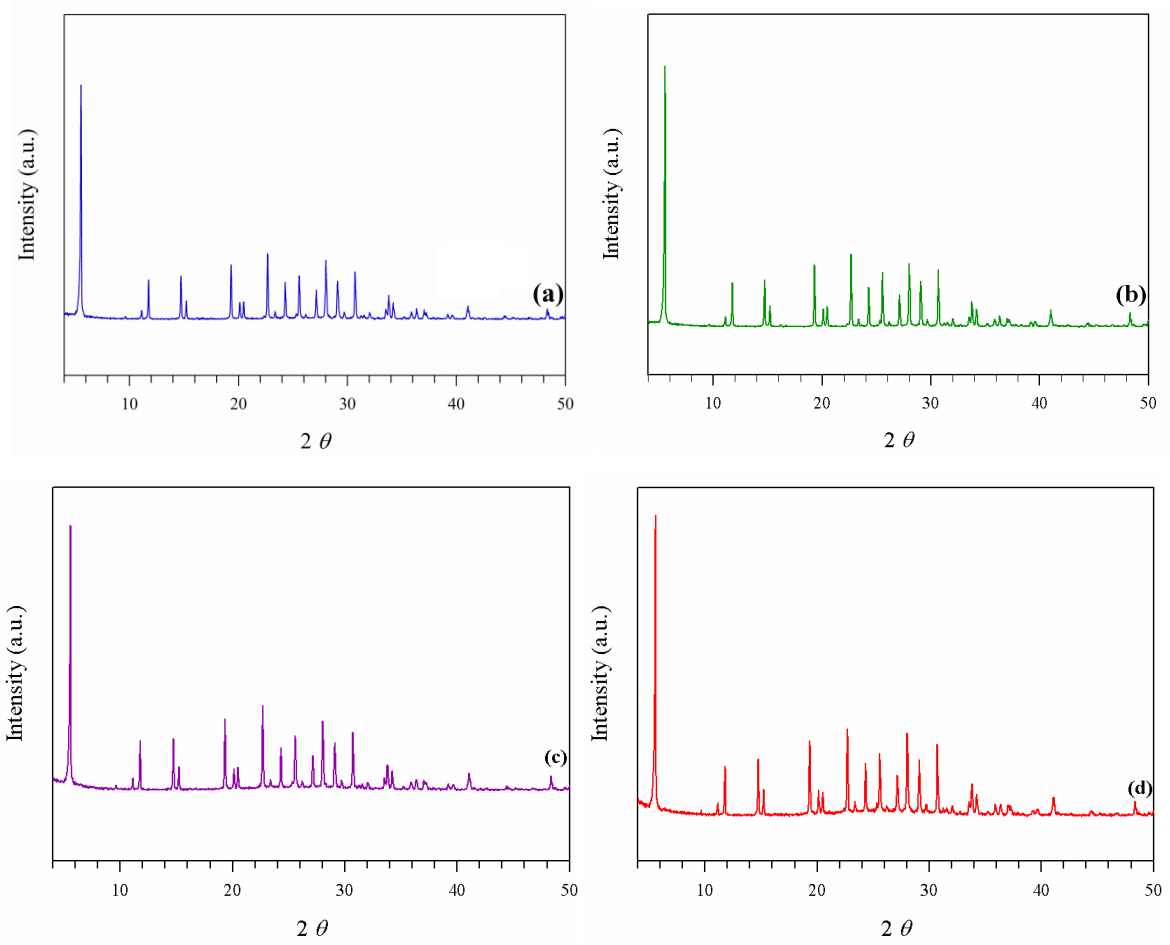

Figure 4.33. XRD patterns of LTL crystals attained at 150 °C for 3 days using $1Al_2O_3$:$x$$SiO_2$:$y$$GeO_2$:10.9 K_2O:950 H_2O:80TEG. (where $x+y$ = 20, x/y = 99, 65, 49, 39). (a) x/y = 99 (M2-80TEG-150-0.2Ge); (b) x/y = 65 (M2-80TEG-150-0.3Ge); (c) x/y = 49 (M2-80TEG-150-0.4Ge); (d) x/y = 39 (M2-80TEG-150-0.5Ge).

Table 4.8 shows a summary of LTL crystals dimensions for M2. The measurement of the dimensions is only recorded for the three first samples (M2-80TEG-150-0.2Ge, M2-TEG-80-150-0.3Ge, and M2-80TEG-150-0.4Ge). In the last sample, M2-80TEG-150-0.5Ge, the measurement is not reported due to the indistinguishable morphology. The increase of GeO_2 content leads to increase both the diameter and the length of the crystals. However, the increase is much lower than the diameter and length sizes reported in

Table **4.7** using M1. The aspect ratio using M2 is increased due to the increase of the diameter. Based on the trend observed in Table 4.8, it may suggest that the direct dissolution of GeO2 in KOH enhances Ge solubility in the precursor solution, which may yield the increase in number of nuclei and the crystallization rate. Thus, the enhancement is clearly noted in the reduction of both the diameter and length of LTL crystals. The result is in parallel with those observed in Ge-ITQ-7 zeolites.[90,104]

Table 4.8. Summary of dimensions of LTL crystals attained using M2

Sample ID	Diameter, D(μm)	Length, L (μm)	Aspect Ratio, L/D
M2-80TEG-150-0.2Ge	0.97 ± 0.08	0.62 ± 0.09	0.64
M2-80TEG-150-0.3Ge	0.97 ± 0.09	0.79 ± 0.09	0.82
M2-80TEG-150-0.4Ge	1.07 ± 0.06	0.93 ± 0.17	0.87
M2-80TEG-150-0.5Ge*	0.88 ± 0.07	0.82 ± 0.11	0.93

*Dimensions of M2-80TEG-150-0.5Ge were taken from Figure 4.34 (e)

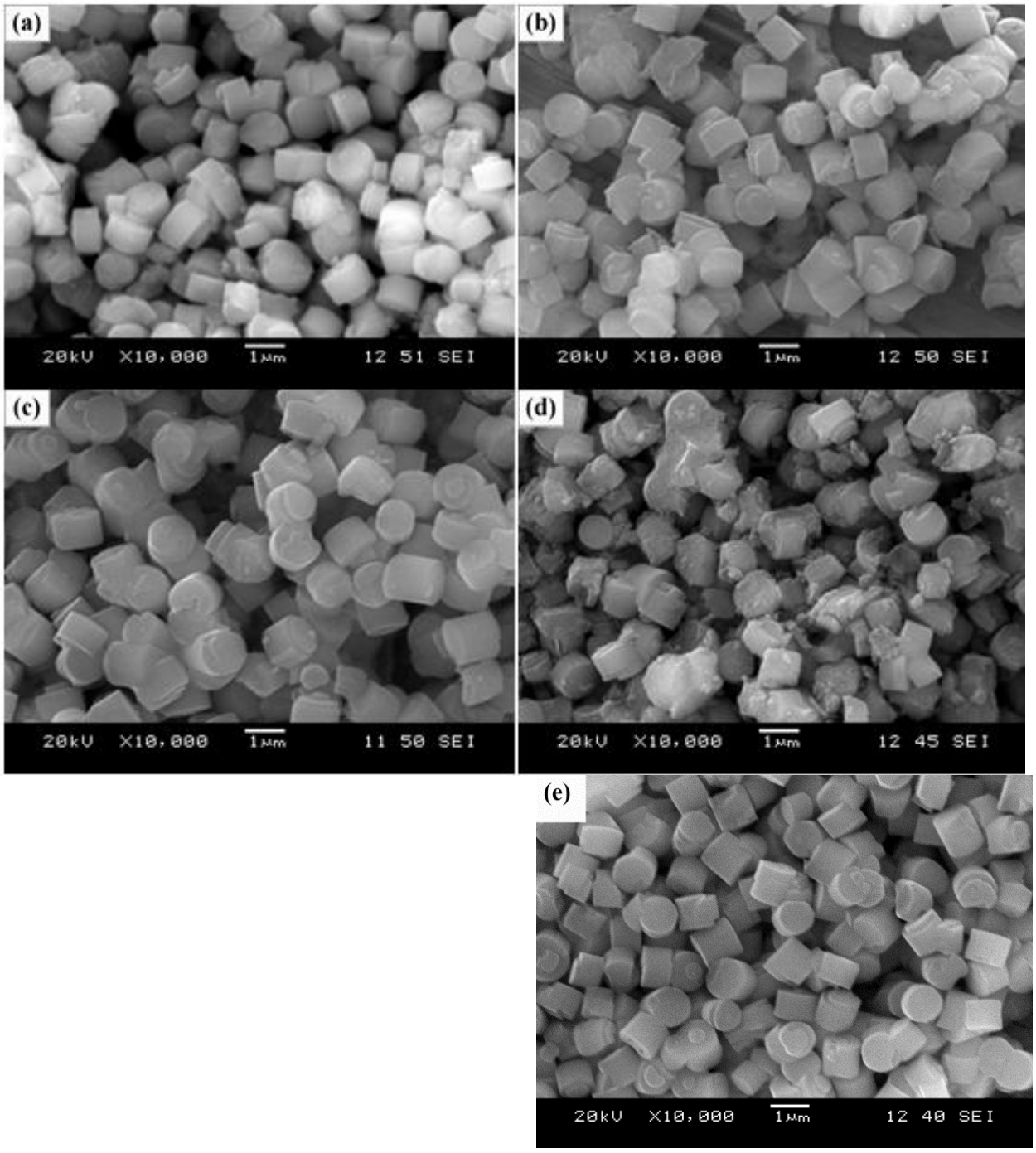

Figure 4.34. SEM images of LTL crystals attained at 150 °C for 3 days. (a) M2-80TEG-150-0.2Ge; (b) M2-80TEG-150-0.3Ge; (c) M2-80TEG-150-0.4Ge; (d)-(e) M2-80TEG-150-0.5Ge. The scale bar is 1 μm.

4.2.3. Third Synthesis Procedure (M3)

Figure 4.35 shows the PXRD patterns of resulting crystals using M3. The crystallinity of LTL phase is maintained without noticing any amorphous material or impurity.

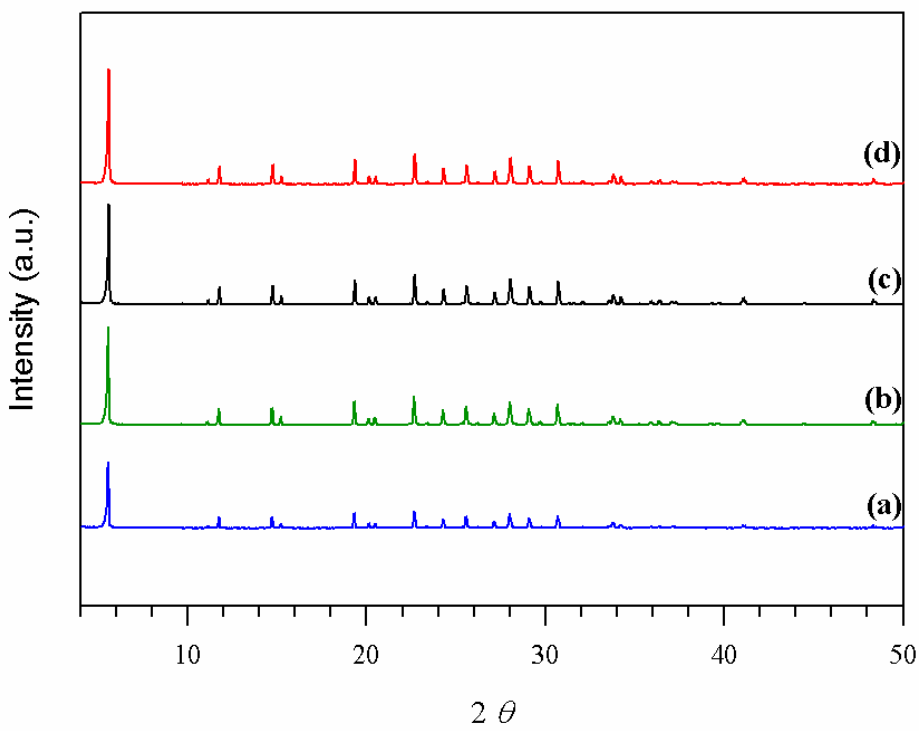

Figure 4.35. Powder XRD patterns of LTL crystals attained at 150 °C for 3 days using $1Al_2O_3$: $xSiO_2$: $yGeO_2$: $10.9K_2O$: $950H_2O$:80TEG. (where $x+y$ = 20, x/y= 99, 65, 49, 39). (a) x/y = 99 (M3-80TEG-150-0.2Ge); (b) x/y = 65 (M3-80TEG-150-0.3Ge); (c) x/y = 49 (M3-80TEG-150-0.4Ge); (d) x/y = 39 (M3-80TEG-150-0.5Ge).

Figure 4.36 shows the SEM images of LTL crystals attained using M3. The cylindrical morphology of the crystals is maintained using this synthesis approach. Interestingly, using this approach, it is observed the appearance of flakes on the surface of LTL crystals even at a lower GeO_2 content in the precursor solution. The difference is illustrated when M3-80TEG-150-0.2Ge (Figure 4.36 (a)) sample is compared to either M1-80TEG-150-0.2Ge (Figure 4.33(a)) or M2-80TEG-150-0.2Ge (Figure 4.34 (a)), where the flakes are not observed. The presence of the flakes on the surface of the discrete crystals may be attributed to specific interactions between the Al and Ge sources. However, it is not possible to identify these interactions in this study alone. Further studies must be conducted in order to investigate this phenomenon thoroughly.

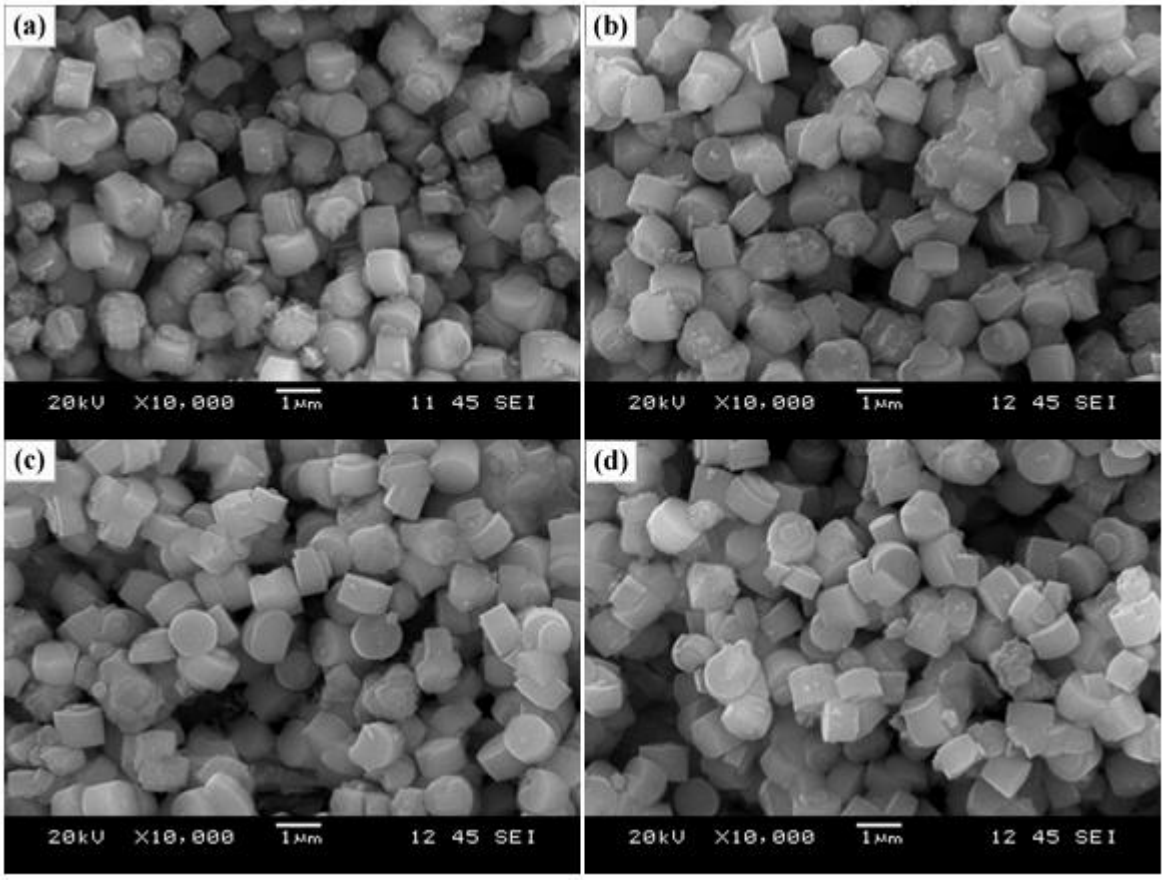

Figure 4.36. SEM images of LTL crystals attained at 150 °C for 3 days. (a) M3-80TEG-150-0.2Ge; (b) M3-80TEG-150-0.3 Ge; (c) M3-80TEG-150-0.4Ge; (d) M3-80TEG-150-0.5Ge. The scale bar is 1 μm.

Table 4.9 shows a summary of the dimensions of LTL crystals. The aspect ratio do not follow a linear relation as observed in M1 and M2 methods when the Ge content is increased. A similar trend is observed when the length of the crystals is analyzed. The M3 method shows that the uniformity of the crystals is decreased. According to Cheng *et al*,[98] the introduction of Al hindered the growth while Ge enhanced the growth of Ge,Al-Silicalite-1. Thus, the nonuniformity of the crystals may be an indication of the competition among these two different cations in order to be incorporated into the LTL framework**.**

Table 4.9. Summary of dimensions of LTL crystals attained using M3.

Sample ID	Diameter, D(μm)	Length, L (μm)	Aspect Ratio, L/D
M3-80TEG-150-0.2Ge	0.98 ± 0.09	0.70 ± 0.04	0.71
M3-80TEG-150-0.3Ge	1.02 ± 0.04	0.68 ± 0.09	0.67
M3-80TEG-150-0.4Ge	1.06 ± 0.06	0.72 ± 0.06	0.67
M3-80TEG-150-0.5Ge	0.98 ± 0.09	0.73 ± 0.03	0.75

4.2.4. XRF Analyses

Table 4.10 shows the Si/Ge ratio of the resulting samples from M1 to M3, which are obtained using XRF analyses. These results are compared to the initial Si/Ge ratio in the precursor solution. Among the three methods, M3 shows the highest Ge content in LTL samples, followed by M2 and M1. The XRF analyses clearly show that the different approaches utilized to include Ge in the precursor solution alter the Ge content in the final products. It is also observed the low incorporation of Ge in the LTL framework. This may be attributed to the use of high pH in the precursor solutions which decreases the Ge incorporation. Studies[95,97,102] have shown that the decrease in the pH to a value of 8 allows the increment of the Ge content. The low pH is achieved by using fluoride[89,90,95] media which highly differs from our alkaline media. However, on the basis of these results it is possible to incorporate germanium under these conditions.

Table 4.10. Bulk Compositions of the three methods as determined by XRF

Si/Ge, initial	Si/Ge,M1	Si/Ge,M2	Si/Ge,M3
99	1705.84	1463.31	1009.99
65	759.66	560.49	879.06
49	653.93	576.56	225.73
39	321.05	231.94	174.61

Based on the available data, it is not possible to identify if the higher content of Ge observed in M3 is due to the complete incorporation of Ge in the LTL framework or to an overlayer formation on the surface of the crystal. The Ge overlayer has been reported in Ge-ZSM-5[97] and may be due to the higher solubility of Ge in the alkaline media and the differences in the cations sizes (Al^{3+} and Ge^{4+}).

4.2.5. NMR Analyses

The incorporation of Ge into the precursor solution leads to a decrease in the synthesis duration from 6 to 3 days as well as assisting to decrease the aspect ratio of LTL crystals. Based on these results, I hypothesize that some of the GeO_2 added into the precursor solution might be interacting with TEG molecules. This may be one possible explanation of why we have been observing the attainment of LTL phase at the conditions already mentioned.

Previously, ^{13}C-NMR measurements were conducted to understand why TEG presents the most outstanding performance to attain the LTL phase among the three co-solvents used. These analyses allow us to understand that the chemical structure of TEG molecules are kept intact after the aging of the precursor solution. Thus, ^{13}C-NMR analyses are conducted to M2-80TEG-0.2Ge, M2-80TEG-0.4Ge, M3-80TEG-0.2Ge, and M3-80TEG-0.4Ge in order to verify the interaction between TEG and

GeO_2 in the aged precursor solutions.

Table 4.11 shows the summary of resonance signals in ^{13}C-NMR spectra of pure TEG, TEG aged in the precursor solution, M2-80TEG-0.2Ge, M2-80TEG-0.4Ge, M3-80TEG-0.2Ge, and M3-80TEG-0.4Ge in the zeolite precursor solution. The resonance signals of TEG spectrum of the aged precursor solutions containing GeO_2 have increased the chemical shifting when compared with the spectrum of pure TEG. The higher shifting may be due to the chemical reaction of TEG with the other chemical components in the precursor solution. For instance, Ossenkamp *et al*[124] showed that when different alcohols groups react with silica, there is an increase in the chemical shifting that proves the entrapment of the alcohol molecule with the silica. However, the higher chemical shifting in precursor solutions containing GeO_2 may also be due to its interaction with TEG. This stronger interaction may be due to the dissolution of Ge in the alkaline media of the precursor solution.[102] Thus, the presence of GeO_2 assists to change the chemical environment of TEG.

It is also observed that the chemical shifting of TEG is independent of the GeO_2 content. Therefore, this result may imply that only a specific amount of GeO_2 interacts with the TEG and that the different synthesis approaches lead to the similar interactions of TEG molecules when the precursor solution is aged for 16 hours. Figure 4.37 to Figure 4.40 illustrate the ^{13}C-NMR spectra of the different aged precursor solutions containing GeO_2.

Table 4.11. Summary of resonance signals in ^{13}C-NMR spectra of pure TEG, TEG aged in the precursor solution, and TEG and Ge contained in zeolite precursor solution

	TEG, pure	**TEG, aged**	**M2-80TEG-0.2Ge**	**M3-80TEG-0.2Ge**	**M2-80TEG-0.4Ge**	**M3-80TEG-0.4Ge**
(A)	72.307	72.653	72.628	72.617	72.61	72.61
(B)	69.93	70.29	70.327	70.342	70.36	70.348
(C)	60.96	61.586	61.671	61.679	61.69	61.689

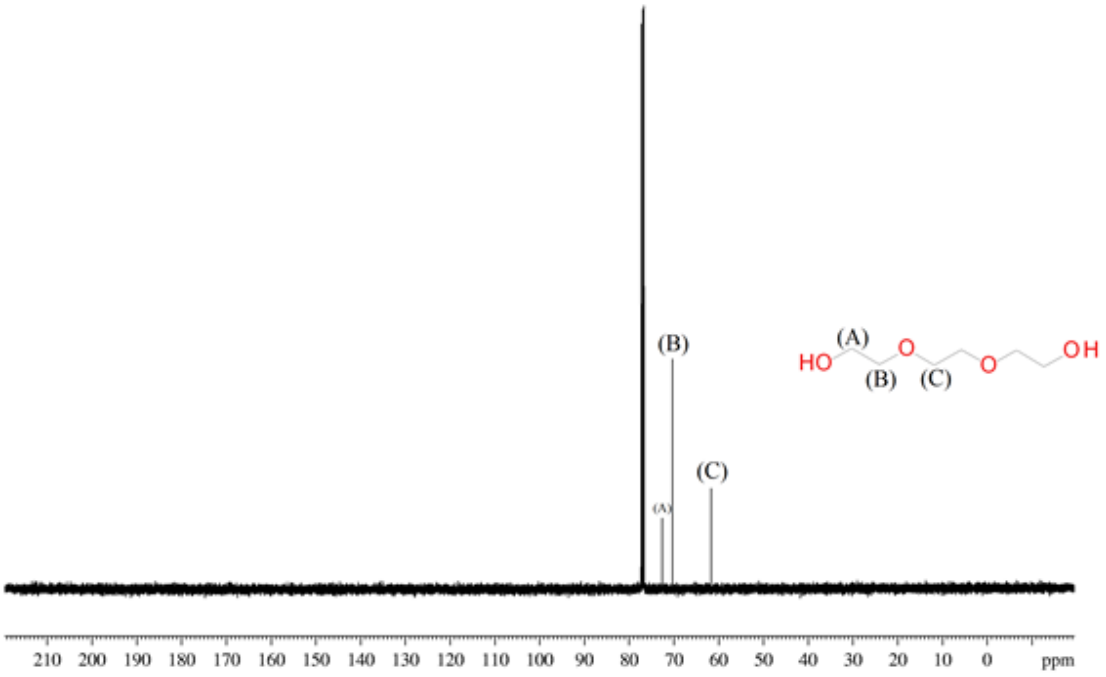

Figure 4.37. ^{13}C-NMR spectrum for M2-80TEG-0.2Ge ($CDCl_3$, 400 MHz)

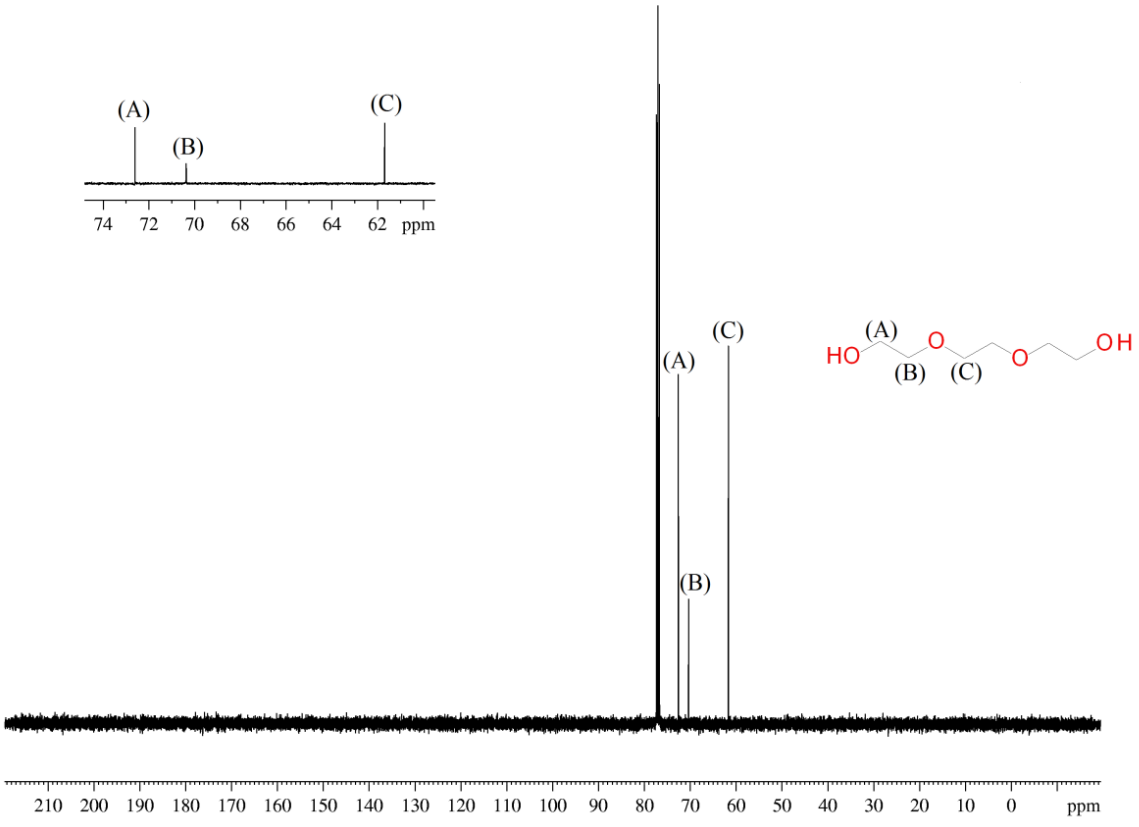

Figure 4.38. ^{13}C-NMR spectrum for M2-80TEG-0.4Ge ($CDCl_3$, 400 MHz)

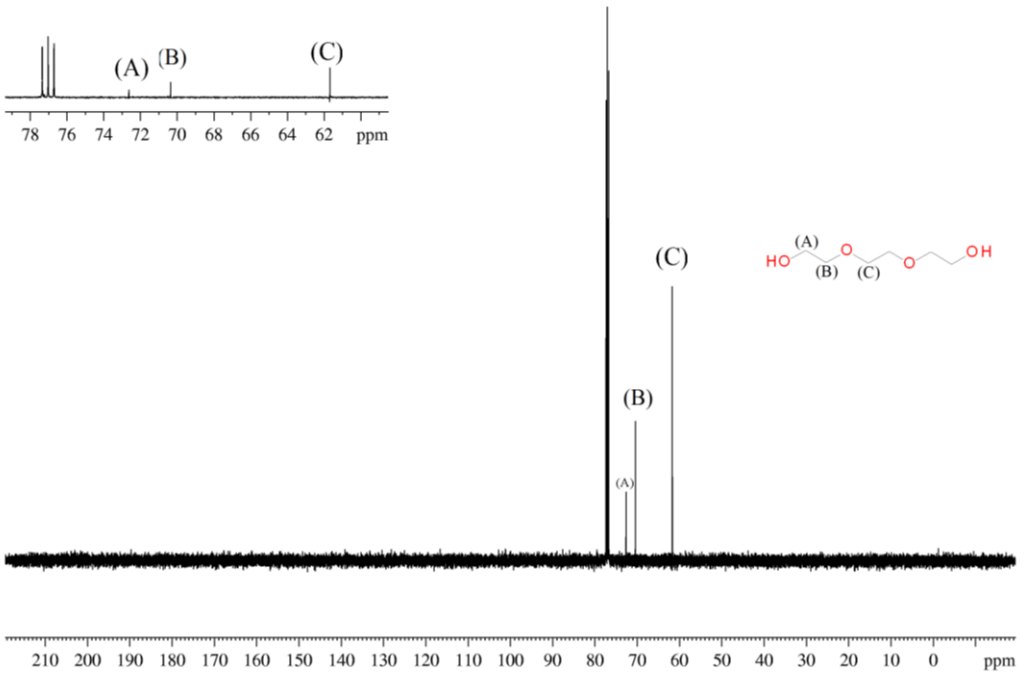

Figure 4.39. ^{13}C-NMR spectrum for M3-80TEG-0.2Ge ($CDCl_3$, 400 MHz)

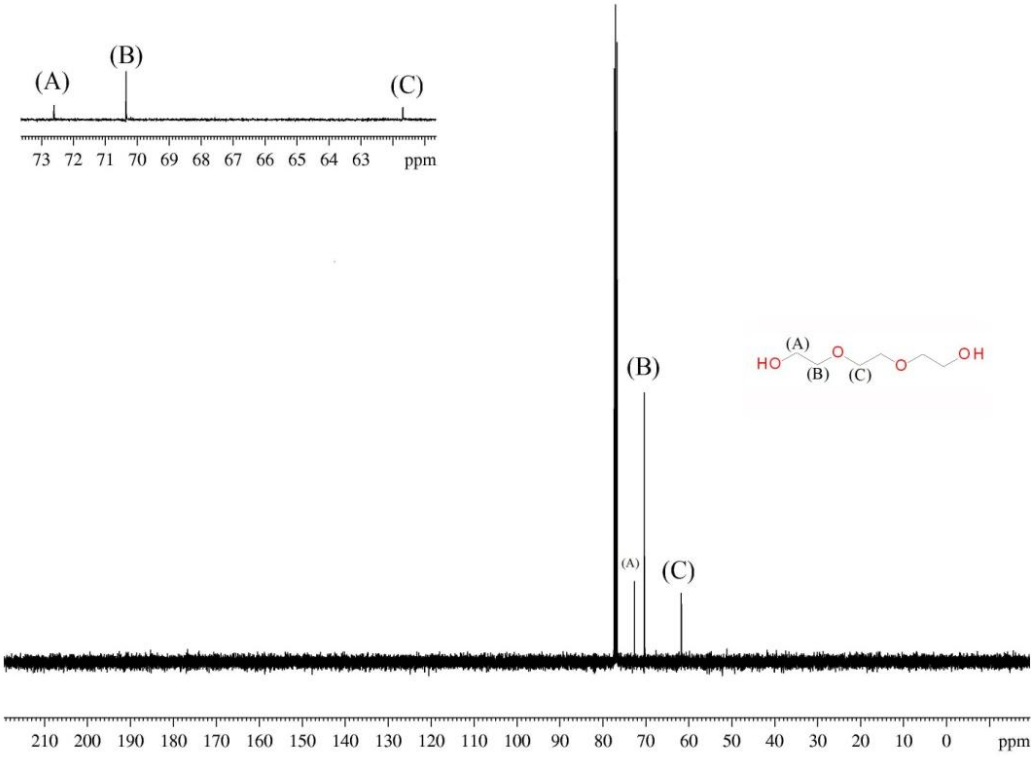

Figure 4.40. ^{13}C-NMR spectrum for M3-80TEG-0.4Ge ($CDCl_3$, 400 MHz)

4.2.6. FTIR Spectra Analyses

Figure 4.41 and Figure 4.42 depict the FTIR spectra conducted to observe if the amount of GeO_2 and the different synthesis approaches have any effect in the LTL framework. In Figure 4.41, the samples labeled as M2-80TEG-0.2Ge and M3-80TEG-0.2Ge are compared with a sample synthesized without using any co-solvent or GeO_2 (hereafter, pure LTL). Figure 4.41 (a) represents a pure LTL[55] sample. Figure 4.41 (b) represents LTL attained using M2-TEG-80-0.2, while Figure 4.41 (c) shows FTIR spectrum for LTL attained using M3-80TEG-0.2Ge. Figure 4.42 shows the FTIR spectra using higher amount of GeO_2. The samples are: M2-80TEG -0.4Ge (Figure 4.42 (b)) and M3-80TEG-0.4Ge (Figure 4.42 (c)). These spectra are also compared to pure LTL sample (Figure 4.42 (a)).

In both figures, it is observed that the major feature peaks of LTL are maintained in all spectra. However, three main differences are observed between the spectra of Ge-included LTL crystals and pure LTL crystals. First, the signal around 584 cm^{-1} in Figures 4.41(b)-(c) gradually disappears from the spectra when compared to Figure 4.41 (a). Furthermore, this inhibition is more prominent when higher amount of Ge is used as observed in Figure 4.42 (b)-(c). Second, the humps observed at 3474 cm^{-1} and 3604 cm^{-1} in the pure LTL sample (Figure 4.41 (a)) is flattened as the synthesis approach and the amount of GeO_2 change. In Figure Figure 4.41, the flatting is more prominent in Figure 4.41 (c) than (b), while in Figure 4.42, the hump is greatly leveled when the GeO_2 content is increased in M2-80TEG-0.4Ge. In Figure 4.42 (c), it appears to remain constant regardless of Ge content. Third, the previous FTIR analysis conducted to 80TEG-150-6 sample (Figure 4.28(c), which is Ge-free) shows several absorbance peaks around 2800 to 3000 cm^{-1}. The C-H stretching feature is not observed in the samples containing Ge and TEG.

The aforementioned observations obtained from FTIR analyses can be rationaled as follows. First, the peak at 584cm^{-1} belongs to the vibration of D6R units in LTL framework. The disappearance of this peak may be an indication of the Ge in LTL framework, where Ge atoms might be stabilizing the vibration of D6R units. Studies show the preferential incorporation of Ge atoms towards secondary unit buildings specifically, D4R units in ITQ-7 zeolites.[90] It is observed that Ge decreases the T-O-T angle (T = Ge or Si) by increasing the T-O distance and therefore, the units are stabilized.[89,90,129] Thus, it may be speculated, based on our FTIR results and the observations in literature that Ge prefers to be incorporated in the secondary unit buildings of LTL, which are D6Rs. On the other hand, Kosslick and Fricke[100] reported the appearance of a peak at 670 cm^{-1} in their FTIR spectra of Ge-ZSM-5. The peak belongs to Ge-O-Si bonding, confirming the isomorphous substitution of Si by Ge. However, the

presence of this peak is not observed in our FTIR results. This may be due to the lower GeO_2 content utilized in LTL syntheses in alkaline media when compared with the GeO_2 content used to synthesize ZSM-5 in fluoride media by Kosslick and Fricke.[100]

Second, the bands at higher wavenumber (3474 and 3709 cm^{-1}) represent O-H stretching. However, the decrease in the humps is more pronounced in the samples containing both Ge and TEG. This may be attributed to the affinity of Ge ions to interact with OH group. Thus, an increase in Ge content leads to a decrease in the incorporation of OH groups in the LTL framework. Another possible explanation is, based on the results from ^{13}C NMR analyses, it is suggested that due to the alkaline media of the precursor solution, an oxidation occurs in TEG molecules. The Ge ions may replace some of the H ions attached to the oxygen at the end of the TEG chain. Thus, the stretching of OH groups at higher wavelengths is not as pronounce as the pure LTL. This could support our ^{13}C NMR results, in which the chemical shifting of the carbons next to the –OH groups demonstrates a downward shifting.

Third the peaks whose wavelength between 2800 to 3000 cm^{-1} represent the C-H stretching bonds from TEG molecules. However, these bands disappear in the FTIR spectra of the samples containing both TEG and GeO_2. This could be an indication of the low concentration of TEG molecules in the LTL framework. The presence of TEG molecules in LTL framework is detected by the appearance of the peak shoulder around 1190 cm^{-1} (indexed with arrows in both figures), which represent C-O bonds of TEG molecules.

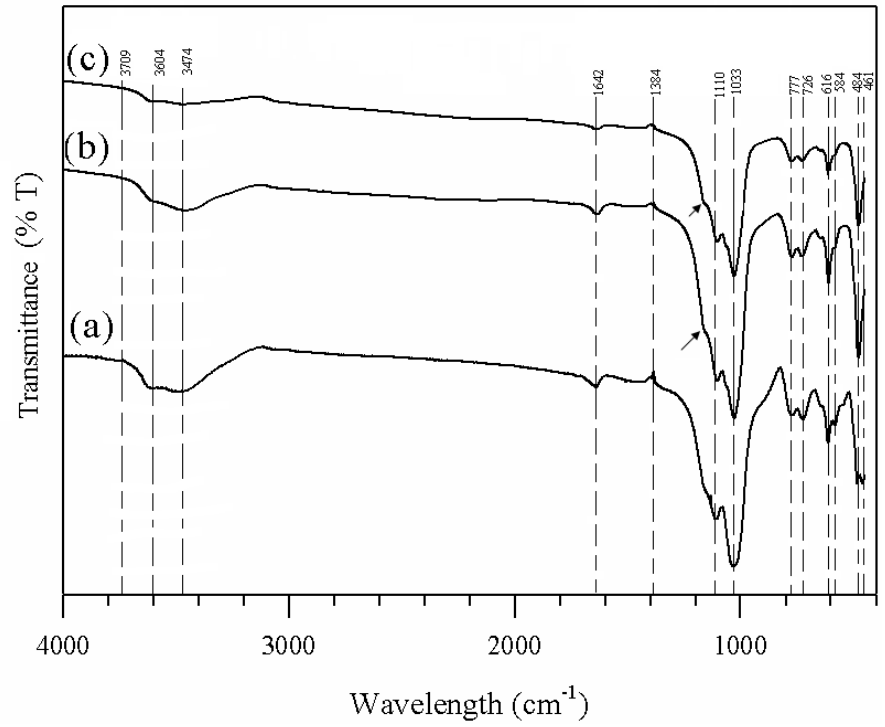

Figure 4.41. FTIR spectra of LTL acquired using different synthesis approaches. (a) LTL synthesized based on the method described by Lee *et al;*[55] (b) LTL attained using M2-80TEG-0.2Ge ; (c) LTL attained using M3-80TEG-0.2Ge. The arrows point out to the shoulder peak at 1190 cm^{-1}.

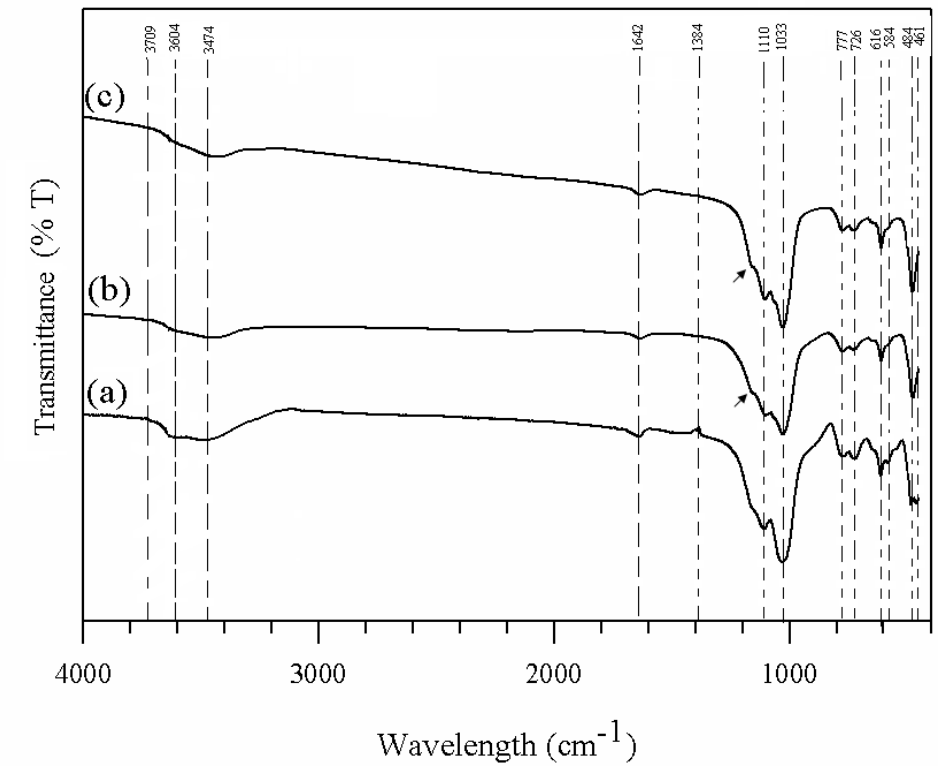

Figure 4.42. FTIR spectra of LTL acquired using different synthesis approaches. (a) LTL synthesized based on the method described by Lee *et al;*[55] (b) LTL attained using M2-80TEG-0.4Ge; (c) LTL attained using M3-80TEG-0.4Ge. The arrows point out to the shoulder peak at 1190 cm^{-1}

CHAPTER 5
CONCLUSIONS

The syntheses of zeolite L (LTL) were studied by the use of co-solvents in high water content media. Three different co-solvents were used: Ethylene Glycol (EG), Diethlylene Glycol (DEG), and Triethylene Glycol (TEG). The synthesis conditions, such as temperature (150 and 180 °C), concentration of co-solvent (30 and 80 moles) and synthesis duration (3 and 6 days) were varied to study the co-solvent effect.

The use of higher temperature (180 °C) and the variation of the synthesis duration led to the co-existence of impurity phases (cancrisilite and zeolite W) and zeolite L phase. Among the three co-solvents, TEG promoted the attainment of LTL phase, while DEG inhibited the formation of LTL phase and the use of EG did not assist in the attainment of LTL phase. It is concluded that the LTL phase is thermodynamically metastable using higher temperature. The appearance of LTL phase greatly depended on the adjustment of the synthesis conditions. SEM analysis showed a cylinder-like morphology of the LTL crystals with an aspect ratio of 1.53 using 80TEG-180-3.

On the other hand, the syntheses conducted at 150 °C and using 30 moles of the co-solvents for 3 days led to form an amorphous phase regardless of the co-solvent utilized. An increase in the synthesis duration, using 30 moles of any of the co-solvents, facilitated the formation of LTL phase. However, depending on the co-solvent used, it was observed the co-existence of LTL phase and amorphous materials (EG and DEG) as well as the formation of LTL and zeolite T phase (TEG). A pure and highly crystalline LTL phase was attained when the TEG amount was increased to 80 moles and the synthesis duration was carried out for 6 days. SEM analyses indicated that the morphology was greatly changed when varying the content of the co-solvents. At lower co-solvent content and longer synthesis duration, the morphology of the attained crystals were: long hexagonal crystals when using EG, a mixture of coin-like shape and long stick-like shape crystals when using DEG and single coin-like shape and a bundle of narrow crystals when using TEG. On the other hand, the crystals attained using TEG at higher concentration and longer synthesis time yielded a uniform cylinder-like structure with an aspect ratio of about 1.

The effect of the aging time was varied to investigate if the impurity phase, specifically cancrisilite, was inhibited. It was found that, the aging time of the precursor solution greatly reduced the

appearance of the cancrisilite peaks when using TEG as the co-solvent at 180 °C for 3 days. It is proposed that the suppression of cancrisilite lies in the range of 17.5-32 hours. NMR analyses indicated that the structures of the different co-solvents are not modified after the aging of the precursor solution at room temperature. Moreover, FTIR analyses showed that the overall structure of LTL framework is maintained as well as the presence of TEG molecules in the LTL framework.

The second part of this work focused on developing different synthesis procedures that permitted to study the isomorphous substitution of Si by Ge and maintaining the crystallinity of LTL at the same time. The precursor solution was prepared in alkaline media. The incorporation of Ge in the precursor solution allowed attaining LTL crystals just after 3 days at 150 °C. Moreover, from PXRD analyses showed a pure crystalline LTL phase without the presence of impurities (i.e., zeolite T). In terms of the crystal morphology, it was observed that the cylinder-like shape was maintained using Ge. The aspect ratio of the crystal was also reduced when compared to the aspect ratio of the crystals attained using only TEG. This observation may be attributed to the increase in the number of nuclei.

Even though, the Ge content used in this study was low (0.02-0.13 g GeO_2), XRF analyses showed the presence of Ge in the LTL framework. It was noticed that a higher GeO_2 amount in the precursor solution led to higher amount of Ge in the corresponding LTL crystals. It is interesting to observe that the Ge content in the framework is sensitive to synthesis approach used from this work.^{13}C NMR indicated that even with the inclusion of Ge in the precursor solution, TEG molecules maintained their chemical structure. FTIR analyses showed that the LTL framework is maintained regardless the Ge content and the synthesis approach utilized. However, it was observed differences between the FTIR of the samples containing Ge and pure LTL, which may indicate the presence of Ge in the framework of LTL. This difference is based on the disappearance of a wavelength band at which represents D6R units; this disappearance may indicate that Ge atoms stabilize this structure.

This work clearly shows that the addition of co-solvents to LTL syntheses allows tuning the morphology of LTL crystals. The LTL phase can be attained using lower synthesis temperature and lower synthesis duration. In the case of the isomorphous substitution, the proposed synthesis approaches successfully attained highly crystalline LTL phase as well as the study of the incorporation of Ge in the LTL framework. However it was not possible to investigate the location of the Ge atoms in the framework of LTL. Further studies are required to understand the incorporation of Ge in the LTL framework.

CHAPTER 6
RECOMMENDATIONS

Zeolite L (LTL) presents excellent potential in the aromatization of n-alkanes or as host guest materials for harvesting solar energy. These applications are highly correlated with the size and the morphology of zeolite crystals. Although this thesis clearly shows that the co-solvent synthesis approach permits the tuning of the morphology and size of LTL crystals towards the aforementioned applications. Much interesting future work still remains and is described as follows:

6.1 Influence of The Co-Solvents Concentration and Hydrothermal Conditions in LTL Attainment

This work only used two different co-solvent concentrations: 30 and 80 moles. The successful attainment of a highly crystalline material was attained using 80 moles of TEG at 150 °C for 6 days. Thus, it would be appropriate to investigate the effect of co-solvent concentration on the attainment of LTL phase systematically. Additionally, several questions may emerge from this investigation, such as: the correlations between the co-solvent concentration and the synthesis duration and LTL crystal morphology. Thus, this study might shed light on how the chain length and the OH groups of co-solvent molecules are affecting the LTL attainment.

Moreover, it was observed that the colour of the precursor solution using TEG was initially milky white. After 16 hours of aging, the colour changed to beige as observed in Figure 6.1. It is interesting to note that this colour change occurred at ambient temperature (25 °C). Although, NMR studies did not show any significant chemical shifting of the co-solvents structures, it has been reported that KOH acts as a catalyst for the ethoxylation and propoxylation of different co-solvents.[130] Thus, we might speculate that there is a correlation between KOH and the co-solvents. The change in colour was not observed when using EG and partially observed using DEG. Consequently, a further study using NMR techniques (^{1}H and ^{13}C NMR) should be implemented to understand the interactions between KOH and three glycols. The answer of this question would also assist to determine the relation between how the amount of carbons affects the LTL attainment.

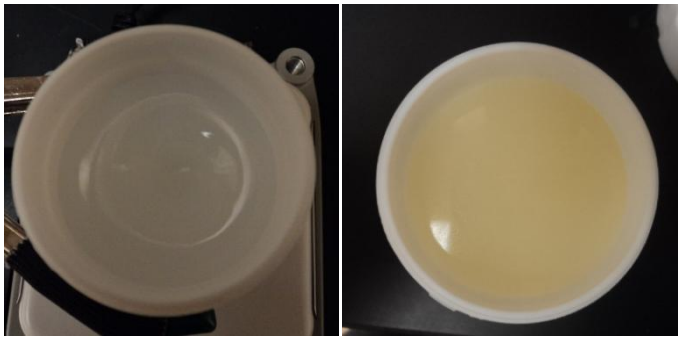

Figure 6.1 Precursor solution using TEG; Initial colour precursor solution: milky white (left side); Final colour precursor solution after 16 hours aging (right side).

The hydrothermal synthesis is generally conducted in static conditions to attain zeolites. However, it has been observed that the use of dynamic conditions assists to shorten the crystallization time[131] as well as to decrease impurity phases.[132] It would be interesting to study this parameter in order to observe what affects the shape of the final products attained after hydrothermal synthesis and the LTL phase formation. For instance, Figure 6.2 shows the different shapes attained when using the different co-solvents (80 moles) synthesized at 150 °C during 3 days. PXRD analysis shows amorphous materials in 80EG-150-3 and 80DEG-150-3, while 80TEG-150-3 presents amorphous materials and a weak LTL phase.

Figure 6.2 Final products attained after hydrothermal synthesis using different co-solvents;. 80EG-150-3 (larger cylinder, front facing); 80DEG-150-3 (compact cylinder, middle); 80TEG-150-3 (pellet, back).

6.2 Aging Effect at Lower Temperatures

The aging time of this study was selected according to the one reported by Lee et al[55]. However, their synthesis was carried out using high temperature without using co-solvents. Hence, a further study should be implemented to obtain the appropriate aging time depending on the different type of co-solvents and the temperature used in order to attain LTL phase.

Furthermore, based on the results obtained in section 4.1.5, it was observed that at higher temperatures, the aging of the precursor solution with TEG allowed to reduce the impurities observed in PXRD. Thus, I suggest that the effect of the aging is analyzed at lower synthesis temperatures, in order to observe if zeolite T is responsive to this parameter. Moreover, it is observed that the crystallization rate using lower temperature is much slower than at high temperature. Thus, besides the impurities reductions, it cannot rule out that the aging effect might also create different interactions during the hydrothermal synthesis at lower temperature which may decrease the reduction of amorphous materials and as a consequence the synthesis duration.

6.3 Thermodynamic Stability of LTL Phase

The PXRD analyses (Figure 4.15 and 4.17) conducted at higher temperatures shows that LTL is thermodynamically unstable regardless of the synthesis conditions (i.e., type and concentration of co-solvent, synthesis duration). This phenomenon is not exclusive of LTL phase and it has been reported when synthesizing different zeolites.[133,134] For instance, from the synthesis of a precursor solution, it was found a transformation from amorphous to faujasite and finally to "P" zeolite. On the other hand, the addition of tetramethylammonium to the precursor solution led to a transformation from amorphous to faujasite and finally to ZSM-4 material.[135] Thus, it is of major importance to investigate the mechanisms of crystallization and transformation of LTL phase when using co-solvents. This study can be implemented at higher temperature and using TEG in the precursor solution. This investigation might also assist to understand the factors that control the nucleation and growth processes.

6.4 Isomorphous Substitution of Si by Ge In LTL Framework

With respect to the isomorphous substitution of Si by Ge, it would be recommendable to increase the Ge content in order to observe the effect on the crystallization of LTL. The increment in the Ge content generally leads to the detriment in the crystallization of the zeolites such as ZSM-5.[97] Moreover, X-ray photoelectron spectroscopy should be implemented to observe if the Ge observed from XRF is

located on the surface of the crystals. The type of Ge source would be also interesting to observe if major interactions might occur between the co-solvents and this Ge source. Moreover, based on our results, it appears that a strong interaction exists between Al and Ge ions. The understanding of this interaction will help to better understand the isomorphous substitution of Si by Ge in LTL framework.

REFERENCES

(1) Flanigen, E. M.; Jansen, J. C.; Bekkum, H. v. *Introduction to Zeolite Science and Practice*; Elsevier Science, **1991**.
(2) Cejka, J.; Corma, A.; Zones, S. *Zeolites and Catalysis, Synthesis, Reactions and Applications*; Wiley-VCH, **2010**.
(3) Katz, R. N. *Ceram. Ind.* **2001**, *151*, 16.
(4) Arruebo, M.; Dong, J.; Anderson, T.; Gu, X.; Gray, G.; Bennett, R.; Nenoff, T. M.; Kartin, M.; Johnson, K.; Falconer, J.; others "Novel modified zeolites for energy-efficient hydrocarbon separations," Sandia National Laboratories, **2006.**
(5) Resource Processing Industries, B.; Government of Canada, I. C., **2004**. http://www.ic.gc.ca/eic/site/hfc-hpc.nsf/eng/mc00062.html (Accessed July **2011**)
(6) Resource Processing Industries, B.; Government of Canada, I. C. **2004**. http://www.ic.gc.ca/eic/site/hfc-hpc.nsf/eng/mc00107.html (Accessed July **2011**)
(7) Cundy, C. S.; Cox, P. A. *Micropor. Meso. Mater.* **2005**, *82*, 1.
(8) Davis, M. E.; Lobo, R. F. *Chem. Mater.* **1992**, *4*, 756.
(9) Trakarnroek, S.; Jongpatiwut, S.; Rirksomboon, T.; Osuwan, S.; Resasco, D. E. *Appl. Catl. A.* **2006**, *313*, 189.
(10) Megelski, S.; Lieb, A.; Pauchard, M.; Drechsler, A.; Glaus, S.; Debus, C.; Meixner, A. J.; Calzaferri, G. *J. Phys. Chem. B.* **2001**, *105*, 25.
(11) Larlus, O.; Valtchev, V. P. *Chem. Mater.* **2004**, *16*, 3381.
(12) Ko, Y. S.; Ahn, W. S. *Korean Chem. Soc., Bull* **1999**, *20*, 1
(13) Treacy, M. M. J. *Micropor. Meso. Mater.* **1999**, *28*, 271.
(14) Gaona-Gómez, A.; Silveira, G. d.; Doan, H.; Cheng, C.-H. *Chem. Commun.* **2011**, *47*, 5876.
(15) Brent, R.; Lobo, A. J. W.; Lewis, D. W.; Anderson, M. W. *J. Phys. Chem. C.* **2010**, *114*, 18240.
(16) Latham, K.; Round, C. I.; Williams, C. D. *Micropor. Meso. Mater.* **2000**, *38*, 333.
(17) van de Water, L. G. A.; van der Waal, J. C.; Jansen, J. C.; Maschmeyer, T. *J. Catal.* **2004**, *223*, 170.
(18) Szostak, R. *Molecular sieves: principles of synthesis and identification*; Springer, 1998.
(19) Morris, R. E.; Weigel, S. J. *Chem. Soc. Rev.* **1997**, *26*, 309.
(20) Barrer, R. M. *Hydrothermal chemistry of zeolites*; Academic Press, **1982**.
(21) Jacobs, P. A. *Zeolite chemistry and catalysis: proceedings of an international symposium, Prague, Czechoslovakia, September 8-13, 1991*; Elsevier, **1991**.
(22) Auerbach, S. M.; Carrado, K. A.; Dutta, P. K. *Handbook of zeolite science and technology*; M. Dekker, **2003**.
(23) Cundy, C. S.; Cox, P. A. *Chem. Rev.* **2003**, *103*, 663.
(24) Baerlocher, C.; Baerlocher, C.; McCusker, L. B.; Olson, D. *Atlas of zeolite framework types*; Elsevier, **2007**.
(25) Van Santen, R. A. *J. Phys. Chem.* **1984**, *88*, 5768.
(26) Kulprathipanja, S. *Zeolites in Industrial Separation and Catalysis*; Wiley-VCH, 2010.
(27) Barrer, R. M. *Zeolites* **1981**, *1*, 130.
(28) Lok, B. M.; Cannan, T. R.; Messina, C. A. *Zeolites* **1983**, *3*, 282.
(29) Occelli, M. L.; Innes, R. A.; Pollack, S. S.; Sanders, J. V. *Zeolites* **1987**, *7*, 265.
(30) Kerr, G. T. *J. Phys. Chem.* **1966**, *70*, 1047.
(31) Lu, B.; Tsuda, T.; Oumi, Y.; Itabashi, K.; Sano, T. *Micropor. Meso. Mater.* **2004**, *76*, 1.

(32) Lai, Z.; Bonilla, G.; Diaz, I.; Nery, J. G.; Sujaoti, K.; Amat, M. A.; Kokkoli, E.; Terasaki, O.; Thompson, R. W.; Tsapatsis, M.; Vlachos, D. G. *Science* **2003**, *300*, 456.
(33) Casci, J. L. *Micropor. Meso. Mater.* **2005**, *82*, 217.
(34) Miller, J. T.; Agrawal, N. G. B.; Lane, G. S.; Modica, F. S. *J. Catal.* **1996**, *163*, 106.
(35) Huo, Q.; Dou, T.; Zhao, Z.; Pan, H. *Appl. Catl. A.* **2010**, *381*, 101.
(36) Wang, Y.; Li, H.; Liu, B.; Gan, Q.; Dong, Q.; Calzaferri, G.; Sun, Z. *J. Solid State Chem.* **2008**, *181*, 2469.
(37) Pauchard, M.; Devaux, A.; Calzaferri, G. *Chem.– Eur. J.* **2000**, *6*, 3456.
(38) Megelski, S.; Calzaferri, G. *Adv. Funct. Mater.* **2001**, *11*, 277.
(39) Li, J.; Pfanner, K.; Calzaferri, G. *J. Phys. Chem.* **1995**, *99*, 2119.
(40) Gfeller, N.; Megelski, S.; Calzaferri, G. *J. Phys. Chem. B.* **1999**, *103*, 1250.
(41) Gfeller, N.; Calzaferri, G. *J. Phys. Chem. B.* **1997**, *101*, 1396.
(42) Calzaferri, G.; Huber, S.; Maas, H.; Minkowski, C. *Angew. Chem. Int. Ed*. **2003**, *42*,3732.
(43) Calzaferri, G.; Gfeller, N. *J. Phys. Chem.* **1992**, *96*, 3428.
(44) McCusker, L. B.; Liebau, F.; Engelhardt, G. *Pure Appl. Chem.* **2001**, *73*, 381.
(45) Terasaki, O.; Thomas, J. M.; Millward, G. R. *Proceedings of the Royal Society of London. Series A, Mathematical and Physical Sciences* **1984**, *395*, 153.
(46) Barrer, R. M.; Villiger, H. *Kristallogr.* **1969**, *128*, 352.
(47) Ohsuna, T.; Horikawa, Y.; Hiraga, K.; Terasaki, O. *Chem. Mater.* **1998**, *10*, 688.
(48) van Koningsveld, H. *Schemes for Building Zeolite Framework Models:* http://www.iza-structure.org/databases/LTL.pdf. (Accessed April **2012**).
(49) Breck, D. W.; Acara, N. A., Paten, U.S 2,711,565 **(1958).**
(50) Wortel, T. M.; Paten, U.S 4,544,539 (**1985)**.
(51) Tsapatsis, M.; Lovallo, M.; Okubo, T.; Davis, M. E.; Sadakata, M. *Chem. Mater.* **1995**, *7*, 1734.
(52) Bhat, S. D.; Niphadkar, P. S.; Gaydhankar, T. R.; Awate, S. V.; Belhekar, A. A.; Joshi, P.N. *Micropor. Meso. Mater.* **2004**, *76*, 81.
(53) Ruiz, A. Z.; Brühwiler, D.; Ban, T.; Calzaferri, G. *Monatsh. Chem.* **2004**, *136*, 77.
(54) Ko, Y. S.; Ahn, W. S. *Korean Chem. Soc., Bull*, *20*, 1.
(55) Lee, Y. J.; Lee, J. S.; Yoon, K. B. *Micropor. Meso. Mater.* **2005**, *80*, 237.
(56) Ban, T.; Saito, H.; Naito, M.; Ohya, Y.; Takahashi, Y. *J. Porous Mater.* **2007**, *14*, 119.
(57) Ko, Y. S.; Ahn, W. S. *Korean J. Chem. Eng.* **2008**, *25*, 1546.
(58) Sherman, J. *Chem. Commun.* **2003**, 1617.
(59) White, J.; Dutta, P. K.; Shqau, K.; Verweij, H. *Micropor. Meso. Mater.* **2008**, *115*, 389.
(60) Brent, R.; Anderson, M. W. *Angew. Chem. Int. Ed.* **2008**, *120*, 5407.
(61) Xu, R.; Pang, W.; Yu, J.; Huo, Q.; Chen, J. *Chemistry of Zeolites and Related Porous Materials-Synthesis and Structure*; John Wiley & Sons, **2007**.
(62) Bibby, D. M.; Dale, M. P. *Nature* **1985**, *317*, 157.
(63) Qisheng, H.; Shouhua, F.; Ruren, X. *J. Chem. Soc., Chem. Commun.* **1988**, 1486.
(64) Huo, Q.; Xu, R. *J. Chem. Soc., Chem. Commun.* **1990**, 783.
(65) Gao, Q.; Chen, J.; Li, S.; Xu, R. *Micropor. Mater.* **1996**, *7*, 219.
(66) Xu, W.; Li, J.; Liu, G. *Zeolites* **1990**, *10*, 753.
(67) Li, J.; Liu, G.; Xu, W.; Ma, Q. *Zeolites* **1992**, *12*, 343.
(68) Kuperman, A.; Nadimi, S.; Oliver, S.; Ozin, G. A.; Garces, J. M.; Olken, M. M. *Nature* **1993**, *365*, 239.
(69) Barrett, P. A.; Camblor, M. A.; Corma, A.; Jones, R. H.; Villaescusa, L. A. *J. Phys. Chem. B.* **1998**, *102*, 4147.
(70) Yang, X.; Albrecht, D.; Caro, J. *Micropor. Meso. Mater.* **2007**, *100*, 95.

(71) Rakoczy, R. A.; Traa, Y.; Kortunov, P.; Vasenkov, S.; Kärger, J.; Weitkamp, J. *Micropor. Meso. Mater.* **2007**, *104*, 179.
(72) Marthala, V. R. R.; Hunger, M.; Kettner, F.; Krautscheid, H.; Chmelik, C.; Kärger, J. r.; Weitkamp, J. *Chem. Mater.* **2011**, *23*, 2521.
(73) Chen, X.; Yan, W.; Yu, J.; Cao, X.; Xu, R. In *From Zeolites to Porous MOF Materials - The 40th Anniversary of International Zeolite Conference, Proceedings of the 15th International Zeolite Conference*; Ruren Xu, Z. G., Ed.; Elsevier, **2007**; *170*, 432.
(74) Chen, X.; Yan, W.; Cao, X.; Xu, R. *Micropor. Meso. Mater.* **2010**, *131*, 45.
(75) Nakamura, T.; Inui, T.; Inoue, M.; Miyake, T. *J. Mater. Sci.* **2006**, *41*, 4335.
(76) Fukunaga, T.; Katsuno, H. *Catal. Surv. Asia* **2010**, *14*, 96.
(77) Ruiz, A. Z.; Br\ühwiler, D.; Ban, T.; Calzaferri, G. *Monatsh. Chem.* **2005**, *136*, 77.
(78) Calzaferri, G.; Pauchard, M.; Maas, H.; Huber, S.; Khatyr, A.; Schaafsma, T. *J. Mater. Chem.* **2002**, *12*, 1.
(79) Calzaferri, G.; Bossart, O.; Brühwiler, D.; Huber, S.; Leiggener, C.; Van Veen, M. K.; Ruiz, A. Z. *C. R. Chim.* **2006**, *9*, 214.
(80) Fricke, R.; Kosslick, H.; Lischke, G.; Richter, M. *Chem. Rev.* **2000**, *100*, 2303.
(81) Lewis, D. W.; Catlow, C. R. A.; Sankar, G.; Carr, S. W. *J. Phys. Chem.* **1995**, *99*, 2377.
(82) Yang, P. *The chemistry of nanostructured materials*; World Scientific, **2003**.
(83) B.Nagy, J.; Aiello, R.; Giordano, G.; Katovic, A.; Testa, F.; Kónya, Z.; Kiricsi, I.; Karge, H., Weitkamp, J., *Molecular Sieves- Science and Technology.* Springer. **2007.**
(84) Dartt, C. B.; Davis, M. E. *Appl. Catl. A:* **1996**, *143*, 53.
(85) Li, S.; Tuan, V. A.; Falconer, J. L.; Noble, R. D. *Micropor. Mesopor. Mater.* **2003**, *58*, 137.
(86) Li, S.; Tuan, V. A.; Noble, R. D.; Falconer, J. L. *Ind. Eng. Chem. Res.* **2001**, *40*, 6165.
(87) Xu, C.; Guan, J.; Wu, S.; Jia, M.; Wu, T.; Kan, Q. *Reaction Kinetics, Mechanisms and Catalysis* **2010**, *99*, 193.
(88) Johnson, G. M.; Tripathi, A.; Parise, J. B. *Chem. Mater.* **1998**, *11*, 10.
(89) Sastre, G.; Pulido, A.; Castañeda, R.; Corma, A. *J. Phys. Chem. B.* **2004**, *108*, 8830
(90) Blasco, T.; Corma, A.; Díaz-Cabañas, M. J.; Rey, F.; Vidal-Moya, J. A.; Zicovich-Wilson, C. M. *J. Phys. Chem. B.* **2002**, *106*, 2634.
(91) Kamakoti, P.; Barckholtz, T. A. *J. Phys. Chem. C.* **2007**, *111*, 3575.
(92) O'Brien, M. G.; Beale, A. M.; Kuipers, B. W. M.; Erné, B. H.; Lewis, D. W.; Catlow, C. R. A. *J. Phys. Chem. C* **2009**, *113*, 18614.
(93) Corma, A.; Navarro, M. T.; Rey, F.; Rius, J.; Valencia, S. *Angew. Chem. Int. Ed.* **2001**, *113*, 2337.
(94) Li, Q.; Navrotsky, A.; Rey, F.; Corma, A. *Micropor. Mesopor. Mater.* **2003**, *59*, 177.
(95) van de Water, L. G. A.; van der Waal, J. C.; Jansen, J. C.; Cadoni, M.; Marchese, L.; Maschmeyer, T. *J. Phys. Chem. B.* **2003**, *107*, 10423.
(96) Camblor, M. A.; Lobo, R. F.; Koller, H.; Davis, M. E. *Chem. Mater.* **1994**, *6*, 2193.
(97) Ghosh, A.; Vargas, N. G.; Mitchell, S. F.; Stevenson, S.; Shantz, D. F. *J. Phys. Chem. C.* **2009**, *113*, 12252.
(98) Cheng, C.-H.; Juttu, G.; Mitchell, S. F.; Shantz, D. F. *J. Phys. Chem. B.* **2006**, *110*, 2488.
(99) Gabelica, Z.; Guth, J.-L. *Angew. Chem. Int. Ed.* **1989**, *28*, 81
(100) Kosslick, H.; Tuan, V. A.; Fricke, R.; Peuker, C.; Pilz, W.; Storek, W. *J. Phys. Chem.* **1993**, *97*, 5678.
(101) Tuan, V. A.; Falconer, J. L.; Noble, R. D. *Micropor. Mesopor. Mater.* **2000**, *41*, 269.
(102) Cheng, C.-H.; Juttu, G.; Mitchell, S. F.; Shantz, D. F. *J. Phys. Chem. B.* **2006**, *110*, 21430.
(103) Corma, A.; Díaz-Cabañas, M. J.; Fornés, V. *Angew. Chem. Int. Ed*. **2000**, *39*, 2346.

(104) Corma, A.; Diaz-Cabanas, M. J.; Domine, M. E.; Rey, F. *Chem. Commun.* **2000,** 137.
(105) Leiva, S.; Sabater, M. J.; Valencia, S.; Sastre, G.; Fornés, V.; Rey, F.; Corma, A. *C. R. Chim.* **2005**, *8*, 369.
(106) Cook, J. D.; Thompson, R. W. *Zeolites* **1988**, *8*, 322.
(107) Treacy, M. M. J.; Higgins, J. B.; Commission, I. Z. A. S. *Collection of simulated XRD powder patterns for zeolites*; Elsevier, **2007**.
(108) Skoog, D. A.; Holler, F. J.; Crouch, S. R. *Principles of Instrumental Analysis*; Thomson Brooks/Cole, **2007**.
(109) Settle, F. A. *Handbook of instrumental techniques for analytical chemistry*; Prentice Hall PTR, **1997**.
(110) Pichat, P.; Franco-Parra, C.; Barthomeuf, D. *J. Chem. Soc. Farad. T. I.* **1975**, *71*, 991.
(111) Balcı, M. *Basic 1h- And 13c-NMR Spectroscopy*; Elsevier, **2005**.
(112) Pavia, D. L. *Introduction to Spectroscopy*; Brooks/Cole, Cengage Learning, **2009**.
(113) Jambor L.J, V. D. A. *Am. Mineral.* **1993**, *78*, 1314.
(114) J.W. Anthony, R. A. B., K.W. Bladh, M.C. Nichols *Handbook of Mineralogy, Mineralogical Society of America*, **2011**.
(115) Zhou, R.; Zhong, S.; Lin, X.; Xu, N. *Micropor. Mesopor. Mater.* **2009**, *124*, 117.
(116) Mirfendereski, M.; Mohammadi, T. *Powder Technol.* **2011**, *206*, 345.
(117) Huang, Y.; Yao, J.; Zhang, X.; Kong, C.; Chen, H.; Liu, D.; Tsapatsis, M.; Hill, M. R.; Hill, A. J.; Wang, H. *CrystEngComm* **2011**, *13*, 4714.
(118) Xu, R.; Pang, W.; Huo, Q. *Modern Inorganic Synthetic Chemistry*; Elsevier, **2010.**
(119) Joshi, P. N.; Kotasthane, A. N.; Shiralkar, V. P. *Zeolites* **1990**, *10*, 598.
(120) Iwasaki, A.; Hirata, M.; Kudo, I.; Sano, T.; Sugawara, S.; Ito, M.; Watanabe, M. *Zeolites* **1995**, *15*, 308.
(121) Sig Ko, Y.; Seung Ahn, W. *Powder Technol.* **2004**, *145*, 10.
(122) Tosheva, L.; Valtchev, V. P. *Chem. Mater.* **2005**, *17*, 2494.
(123) Ferchiche, S.; Warzywoda, J.; Sacco, A. *Inter. J. Inorg. Mater.* **2001**, *3*, 773.
(124) Ossenkamp, G. C.; Kemmitt, T.; Johnston, J. H. *Langmuir* **2002**, *18*, 5749.
(125) Lahodny-Sarc, O.; White, J. L. *J. Phys. Chem.* **1971**, *75*, 2408.
(126) Hennessy, B.; Megelski, S.; Marcolli, C.; Shklover, V.; Bärlocher, C.; Calzaferri, G. *J. Phys. Chem. B.* **1999**, *103*, 3340.
(127) Socrates, G. *Infrared and Raman characteristic group frequencies: tables and charts*; Wiley, **2004**.
(128) Gaona-Gómez, A.; Cheng, C.-H. *Micropor. Mesopor. Mater.* **2012**, *153*, 227.
(129) Corma, A.; Diaz-Cabanas, M. J.; Garcia, H.; Palomares, E. *Chem. Commun.* **2001,** 2148.
(130) Di Serio, M.; Tesser, R.; Dimiccoli, A.; Santacesaria, E. *Ind. Eng. Chem. Res.* **2002**, *41*, 5196.
(131) Camblor, M. A.; Mifsud, A.; Pérez-Pariente, J. *Zeolites* **1991**, *11*, 792.
(132) Asensi, M. A.; Corma, A.; Martínez, A.; Derewinski, M.; Krysciak, J.; Tamhankar, S. S. *Appl. Catl. A.* **1998**, *174*, 163
(133) Matijasic, A.; Patarin, J. *Micropor. Mesopor. Mater.* **1999**, *29*, 405.
(134) Čimek, A.; Komunjer, L.; Subotić, B.; Široki, M.; Rončević, S. *Zeolites* **1991**, *11*, 258.
(135) Dwyer, F. G.; Chu, P. *J. Catal.* **1979**, *59*, 263.
(136) Gottlieb, H. E.; Kotlyar, V.; Nudelman, A. *J. Org. Chem.* **1997**, *62*, 7512.

APPENDICES

Appendix A. ^{1}HNMR and ^{13}C NMR Spectra for Pure Co-Solvents

Figure A.1 illustrates the ^{1}H-NMR spectra for EG. Two peaks are observed, where the peak of 4.79 ppm corresponds to the solvent residual (D_2O) and the other peak represents the EG molecule. The single peak around 3.61 ppm is attributed to the chemical shift of H atoms of $–CH_2–$ units at, position (A) in Figure A.1. The ^{1}H-NMR shift observed for EG is comparable to that reported by Gottlieb *et al*,[136] where the chemical shift for EG is 3.65 ppm. The difference (± 0.04 ppm) between the two values may be attributed to the accuracy of the ^{1}H-NMR measurement which lies in the range of ± 5%.[109] Moreover, the magnified figure shows two peaks with resonance signals of 3.613 and 3.606 ppm. It is believed that these peaks are the result of interactions of the molecule with the solvent and does not belong to the molecule structure.

Figure A.2 shows the ^{1}H-NMR for the DEG molecule. The peak around 4.79 ppm corresponds to the solvent residual (D_2O). A set of two main multiplets are formed. Basically, the two main multiplets are formed because of the –O– unit located in the middle of the DEG molecule. It is observed a deshielding effect due to the presence of –OH groups. The peak with a resonance signal of 3.71 ppm corresponds to the $–CH_2$ groups adjacent to the –OH at position (A). The peak with a resonance of 3.62 ppm corresponds to the hydrogen atoms of $–CH_2–$ groups at position (B) in Figure A.2 (b)

Figure A.3 illustrates the ^{1}H-NMR benchmark for TEG. As the TEG ^{1}H-NMR spectrum is compared to that of DEG, both figures share similarities. The only difference between them is that TEG has a longer chain. This characteristic can be observed in the resonance signal at 3.70 ppm, which may represent the hydrogen atoms of $–CH_2–$ unit at position (B) in Figure A.3 (c). The resonance signal for the hydrogen atoms of $–CH_2–$ groups at position (A) in Figure A.3 (c) is 3.73 ppm. The hydrogen atoms at position (C) in Figure A.3 (c) correspond to a resonance signal of 3.61 ppm.

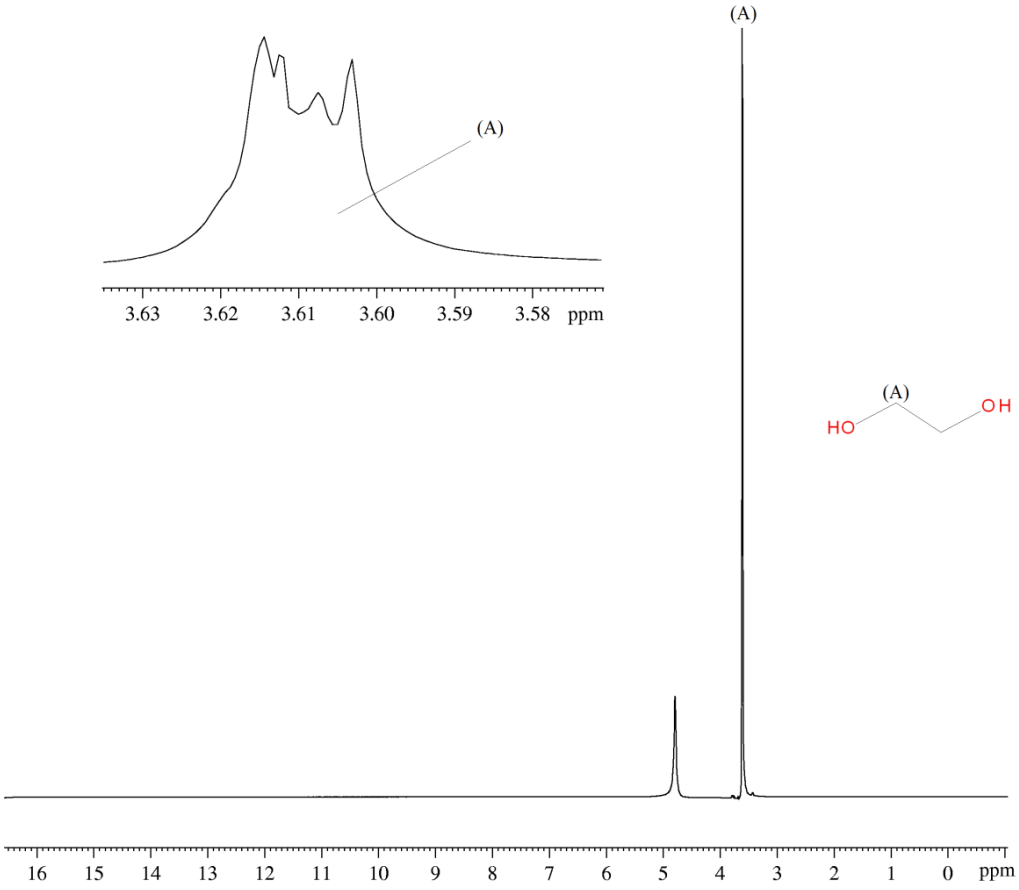

Figure A.1. ^{1}H-NMR spectrum for pure EG (D_2O, 400 MHz)

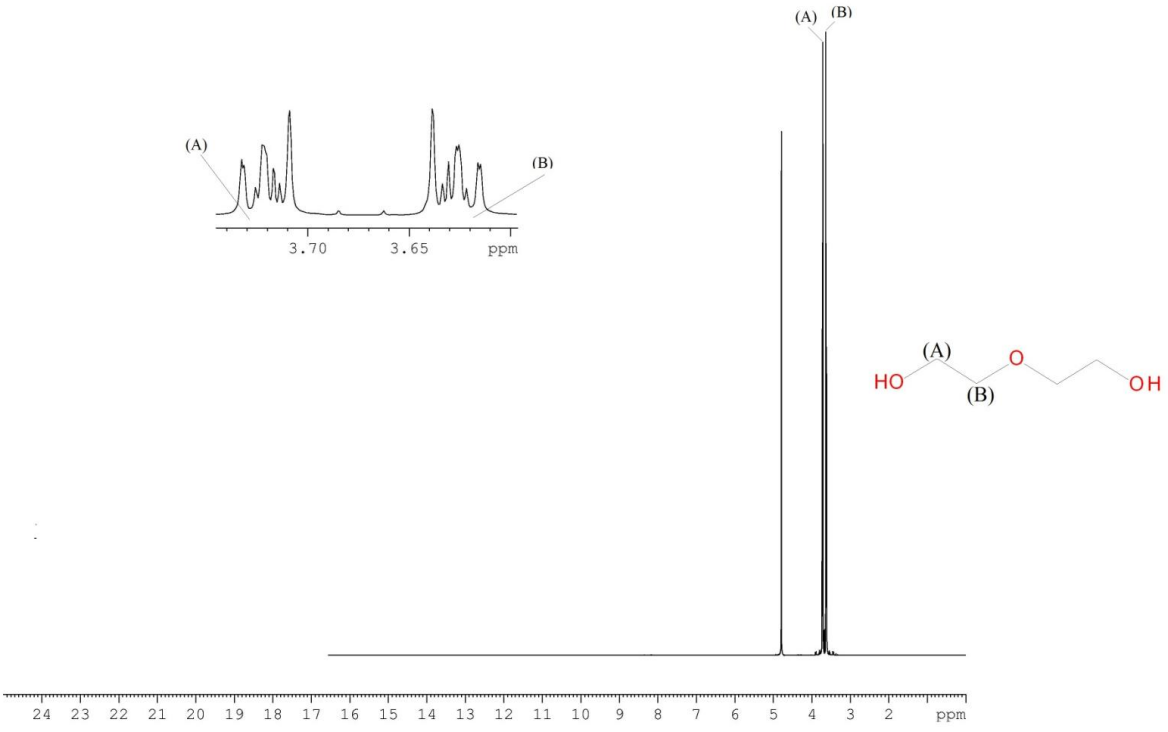

Figure A.2. ^{1}H-NMR spectrum for pure DEG (D_2O, 400 MHz**)**

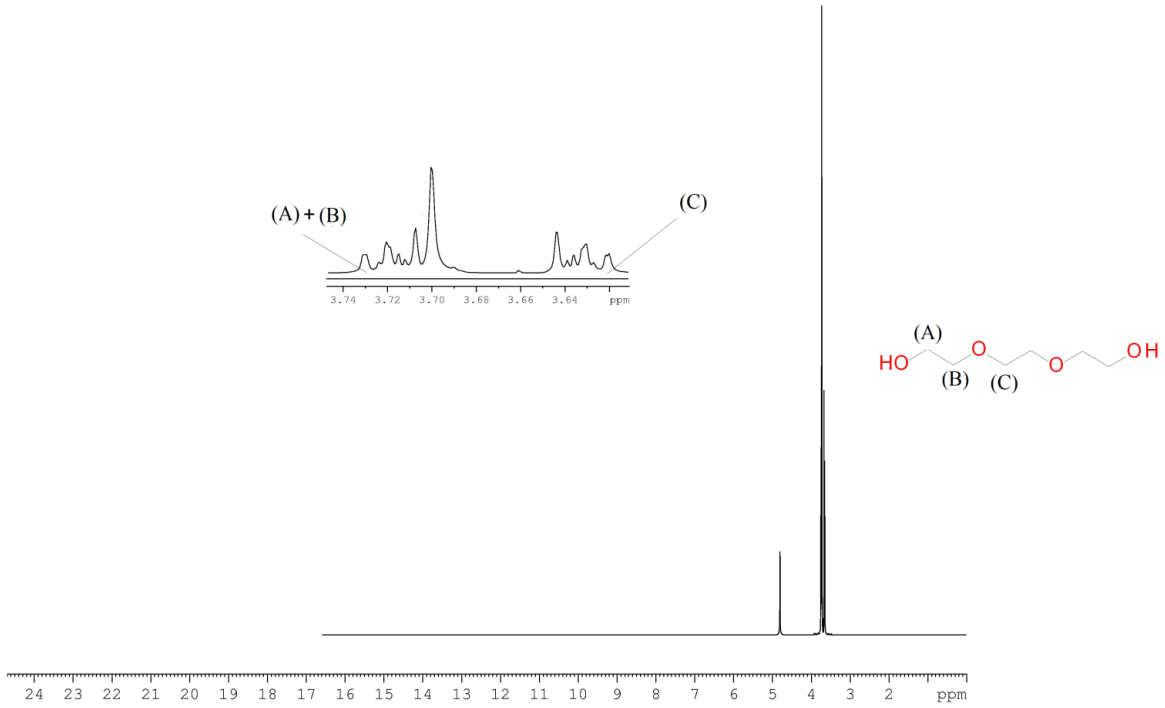

Figure A.3. ^{1}H-NMR spectrum for pure TEG (D_2O, 400 MHz).

Figure A.4, Figure A.5, and Figure A.6 show ^{13}C-NMR spectra of pure EG, DEG, and TEG correspondingly.

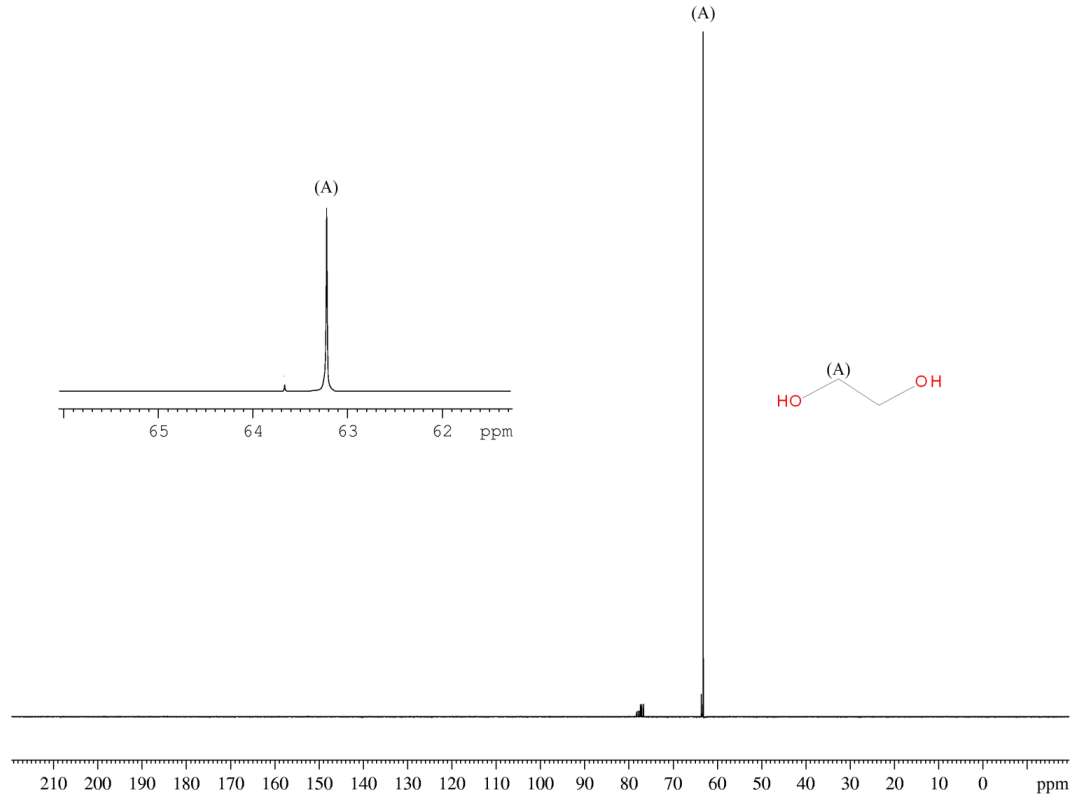

Figure A.4. ^{13}C-NMR spectrum for pure EG ($CDCl_3$, 400 MHz)

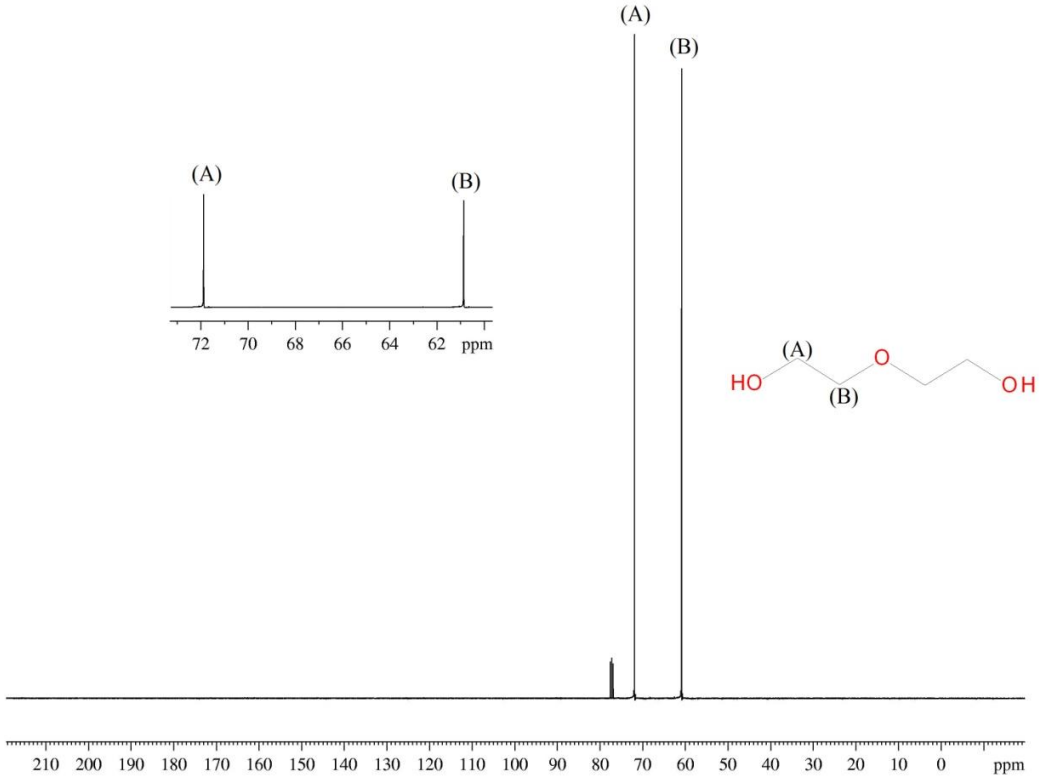

Figure A.5. ^{13}C-NMR spectrum for pure DEG ($CDCl_3$, 400 MHz)

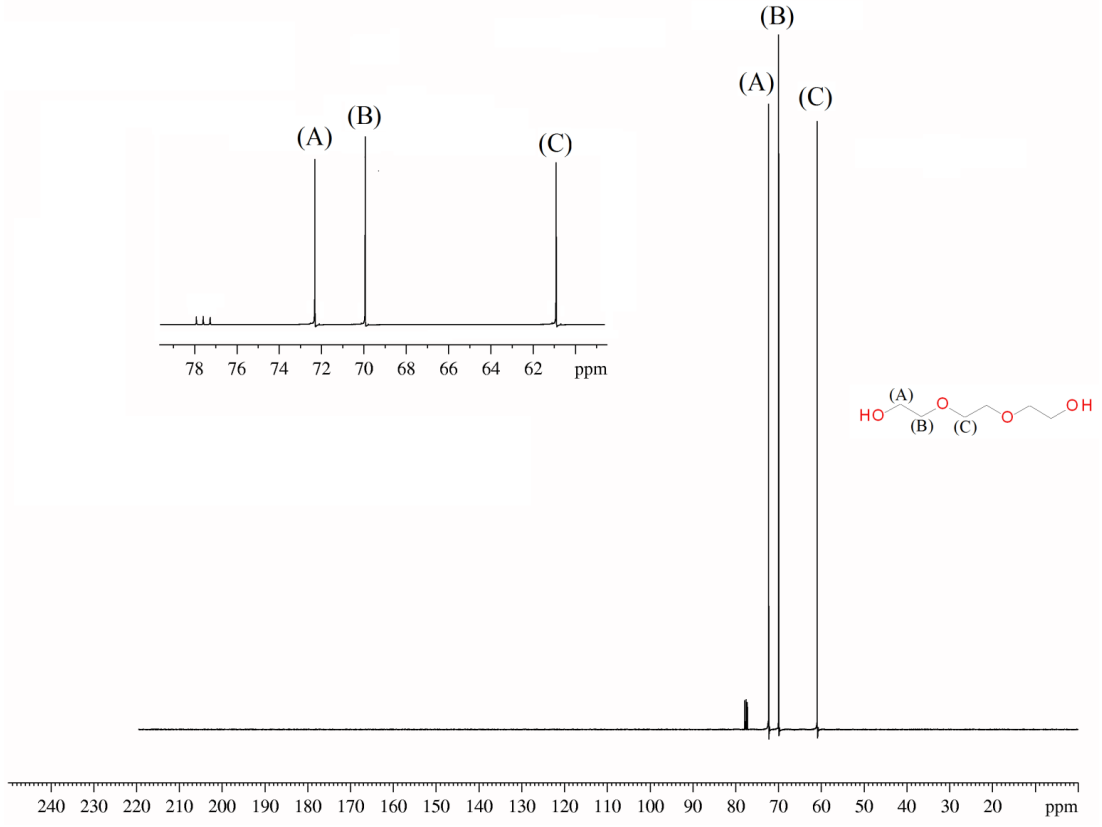

Figure A.6. ^{13}C-NMR spectrum for pure TEG ($CDCl_3$, 400 MHz)

Appendix B. Experimental Reproducibility of Zeolite L (LTL) phase

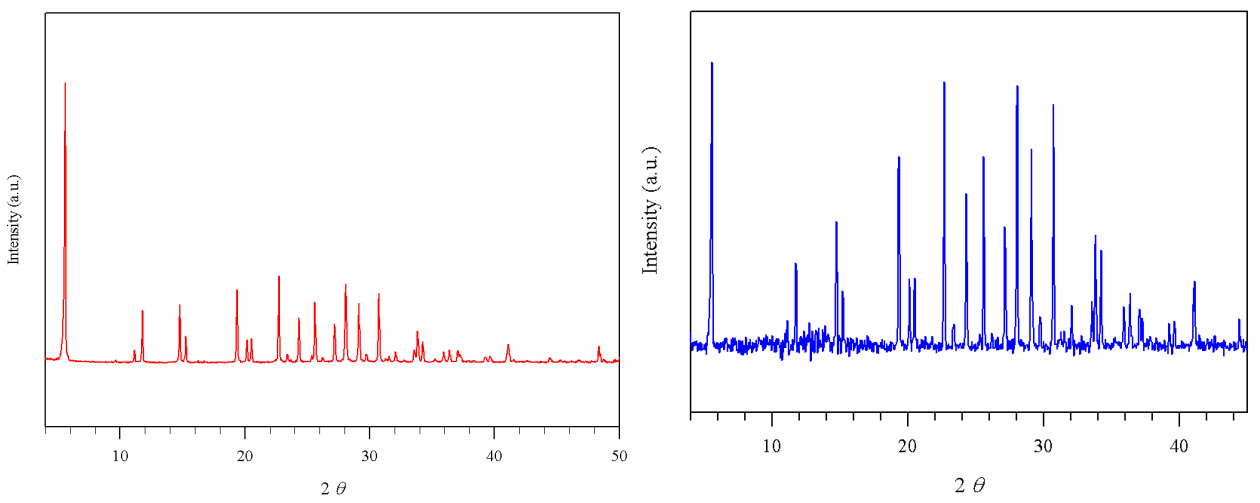

Figure B.1. Powder XRD patterns attained at 150°C for 6 days using $1Al_2O_3$:$20SiO_2$:$10.9K_2O$: 950 H_2O: 80 $C_6H_{14}O_4$; Addition sequence changed. Solution A to Solution B. (Left pattern); Adopted addition sequence in all the syntheses conducted in this study. Solution B to Solution A. (right pattern). The pattern at the left side was analyzed at University of Toronto. The pattern at the right side was analyzed at MacMaster University. Both patterns show a crystalline LTL phase.

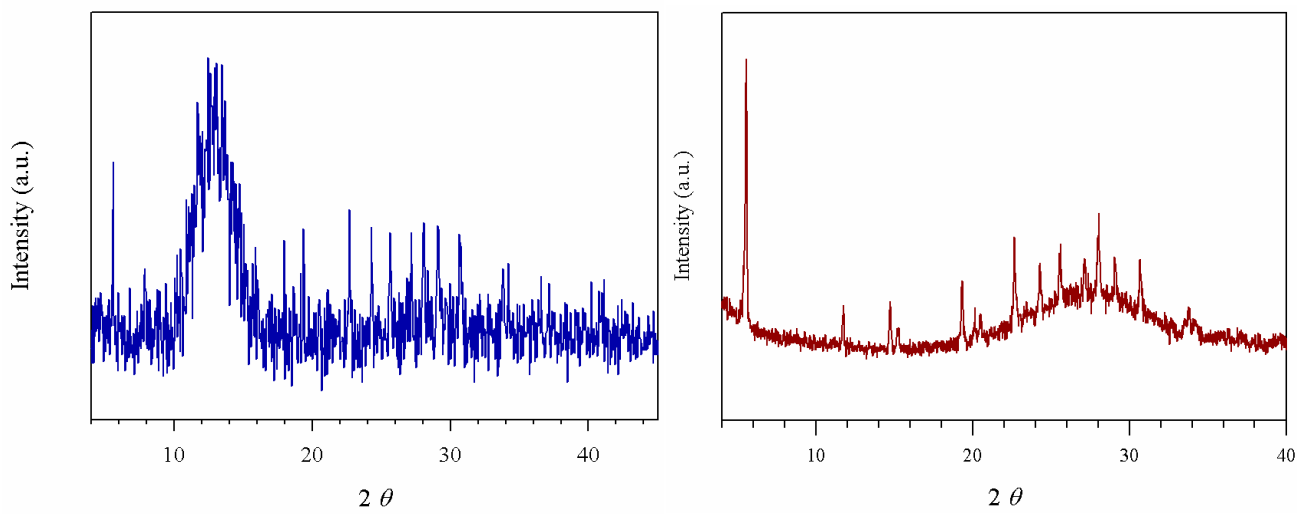

Figure B.2. Powder XRD patterns attained at 150°C for 3 days using $1Al_2O_3$:$20SiO_2$:$10.9K_2O$: 950 H_2O: 80 $C_6H_{14}O_4$. PXRD analyses conducted at MacMaster Univeristy (left pattern); PXRD analysis conducted at University of Toronto (right pattern). Both PXRD patterns shows the co-existence of amorphous materials and crystalline LTL phase.

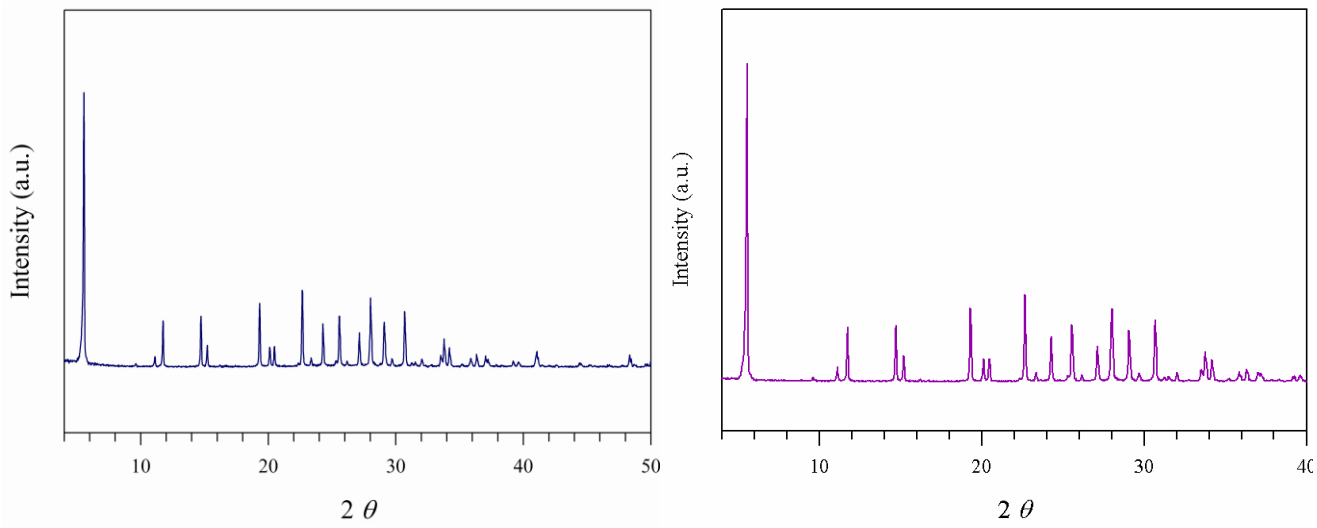

Figure B.3. Powder XRD patterns of LTL crystals attained at 150 °C for 3 days using $1Al_2O_3$:$xSiO_2$:$yGeO_2$:10.9 K_2O:950 H_2O:80TEG. (where $x+y$ = 20, x/y = 99); (a) x/y = 99 (M2-80TEG-150-0.2Ge). Both PXRD analyses were conducted at University of Toronto.